AD-A136 729 STRESS CORROSION OF CERAMIC MATERIALS(U) NATIONAL BUREAU OF STANDARDS WASHINGTON D C INORGANIC MATERIALS DIV* S W FREIMAN ET AL. 01 NOV 83 N00014-79-F-0030 1/2

UNCLASSIFIED F/G 11/2 NL

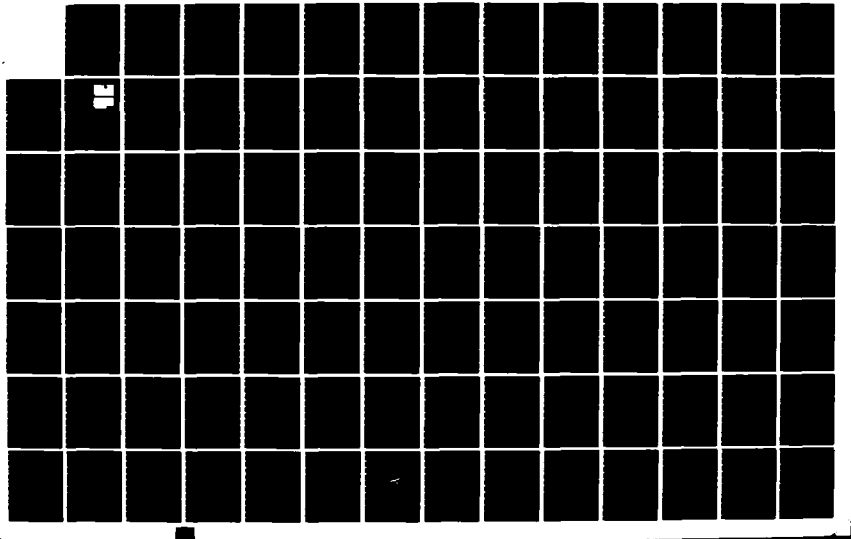

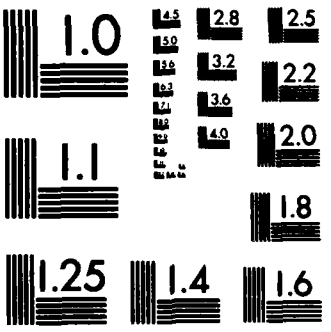

MICROCOPY RESOLUTION TEST CHART
NATIONAL BUREAU OF STANDARDS-1963-A

(12)

A136729

STRESS CORROSION OF CERAMIC MATERIALS

S.W. Freiman, B.R. Lawn

and

G.S. White, A.C. Gonzalez, R.F. Cook,
P. Chantikul, H. Richter, E.R. Fuller, Jr.,
S.M. Wiederhorn and T.A. Michalske

Annual Report

October 1, 1982 - September 30, 1983

ONR Contract No. N00014-79-F-0030
NBS Project No. 5610454

for

Office of Naval Research
Code 431
Arlington, VA 22217

by

National Bureau of Standards
Inorganic Materials Division
Washington, DC 20234

October 1983

SECURITY CLASSIFICATION OF THIS PAGE (When Data Entered)

REPORT DOCUMENTATION PAGE

READ INSTRUCTIONS BEFORE COMPLETING FORM

1. REPORT NUMBER	2. GOVT ACCESSION NO. AD-A136729
3. RECIPIENT'S CATALOG NUMBER	
4. TITLE (and Subtitle) Stress Corrosion of Ceramic Materials	5. TYPE OF REPORT & PERIOD COVERED Annual 1 ~~Nov~~ Oct. 1982 - 31 Oct. 1983
	6. PERFORMING ORG. REPORT NUMBER
7. AUTHOR(s) S. W. Freiman, B. R. Lawn, G. S. White, A. C. Gonzalez, R. R. Cook, P. Chantikul, H. Richter, E. R. Fuller, Jr., S. M. Wiederhorn, and T. A. Michalske	8. CONTRACT OR GRANT NUMBER(s) N00014-79-F-0030
9. PERFORMING ORGANIZATION NAME AND ADDRESS National Bureau of Standards Inorganic Materials Division Washington, D. C. 20234	10. PROGRAM ELEMENT, PROJECT, TASK AREA & WORK UNIT NUMBERS
11. CONTROLLING OFFICE NAME AND ADDRESS Office of Naval Research 800 North Qunicy Arlington, VA 22217	12. REPORT DATE 1 Nov. 1983
	13. NUMBER OF PAGES 212
14. MONITORING AGENCY NAME & ADDRESS(if different from Controlling Office)	15. SECURITY CLASS. (of this report) Unclassified
	15a. DECLASSIFICATION/DOWNGRADING SCHEDULE

16. DISTRIBUTION STATEMENT (of this Report)
Unlimited

17. DISTRIBUTION STATEMENT (of the abstract entered in Block 20, if different from Report)
Unlimited

18. SUPPLEMENTARY NOTES

19. KEY WORDS (Continue on reverse side if necessary and identify by block number)

Crack growth	Ferroelectric
Fracture	Capacitors
Glasses	Proof testing
Ceramics	Static fatigue

20. ABSTRACT (Continue on reverse side if necessary and identify by block number)

The molecular model for crack growth in SiO_2 has been extended to other materials. An electrostatic model for crack growth has been developed to explain high velocity behavior in silicate glasses. Effects of internal stresses in ferroelectric barium titanate have been demonstrated. Indentation fracture studies have been initiated on multilayer capacitors in order to correlate crack-like defects with electrical failures.

DD FORM 1 JAN 73 1473 EDITION OF 1 NOV 65 IS OBSOLETE
S/N 0102-LF-014-6601

SECURITY CLASSIFICATION OF THIS PAGE (When Data Entered)

STRESS CORROSION OF CERAMIC MATERIALS

STRESS CORROSION OF CERAMIC MATERIALS

SUMMARY

This program consists of three portions: (1) Investigation into the chemistry of stress enhanced crack growth in glasses and ceramics; (2) A study into the basic mechanisms which govern crack growth and fracture in piezoelectric materials, and (3) A study into lifetime prediction procedures for ceramic capacitors using fracture mechanics techniques.

(1) A molecular model was developed explaining stress enhanced crack growth in vitreous SiO_2. During the past year, work on alkali silicate glasses has shown that the presence of Na^+ ions in the glass may modify this mechanism, but that under most conditions fracture is still controlled by the stress aided rupture of Si-O bonds. Further, it has been shown that the model also explains crack growth in Al_2O_3 (sapphire). The same environments which produced enhanced crack growth in SiO_2 also did so in Al_2O_3. It has been shown that more ionically bound solids such as MgF_2 show somewhat modified crack growth behavior in these environments. Infrared reflection spectroscopy is now being used to establish correlations between subcritical crack growth and corrosion behavior of glasses in a number of liquid environments.

In a parallel effort, an electrostatic model for crack growth in glasses has been developed. This model is consistent with the mechanism discussed above. In the absence of strong chemical reactions at crack tips, crack growth rates are predicted to depend on the dielectric constant of the environment and the stress dependence of the dielectric constant in the glass.

This electrostrictive model is consistent with crack growth data obtained on soda-lime-silica glass; data on vitreous silica is being collected.

(2) Indentation fracture techniques are being used to determine effects of the cubic to tetragonal phase transformation on both the strength and fracture toughness of $BaTiO_3$. It has been shown that a $\tilde{\sim}$ 50% decrease in K_{IC} occurs in going from the ferroelectric to the paraelectric state. This decrease occurs monotonically with an increase in temperature up to the Curie point ($\tilde{\sim}$ 120°C). This effect is reversible, the stress required to propagate an indentation induced flaw returning to its original room temperature value after heating up to 150°C and then cooling. This reversibility indicates that the toughness variation is intrinsic to the material and suggests that no change in the indentation induced stress field occurs due to heating above the Curie point. Deviations in strengths from indentation theory predictions were observed at small indentation loads and flaw sizes. This behavior is interpreted in terms of the influence of internal stresses induced by the cubic to tetragonal transformation and is consistent with earlier studies on similar materials. Studies are underway to determine the effect of these localized internal stresses on subcritical crack growth behavior in $BaTiO_3$.

(3) The objective of this part of the program is to determine whether certain electrical breakdowns in ceramic capacitors occur due to cracks which grow between two electrodes under combined mechanically and electrically induced stress fields. Observations of indentation induced cracks in both BX and NPO ceramic capacitor compositions has shown that there is a strong

interaction between cracks and the metal electrode layers in the capacitor, leading to a significantly increased apparent toughness of the material. Dynamic fatigue studies of both the BX and NPO capacitors also suggest significant electrode-crack interactions. Low stressing rate studies on this material containing indentation induced cracks on which an electrical field of 1400 v/cm was imposed, show no effects of this field on the strength. Also no change in crack length for an indentation induced crack was observed on capacitors under the above electrical field. Work on effects of combined mechanical loads and electrical fields on crack extension is being continued.

Reprinted from the Journal of the American Ceramic Society, Vol. 66, No. 4, April 1983

A Molecular Mechanism for Stress Corrosion in Vitreous Silica

TERRY A. MICHALSKE* and STEPHEN W. FREIMAN*,*

Ceramic Development, Sandia Laboratories, Albuquerque, New Mexico 87115

The mechanical strength of most glasses and ceramics decreases with time under static loading in an ambient environment. This strength loss is associated with slow growth of preexisting surface flaws due to stress corrosion by water from the surrounding environment. We studied stress corrosion in vitreous silica exposed to water and several nonaqueous environments; environments which enhance stress-corrosion crack growth in silica contain active groups with electron donor sites on one end and proton donor sites at the other. These results suggest a detailed chemical model for the interaction of the environment with mechanically strained bonds in the solid at the tip of a crack. The proposed model for stress-corrosion crack growth also has implications for the long-term strength behavior of a wide variety of brittle materials.

I. Introduction

A DECREASE in strength with time under load in ambient environments is observed for most glasses and ceramics. This phenomenon, commonly referred to as static fatigue or delayed failure, results, at least in part, from slow growth of preexisting flaws in the materials. The small flaws grow until they are large enough to result in catastrophic failure. Up to now, no conclusive evidence existed for stress corrosion in glasses or ceramics due to any species other than water. In addition, models for crack growth due to water, such as those proposed by Orowan,[1] Charles and Hillig,[2] and Wiederhorn *et al.*,[3] are phenomenological in nature. None of these theories provides an understanding of why water is especially effective in increasing the rate of slow crack growth, nor do they provide a means of predicting the effect of nonaqueous environments on fracture of glass.

In this paper, we present a detailed view of the chemical interaction between strained crack-tip bonds in vitreous silica and water molecules from the environment. We show how such a molecular interpretation of the stress-corrosion process leads to an understanding of the effectiveness of water as a stress-corrosion agent along with the ability to qualitatively predict the effects of various nonaqueous stress-corrosion agents. Experimental results in the form of crack velocity vs stress intensity diagrams will be presented for crack growth in vitreous silica in support of this interpretation. Finally, a brief section is included to demonstrate the coherence of such a molecular interpretation of stress corrosion with current atomistic models of the fracture process.

Presented at the Basic Science Division Joint Fall Meeting with TMS–AIME, Louisville, Kentucky, October 14, 1981 (Paper No. 106–B–81F). Received June 21, 1982; revised copy received October 4, 1982; approved October 21, 1982.

Supported in part by the Office of Naval Research and the Department of Energy.

*Member, the American Ceramic Society.

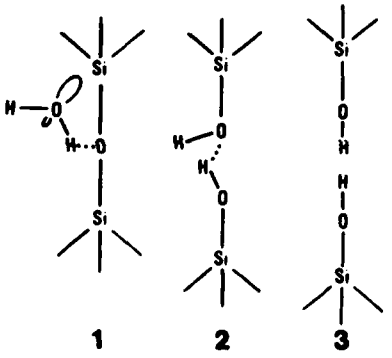

Fig. 1. Representation of proposed reaction between water and strained Si–O–Si bond at crack tip. Reaction steps involve (*1*) adsorption of water to Si–O bond, (*2*) concerted reaction involving simultaneous proton and electron transfer, and (*3*) formation of surface hydroxyl groups.

II. Chemical Bond Rupture in Silica

Network silicates are composed of $[SiO_4]^{-4}$ tetrahedral units linked at their corners by bridging Si–O–Si bonds. On the atomic scale, it is the bridging Si–O bond which supports stress in the material and its rupture is important to the fracture process. At the crack tip in a stressed solid, highly concentrated strain fields are produced. Continuum approximations indicate that the bridging bond experiences strains >20%. The effect of this strain on the bridging Si–O bond can be discussed in terms of decreased bonding overlap and, thus, an increased availability for Si and O atoms to bond with other species.

The structure and bonding in the water molecule are established in the literature. Oxygen atomic orbitals 2*s*, 2*px*, and 2*py* form three hybrid orbitals, two of which σ-bond with hydrogen atoms. The remaining lone-pair orbitals (one hybrid and the remaining *pz*) are directed away from the hydrogen atoms. This arrangement results in a positive charge center opposite the lone-pair orbitals.

The interaction between a strained bridging bond at the crack tip in silica and a water molecule from the environment can be represented by a three-step process (Fig. 1).

Step 1. A water molecule from the environment attaches to a bridging Si–O–Si bond at the crack tip. The water molecule is aligned by: (1) formation of the hydrogen bond with the $O_{(bridging)}$ atom and (2) interaction of the lone-pair orbitals from $O_{(water)}$ with the Si atom. The lone-pair orbital interaction may involve either Van der Waals attraction or some covalent bonding with unoccupied orbitals of Si.

Step 2. A concerted reaction occurs in which proton transfer to the $O_{(br)}$ is accomplished simultaneously with electron transfer from the $O_{(w)}$ to the Si atom. As a result of this reaction, two new bonds are formed, one between $O_{(w)}$ and Si, and one between hydrogen and $O_{(br)}$; the original bridging bond between $O_{(br)}$ and Si is destroyed.

Step 3. Rupture of the hydrogen bond between $O_{(w)}$ and transferred hydrogen occurs to yield surface Si–O–H groups on each fracture surface. Since the hydrogen bond is weak, this step is expected to occur immediately after proton transfer. (Budd[4] proposed a similar mechanism for the dissolution of silica in water; however, it should be noted that the present model for crack growth is not contingent on the removal of material from the fracture surface.)

It is worth noting that the chemical mechanism used here to describe rupture of highly strained crack-tip bonds is in agreement with reactions observed at strained siloxane (SiOSi) bonds present on dehydrated silica surfaces.[5] Spectroscopic results show that dehydrating a silica surface at $T<400°C$ creates strained siloxane surface bonds. When water is readmitted, the strained surface bonds act as sites to dissociatively adsorb water molecules, thus forming two silanol (SiOH) surface groups.

This model for chemical bond rupture has a number of interesting implications. Note first that there is no requirement for prior dissociation of the water molecule, nor do any reaction products

Table I. Properties of Environments Investigated

Environment	Dielectric constant, ϵ'	Dipole moment, $\mu \times 10^{30}$ (C·m)	Water content
Water, H_2O	78	6.17	
Deuterated water, D_2O	78	6.20	
Ammonia, NH_3	22	4.90	1–5% rh
Hydrazine, N_2H_4	52	5.83	5% max
Formamide, CH_3NO	109	12.4	365 ppm*
Acetonitrile, CH_3CN	39	13.1	125 ppm*
Carbon monoxide, CO	1	0.33	1–5% rh
Nitrobenzene, $CH_6H_5NO_2$	34	14.1	
Nitrogen, N_2	1	0	1–5% rh

*By Karl Fisher technique.

need be removed from the surface. This is quite a different picture than that presented by Charles and Hillig.[2] The model is consistent with the concepts of Orowan,[1] who suggested that the driving force for crack growth is the reduction in surface energy by the environment. Second, the model suggests that environments other than water should enhance crack growth if the species possess structural and bonding features similar to those of water, i.e. proton donor sites at one end of the molecule (or groups) and lone-pair orbitals at the other. The environmental molecule (or group) must also be of comparable size with the Si–O bond (≈0.163 nm).

III. Experimental Procedure

To evaluate the stress-corrosion reaction proposed in Section II, crack-growth studies were conducted on vitreous silica† in water, N_2 gas of low relative humidity, and several nonaqueous environments (Table I). The glass was cut into double-cantilever-beam specimens (50 by 12 by 1 mm) having a center groove of about one-half the specimen thickness. The specimens were annealed at 1090°C after machining. A sharp crack was introduced into one end by pressing a sharp point onto the side opposite the groove. Aluminum arms were epoxied to the specimen and crack-growth data obtained using the applied-moment technique[6] by applying deadweight loading and using a 40X traveling microscope with a filar eyepiece to monitor crack motion. All tests other than those in H_2O and deuterated water were conducted inside a Plexiglass‡ chamber. Prior to testing, the chamber was purged with N_2 gas for 5 to 10 min. In the case of NH_3 and CO, these gases were then continuously bled at a constant flow rate into the chamber during testing. For the liquid environments, an N_2 overpressure was maintained to prevent the pickup of moisture from the environment. The effect of the water always present in any environment on the interpretation of the crack-growth data is discussed in the following section.

The measured crack velocities are plotted vs stress intensity factor (K_I) in Fig. 2 for vitreous silica tested in liquid water and N_2 gas of 1 to 2% relative humidity. Note that the functional form $V = V_0 \exp(bK_I)$ was used throughout, since this expression has a better theoretical basis than the commonly used power law. However, the conclusions regarding the data would not be altered through use of the latter. The important features in this plot are:

(1) Crack growth in the low-velocity regime in N_2 gas is enhanced (curve is shifted to lower K_I and V is a measurable function of K_I) by the small amount of water present, as was shown previously by Wiederhorn[7] for soda-lime glass. The relative amount of enhancement is related to the chemical activity of water (i.e. relative humidity) in the environment.[7]

(2) A plateau in crack velocity is observed in the moist N_2. This plateau has been linked to crack growth limited by the rate of water transport to the tip of the moving crack.[7,8] At sufficiently high V, the plateau behavior ends and rapid fracture is observed.

(3) In N_2 gas above the plateau velocity, the V–K_I curve was too steep to obtain measurements, in agreement with the spontaneous failure of vitreous silica observed by Wiederhorn *et al.*[9] in a vacuum of 0.133 Pa.

(4) Liquid water enhances crack growth over the entire range of crack velocities (10^{-9} to 10^{-2} m/s). (At velocities $>10^{-2}$ m/s, cavitation will occur,[10] and no effect of the water will be observed.)

Figure 3 shows the crack-growth curves for ammonia, hydrazine, and formamide along with the curves for N_2 gas and water from Fig. 2. The data points for water and ammonia are shown to indicate the amount of scatter associated with the experimental

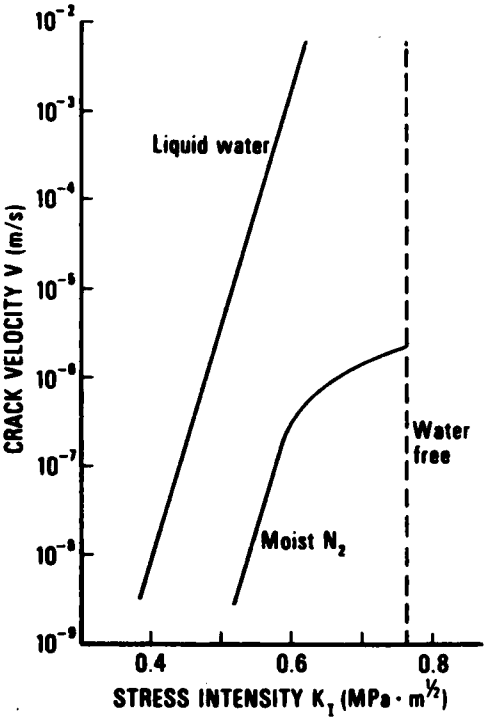

Fig. 2. Effect of water on slow fracture in vitreous silica (curves represent best fit to experimental data).

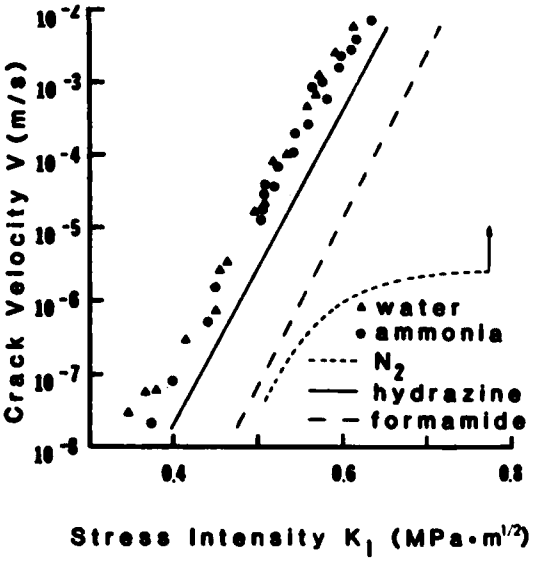

Fig. 3. K_I vs V diagram for vitreous silica at room temperature, showing that water, ammonia, hydrazine, and formamide increase rate of slow crack growth.

*Now with Inorganic Materials, National Bureau of Standards, Washington, DC 22034.
†No. 7940, Corning Glass Works, Corning, NY.
‡Rohm and Haas Co., Philadelphia, PA.

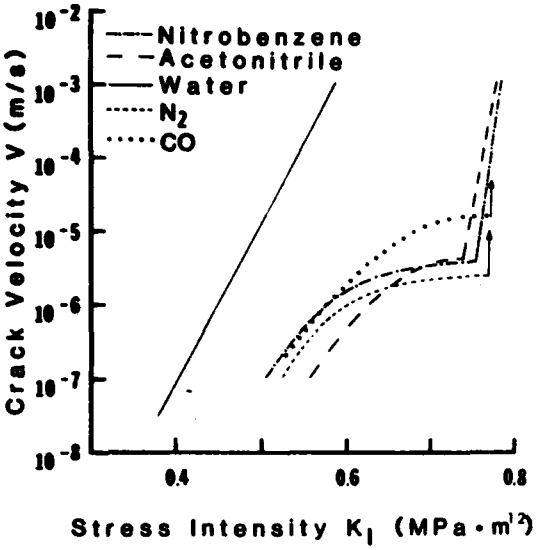

Fig. 4. K_I vs V diagram for vitreous silica at room temperature, showing that carbon monoxide, nitrobenzene, and acetonitrile have little, if any, effect on rate of slow crack growth.

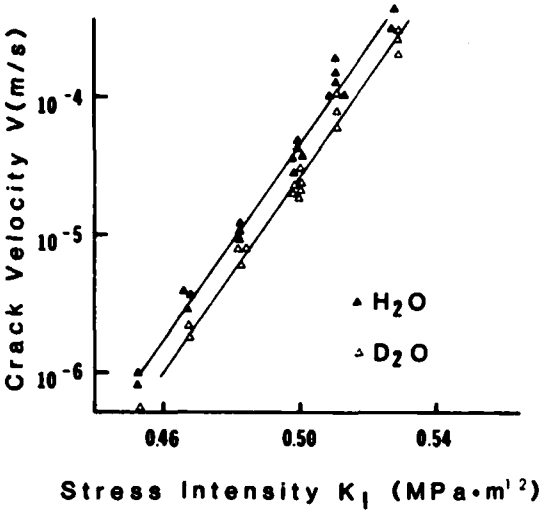

Fig. 5. Comparison of effects of H_2O and D_2O on slow crack growth in vitreous silica at room temperature.

measurements; all other data are represented by best-fit lines. The most important feature of this plot is the absence of any plateau in the curves for ammonia, hydrazine, or formamide. The plateau occurs because crack-growth rates controlled by small amounts of the water in a liquid or gas eventually become limited by the rate at which the water can diffuse to the crack tip. For a water-saturated gas this plateau would occur at 10^{-4} m/s (Ref. 7); it would be significantly lower in a liquid because of viscosity contributions.[3] For a relative humidity of 0.17% in N_2 gas, the plateau would occur at 10^{-7} m/s.[7] This water content is below that known to occur in any of the above environments (Table I). The absence of a plateau in velocity leads to the conclusion that the reaction of ammonia, hydrazine, and formamide at the crack tip controls crack velocities in preference to water present in these environments. The similarity in the slopes of the V–K_I curves in these environments to that in water suggests that stress-activated processes are also similar. It is tempting to attribute significance to the overlap of the data for water and ammonia. However, one must realize that while the ammonia is present as a gas at essentially atmospheric pressure, and so has an activity of 1, the activity of the water referred to the same state is only ≈30/760.

As Fig. 4 indicates, neither carbon monoxide, acetonitrile, nor nitrobenzene controlled crack growth in preference to the small quantities of water present. The V–K_I diagram for each displays a plateau at the approximate velocity expected for the amount of water present. It should be noted that the crack-growth curves in region III vary for each environment, possibly reflecting electrostatic effects of each species on the fracture process, as described by Wiederhorn *et al.*[3]

Finally, Fig. 5 compares crack-growth rates in normal water and deuterated water at room temperature. It can be seen that the slopes of the V–K_I curves are parallel but the curve for deuterated water is displaced to lower velocities.

IV. Discussion

(1) *Implications of Model for Silica*

Figure 3 shows that water, ammonia, hydrazine, and formamide are effective in promoting stress-corrosion crack growth in vitreous silica. Each of these environmental species is similar in that its molecular structure contains the combination of lone-pair electron orbitals opposite a proton, with a separation distance of ≈0.1 nm. This structural similarity is important since it indicates that each of the environments that enhanced stress corrosion is capable of participating in the concerted reaction described in Fig. 1. The schematic drawings of Fig. 6 show the molecular structure of each of the effective stress-corrosion agents. The dashed line represents the bond which is expected to cleave during the crack-tip reaction. In each case, one of the resulting fragments is expected to be a proton which will form a silanol surface group. However, each stress-corrosion environment presents a different remaining fragment which is expected to form a surface compound by bonding with a silicon on the glass surface. The difference in surface compounds for silica fractured in different stress-corrosion environments presents an interesting method for potentially verifying the proposed model for stress-corrosion chemistry. We are currently pursuing surface analysis techniques which will allow identification of these surface compounds.

So far we have shown that environmental species possessing lone-pair orbitals opposite proton donor sites promote stress corrosion in vitreous silica. What is equally important is the evidence that species devoid of this structural similarity do not participate strongly in the stress-corrosion process. As demonstrated in Fig. 4, carbon monoxide, acetonitrile, and nitrobenzene show only enhancement of low-velocity crack growth, which can be directly related to the low-level concentration of water in each. Although each of these environments contains lone-pair orbitals, none has a proton donor site directly across and, except for carbon monoxide, the lone pair is pointing in toward the center of the molecule.

Since reference has been made to correlations between dielectric constant[11] and dipole moment[12] of the environment and slow crack-growth rates, we examined our K_I vs V data for such relations. Table I lists the environments studied in this work along with their respective dipole moment and dielectric constant. No systematic correlations were found between the values from Table I and the slow crack-growth results of Figs. 3 and 4. Nitrobenzene (dipole moment 1.41×10^{-20} C·m) did not control slow crack-growth rates, whereas ammonia (4.9×10^{-29}) C·m was a strong stress-corrosion agent. Formamide ($\varepsilon'=109$) was less effective as a stress-corrosion agent than ammonia ($\varepsilon'(l)=26$) ($\varepsilon'(g)=1$). It is apparent from these comparisons and others which can be made from the present data that studies which report effects of high dipole moment or high dielectric constant on strength may in fact be reporting the effect of water impurities in those environments.

Figure 5 shows that crack-growth rates measured in deuterated water are lower than those measured in normal water. To interpret this hydrogen isotope effect, it will be necessary to discuss the stress-corrosion model in the context of reaction-rate theory. This discussion can begin by examining a schematic of the reaction coordinate for crack-tip bond rupture in a silica specimen which is

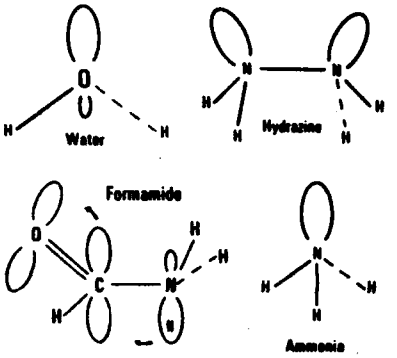

Fig. 6. Representations of water and other nonaqueous species having lone-pair orbitals (electron donor sites) directly across from protons (electron acceptor sites). Dashed line indicates bond expected to cleave during crack-tip interaction.

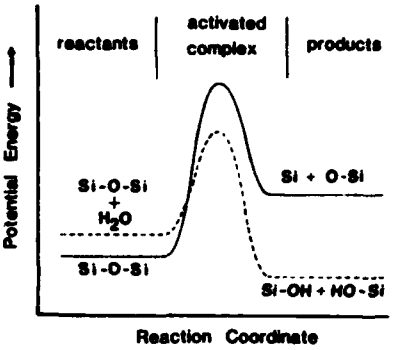

Fig. 7. Representation of reaction coordinate for bond rupture in silica; solid line indicates rupture in vacuum and dashed line rupture with water present.

strained below the critical stress intensity for catastrophic failure (see Fig. 7). The main points of interest on the reaction coordinate are the energy levels of the reactants (bridging bond), the activated complex (that complex which exists at the time of bond rupture), and the products (those species left on the fracture-generated surfaces). In vacuum (solid line), the entire energy of the bridging bond must be overcome before bond rupture can occur. (This energy is supplied in part by mechanical strain as well as by thermal contributions). When water is present (dashed line), the height of the energy barrier to bond rupture is reduced because charge transfer (step 2 of crack-tip interaction) provides an alternate, lower-energy, reaction path. The effect of a reduced energy barrier to reaction can be seen in Eq. (1).

$$k=(RT/Nh)\exp(-\Delta G^{\ddagger}/RT) \tag{1}$$

where k is the reaction-rate constant, N Avogadro's number, h Planck's constant, T temperature, R the gas constant, and $\Delta G^{\ddagger}$ the height of the energy barrier between the reactants and the activated complex. Since the rate constant for a chemical reaction (in this case, bond rupture) is reciprocally dependent on the height of the energy barrier, mechanisms that provide a lower-energy-activated complex will increase crack-growth rates. It should be noted that factors such as the change in the energy of the bridging bond due to adsorbed water (step 1 of crack-tip interaction) and the energy of the reaction products (step 3 of crack-tip interaction) can affect the energy barrier to fracture and, thus, the fracture rate. It will be important in subsequent studies to evaluate the relative importance of all three steps of the bond-rupture process on the fracture rate. At present, the observed isotope effect indicates that the concerted reaction (simultaneous electron and proton transfer) is the rate-limiting step to the chemical bond rupture process. The isotopic effect arises from the difference in ground-state vibrational energies for deuterium and protium which, in turn, results in different activation barriers for the two isotopes. When a proton exchange is involved in the rate-limiting step, a primary (strong) isotope effect is predicted whereby the deuterated reaction is expected to proceed more slowly. Since we do see a decrease in crack velocity for deuterated water, it is reasonable to conclude that proton transfer is involved in the rate-limiting step to fracture.

The preceding discussion has addressed reaction-rate theory in an elementary manner. This topic is treated more rigorously by solvation theory, which parallels closely the reaction involved in stress-corrosion crack g th. Althc olvation chemistry and stress-corrosion chemist , t is cal, both involve reactions which break down bridging b ds in the solid. (In solvation, there is a need to contain the fragments of bond rupture in solution. However, this step is not necessary in stress-corrosion crack growth since broken bonds are separated by mechanical strain.) Reichardt's[13] treatment of solvation theory presents a detailed discussion of possible interactions between solvent molecules and chemical reactions occurring in the solute. His treatment shows how various interactions can influence rate constants for the chemical interactions. Application of solvation theory to stress-corrosion effects can be very helpful in understanding the phenomenon of slow fracture. However, it should be noted that phenomenological studies of chemical kinetics alone do not provide information concerning details of the chemical reaction mechanism and may not be extremely useful for predicting fracture rates in other environments or for other brittle materials.

(2) Predictions for Other Materials

We have shown that the mechanistic model for stress corrosion in silica can be used to predict, qualitatively, the effectiveness of various nonaqueous environments. Recent work has shown that the mechanistic approach is useful not only for predicting stress-corrosion behavior of other oxide materials but can be extended to ionic as well as purely covalent solids. Michalske *et al.*[14] showed that single-crystal sapphire (Al_2O_3) shows slow fracture behavior similar to silica when exposed to the nonaqueous environments discussed in this paper. This result was predicted since the chemistry of the Si–O bond and the Al–O bond are quite similar. However, the same study showed that single-crystal magnesium fluoride (MgF_2) exhibits quite a different susceptibility when exposed to the same environments. Specifically, ammonia, which was very effective in promoting stress corrosion in the oxide materials, was not effective for magnesium fluoride, whereas acetonitrile, which was not effective for the oxides, greatly enhanced fracture rates in magnesium fluoride. These results were interpreted in terms of the change in bond character in going from oxide to fluoride materials. In fluorides, the bridging bond is mostly ionic in character and for this reason electrostatic interactions with the environmental molecules are expected to dominate stress-corrosion behavior. This type of interaction is quite different from the chemical interaction proposed for the oxide system. Experimental investigations of stress corrosion in silicon[15] suggest that aqueous environments have little, if any, effect on fracture rate. This result would also be predicted from the mechanistic model since the silicon-silicon bond is completely covalent and would not exhibit a preference for either end of the water molecule (lone-pair orbital or proton) and, thus, would not easily participate in the concerted reaction hypothesized for stress corrosion in oxides.

Finally, a mechanistic model for the stress-corrosion process has the potential to interface with current atomistic models concerning the physics of fracture. Theoretical work by Fuller *et al.*[16] showed how any arbitrary chemical interaction can be placed in the context of a crack tip in a discrete atomic lattice. It will be important in the future to add experimental parameters obtained in conjunction with mechanistic models for crack growth with theoretical models for crack-tip physics in order to make quantitative predictions of stress corrosion effects.

V. Summary

Crack velocities were measured as a function of K_I for vitreous silica in water and several nonaqueous environments. Results of these studies showed that environments with a molecular structure containing a lone-pair electron orbital across from a proton donor site have the greatest effect on crack growth. A qualitative model is proposed to demonstrate how molecules of this structural type may interact with Si–O bonds at the crack tip. This model enables one to predict the effect of a given environment on crack-growth rates in silica. This molecular model can also be used to predict stress-corrosion effects in other brittle materials.

Acknowledgments: The authors thank Corning Glass Works for providing the glass used in these experiments and S. M. Wiederhorn and J. Houston for helpful discussions.

References

[1]E. Orowan, "The Fatigue of Glass Under Stress," *Nature*, 154, 341–43 (1944).
[2]R. J. Charles and W. B. Hillig, "The Kinetics of Glass Failure by Stress Corrosion"; pp. 511–27 in Symposium sur la Resistance Mechanique du Verre et les Moyens de l'Ameliorer, Union Scientifique Continentale du Verre, 24, Charleroi, Belgium, 1962.
[3]S. M. Wiederhorn, S. W. Freiman, E. R. Fuller, Jr., and C. J. Simmons, "Effects of Water and Other Dielectrics on Crack Growth"; to be published in *Journal of Materials Science*.
[4]S. M. Budd, "The Mechanisms of Chemical Reaction Between Silicate Glass and Attacking Agents," *Phys. Chem. Glasses*, 2 [4] 111–14 (1961).
[5]M. L. Hair, "Hydroxyl Groups in Silica Surface," *J. Non-Cryst. Solids*, 19, 299–309 (1975).
[6]S. W. Freiman, D. R. Mulville, and P. W. Mast, "Crack Propagation Studies in Brittle Materials," *J. Mater. Sci.*, 8, 1527–35 (1973).
[7]S. M. Wiederhorn, "Mechanisms of Subcritical Crack Growth in Glass"; in Fracture Mechanics of Ceramics, Vol. 4. Edited by R. C. Bradt, D. P. H. Hasselman, and F. F. Lange. Plenum, New York, 1974.
[8]C. L. Quackenbush and V. D. Frechette, "Crack-Front Curvature and Glass Slow Fracture," *J. Am. Ceram. Soc.*, 61 [9–10] 402–406 (1978).
[9]S. M. Wiederhorn, H. Johnson, A. M. Diness, and A. H. Heuer, "Fracture of Glass in Vacuum," *J. Am. Ceram. Soc.*, 57 [8] 336–41 (1974).
[10]T. A. Michalske and V. D. Frechette, "Dynamic Effects of Liquids on Crack Growth Leading to Catastrophic Failure in Glass," *J. Am. Ceram. Soc.*, 63 [11–12] 603–609 (1980).
[11]V. K. Moorthy and F. V. Tooley, "Effect of Certain Organic Liquids on Strength of Glass," *J. Am. Ceram. Soc.*, 39 [6] 215–17 (1956).
[12]J. H. Lunsford, "Loss of Strength of Borosilicate Glass in Vapors of Differing Dipole Moments," *J. Am. Ceram. Soc.*, 47 [6] 309 (1964).
[13]C. Reichardt, Solvent Effects in Organic Chemistry. Verlag Chemie, New York, 1979.
[14]T. A. Michalske, S. W. Freiman, and B. Bunker, "A Chemical Approach to Predicting Stress Corrosion Behavior of Brittle Materials"; for abstract see *Am. Ceram. Soc. Bull.*, 61 [3] 414 (1982).
[15]T. J. Chen and W. J. Knapp, "The Fracture of Single-Crystal Silicon Under Several Liquid Environments," *J. Am. Ceram. Soc.*, 63 [3–4] 225–26 (1980).
[16]E. R. Fuller, Jr., B. R. Lawn, and R. M. Thomson, "Atomic Modelling of Chemical Interactions at Crack Tips," *Acta Metall.*, 28, 1405–14 (1980).

Reprinted from the Journal of the American Ceramic Society, Vol. 66, No. 7, July 1983

Relation Between Multiregion Crack Growth and Dynamic Fatigue of Glass Using Indentation Flaws

P. CHANTIKUL*,*

Department of Applied Physics, School of Physics, University of New South Wales, New South Wales 2033, Australia

BRIAN R. LAWN,* HERBERT RICHTER,† and STEPHEN W. FREIMAN*

Fracture and Deformation Division, National Bureau of Standards, Washington, DC 20234

The influence of transport-limited kinetic crack growth on the fatigue properties of soda-lime glass was examined. Dynamic fatigue data were taken on specimens with controlled indentation flaws and were compared with the predicted response from measured crack velocity characteristics. Heptane was used as the operational test environment because of its pronounced crack velocity plateau; control tests in water served to establish a baseline reference for comparing the results. Fractographic observations using a stress wave marker technique showed a complex growth history for flaws broken in heptane compared to that for flaws broken in water. The magnitude of the predicted region II influence is too small to be detected in the dynamic fatigue results, even allowing for the relatively high degree of data reproducibility. The implications of this conclusion for lifetime predictions are discussed.

I. Introduction

THE long-term strength of brittle solids is governed by such factors as flaw size and shape and the susceptibility to chemically enhanced slow crack growth. Implicit in the fracture mechanics treatments of time-dependent strength (fatigue) properties are certain assumptions concerning these factors, e.g. that the flaws respond in essentially the same way as macroscopic cracks and that the crack velocity can be expressed as some simple function (usually power law) of the stress intensity factor. The success of this approach has led, in conjunction with statistical accountability of flaw populations, to useful engineering design schemes.[1,2]

This paper examines the degree to which macroscopic crack velocity data can be used to determine the kinetics of failure in strength testing. In particular, a critical look is taken at the potential complications in lifetime predictions when the crack velocity function shows multiregion behavior.[3] Generally, three such regions are identifiable: region I (low velocities), controlled by rate of reaction between environmental species and crack-tip bonds; region II (intermediate velocities), controlled by rate of transport of environmental species to the tip; region III (high velocities), controlled by electrostatic environment-bond interactions.[4] It is customary to recognize the existence only of region I in the formal derivation of fatigue equations, on the grounds that it is the domain of slowest growth that must control the crack evolution to failure and that in the more concentrated active environments (e.g. water) the higher regions are not strongly evident in the crack velocity response. In addition, it has been argued that natural surface flaws, by virtue of their relatively small size and their continuous accessibility to the external environment at the points of intersection with the free surface,[3-7] may not be subject to conventional region II effects. Considerations of this kind clearly raise questions about the status of macroscopically determined crack velocity functions as a suitable basis for fatigue strength analysis.

The approach adopted here is to run dynamic fatigue tests on glass specimens with controlled flaws, generated by Vickers indentations,[6-11] in an environment with a pronounced region II crack velocity plateau. Although indentation-induced crack systems are subject to intense residual stress fields,[10,12,13] these fields have been well characterized and are readily accommodated into the fracture mechanics formalism.[6,14] The element of control significantly reduces the statistical aspect, and allows for monitoring of the crack evolution to failure. In the present study, this monitoring is accomplished by imposing periodic stress markers onto the frac-

Received October 14, 1982; revised copy received February 11, 1983; approved February 21, 1983.
Supported by the U. S. Office of Naval Research, Metallurgy and Ceramics Program, and by the Deutsche Forschungsgemeinschaft.
*Member, the American Ceramic Society.
*Now with the Department of Physics, Chulalongkon University, Bangkok, Thailand.
†On leave from Fraunhofer Institut für Werkstoffmechanik, Freiburg, Federal Republic of Germany.

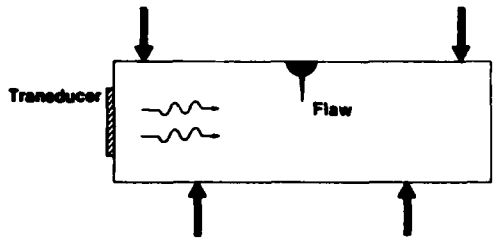

Fig. 1. Schematic of transducer setup for imposing sonic markers on surface of indentation flaw in flexural specimen.

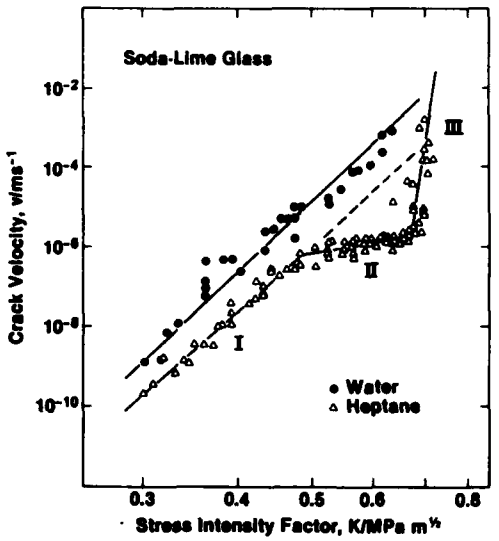

Fig. 2. Crack velocity data for soda-lime glass in heptane (6 specimens) and water (2 specimens) obtained using double-cantilever technique. For heptane, solid lines are segmented least-squares fits to regions I, II, and III; broken line is extrapolation of region I to point of intersection with region III. For water, solid line is prediction from fatigue data.

ture surfaces.[15-17] The dynamic fatigue data are then compared to predictions calculated from v-K curves[3] obtained on double-cantilever-beam specimens.

II. Experimental Procedure

Soda-lime glass was selected as a model material for all tests in this study. Heptane was chosen as the test medium because its low affinity for water (≈50 ppm) leads to a wide region II plateau; also, it has been determined that exposure to air does not lead to an increase in water concentration. Control tests were conducted in water to provide a convenient reference baseline for data analysis. Inert strength tests for parameter calibration were conducted in dry nitrogen gas.[6,7]

(1) Macroscopic Crack Velocity Measurements

Crack velocities were measured on specimens (75 by 12.5 by 1 mm) cut from glass microscope slides, using the double-cantilever configuration with applied-moment loading.[18] A groove ≈0.5 mm deep was cut down the length of one face to guide the crack. The specimens were annealed, precracked, and immersed in the test fluid. An optical microscope was used to monitor the crack growth. Stress intensity factors were calculated from the applied load and specimen dimensions.[18]

[9]The subscript is dropped from K_I, on the understanding that we are always dealing with mode I cracks.

(2) Failure Tests on Controlled-Flaw Specimens

Controlled flaws for strength testing were introduced by indenting with a Vickers pyramid. Flaws of different dimensions were produced by varying the contact load, P, so that any size effect in the region II kinetics might be investigated.[11] All indentations were made in air at a fixed load duration of 10 s, and were left to stand for ≈30 min before strength testing to allow any relaxation in the residual stress field (e.g. due to lateral crack growth[8]) to equalize for all specimens.

The failure tests were conducted in four-point flexure, using a crosshead machine to deliver the bending loads. The rods were carefully oriented so that one set of radial cracks emanating from the indentation corners was normal to the maximum tensile stress. For water, a droplet was simply placed on the indentation site immediately prior to testing; in the case of heptane a liquid bath was necessary because of rapid evaporation. In the latter case the specimens were dried for several minutes in hot air before immersion. Beam theory was used to compute the stress at failure, σ_f. Routine microscopic examination of the broken parts was carried out to confirm that failure originated at the indentation flaw.

(A) Stress Wave Fractography: Stress wave fractographic observations[15-17] were made on annealed glass specimens (150 by 8 by 2 mm) containing 5 N indentations. A transducer mounted at the end of the bend bar generates transverse stress waves normal to the plane of the indentation crack which is to lead to failure (Fig. 1). These waves periodically modify the direction of the maximum tensile stress generated by the external load, without significantly affecting the driving force on the crack. The perturbations leave optically detectable time markers on the fracture surface. Taken in conjunction with the transducer frequency, the markers constitute a pictorial record of the velocity history of the crack system. The major departure from previous studies using this technique is in the lower frequencies attainable, <0.1 Hz (cf. the MHz region conventionally used); under such operating frequencies optically resolvable markers could be produced at crack velocities $<1\ \mu m \cdot s^{-1}$, corresponding to the heptane data plateau region.

(B) Dynamic Fatigue Curves: Fatigue tests were carried out at constant stressing rates, $\dot{\sigma}_a$, on annealed glass rods 5 mm in diam. (inner span 20 mm, outer span 60 mm). An effort was made to cover as wide a stressing-rate range as possible (e.g. by incorporating a piezoelectric load cell into the system for measuring flexural forces at fast rates)[7] to maximize the prospects of detecting any significant shifts in the comparative heptane and water fatigue curves. Inert strengths were measured at the fastest loading rates in flowing dry N_2 gas.

III. Results and Discussion

Let us now show the correspondence between the three sets of observations, i.e. macroscopic crack growth, fractography, and dynamic fatigue.

The macroscopic crack-growth data in Fig. 2 show clear evidence for multiregion velocity behavior in heptane. These data agree with those previously reported for heptane and other alkanes.[19] For a macroscopic crack, the level of the plateau is a function of the concentration of water and the viscosity of the fluid.[4] However, Quackenbush and Frechette[20] and Richter[16] showed that both the crack velocity at which a plateau is observed and the crack-front shape are functions of specimen thickness. The work of these authors suggests that the heptane v-K curve in Fig. 2 is not unique. Whereas regions I and III represent reaction rates intrinsic to the material-environment system, region II is dependent on crack size and shape.

Now consider the flaw-growth patterns in Fig. 3 obtained by stress wave fractography on cracks grown under a constant bending load. In both Figs. 3(*A*) and 3(*B*), corresponding, respectively, to heptane and water, two frequencies have been superimposed to allow coverage of a wide range of velocities. First note that the markers for the specimen tested in water remain closely elliptical in profile, and increase smoothly in spacing, over the entire range of crack growth, corresponding to velocities from 2 $\mu m \cdot s^{-1}$ to

100 mm·s^{-1}, indicative of a single region of crack propagation. The flaw growth in heptane is more complex. The spacing of the markers in the low-frequency domain is nearly constant, and corresponds to a crack velocity of 3 μm·s^{-1}, near the region II plateau. As crack growth proceeds within this region, the crack front becomes increasingly distorted from its initially near-elliptical profile below the tensile surface. Once into the high-frequency domain, corresponding to velocities >1 m·s^{-1}, the front reverts to the elliptical geometry. This difference in behavior between water and heptane environments was reproducible over a number of tests.

Based on the preceding fractographic observations, it would be expected that the fatigue strengths of specimens tested under water and heptane might differ, especially at stressing rates for which the crack spends the largest portion of its growth in region II.

Accordingly, let us examine the possible correspondence between v-K and dynamic fatigue results in terms of indentation fracture mechanics. All mathematical details involved in establishing this correspondence are relegated to the Appendix. We simply note at this point that analytical solutions of the fatigue equations for flaws with residual stresses are obtainable only for single-region crack velocity functions of power-law form, and that these solutions are themselves of power-law form.[14] Figure 4 shows the dynamic fatigue curves predicted from the crack-growth data in heptane, with and without a region II plateau included in the calculations, as well as the experimental dynamic fatigue data in water and heptane. Note that the data have been normalized for indentation load, P, so that all data for each environmental condition might be reduced to a universal curve.

The sequence of operations to obtain the predicted and measured dynamic fatigue curves in Fig. 4 was as follows:

(i) On the assumption that the results for tests in water may be described by single-region behavior over the data range covered, a linear least-squares fit was appropriately made to the logarithmically plotted dynamic fatigue data[11] in Fig. 4. The slope and intercept of this fitted line, in conjunction with inert strength parameters, gives, via a *suitable* set of transformation equations, corresponding values for exponent and coefficient in the glass/water crack velocity equation.

(ii) A linear representation of the result from step (i) was made on the logarithmic crack-velocity/stress-intensity-factor diagram, Fig. 2. The plotted line is seen to pass through the experimental points for a water environment, within the scatter over the data range covered.[8] Thus self-consistency between results from fatigue and velocity tests is established for this single-region system.

(iii) Linear least-squares fits were made to each of the three clearly defined crack velocity regions in Fig. 2. Appropriate exponents and coefficients were evaluated for each fitted segment.

(iv) Using these calibrated velocity parameters, together with the same inert-strength parameters referred to in (i), numerical solutions[12] were obtained for the dynamic fatigue equation (Appendix) for heptane.[9] Two such solutions are plotted in Fig. 4, one with and the other without region II included in the crack velocity function; in the latter case region I is taken to operate up to the extrapolated intersection with the region III curve (Fig. 2).

Even with the relatively high degree of reproducibility achieved by using indentation-induced flaws, the magnitude of any region II influence seems to be too small to be unequivocally distinguished in the dynamic fatigue results for heptane. The fact that the data taken at different loads fall onto the same curve for each environment indicates that flaw size alone is not a primary factor. Similar conclusions were reported by Chandan *et al.*,[5] although their data were less detailed than those presented here.

IV. Concluding Remarks

The foregoing observations suggest that indentation flaws do not show a one-to-one correspondence with macroscopic cracks in their multiregion crack velocity response. This breakdown in correspondence appears to be confined to region II; we recall that for the tests in water, where region I effectively controls the kinetics over the data range considered, mutual consistency is obtained between crack velocity and dynamic fatigue results. Regions I and

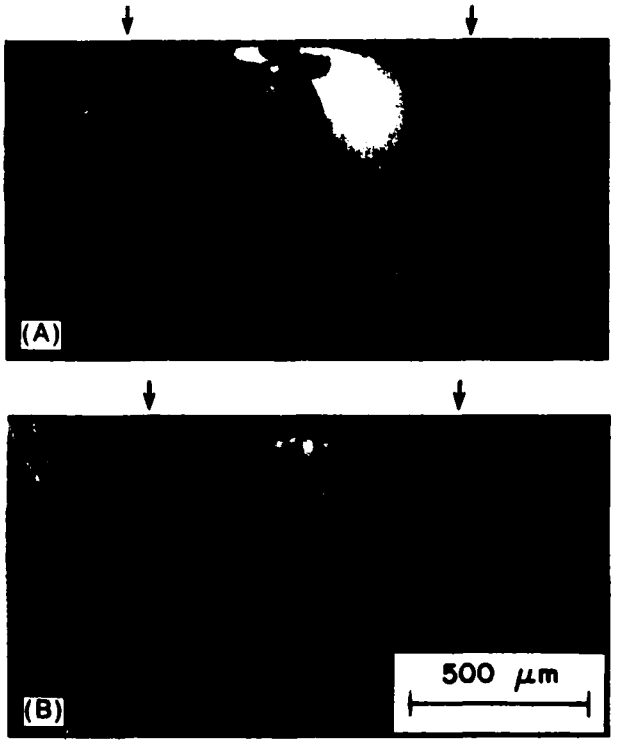

Fig. 3. Fracture surfaces of soda-lime glass from indentations at contact load of 5 N and subsequent bending stress of 35 MPa: (*A*) heptane, marker frequencies 60 mHz and 104 kHz; (*B*) water, 1.1 Hz and 1.9 kHz. (Superposed frequencies in each case simply allow coverage of extended velocity range; arrows indicate points at which markers correspond to transition from lower to higher frequency.) Compare distorted marker pattern in heptane with relatively symmetrical pattern in water.

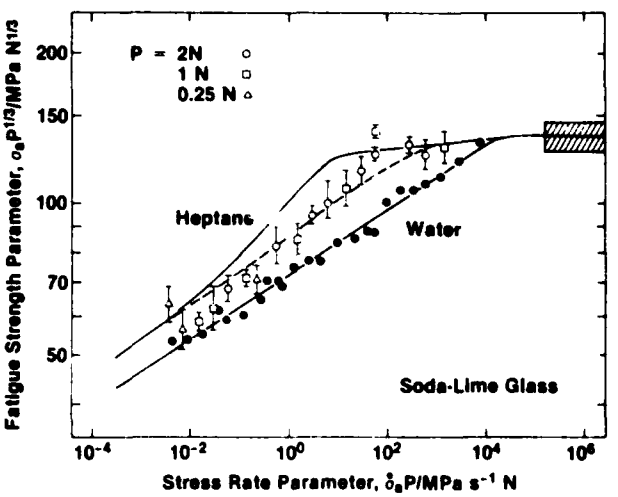

Fig. 4. Normalized dynamic fatigue curves for soda-lime glass in heptane and water. Each data point is mean and standard deviation, in logarithmic coordinates, of 6 to 15 specimens (error bars omitted for water, for clarity). Contact loads P used for heptane are indicated (loads used to obtain control water data covers range 0.05 to 10 N (Ref. 11), but are not differentiated here). Shaded band denotes inert-strength level. Solid line through water data is least-squares fit. Solid line through heptane data is prediction from crack velocity curve with region II included; broken line is corresponding prediction with region II excluded.

[8] In drawing a straight line through the water data in Fig. 2 we intend no statement about the fundamental relation between crack velocity and stress intensity factor; ours is strictly an empirical fitting procedure.

[9] Inclusion of a possible threshold stress intensity factor at 0.3 MPa·m$^{1/2}$ in Fig. 2 did not significantly affect the calculated fatigue curves.

III are intrinsic to the material/environment and would not be expected to depend in any way on crack geometry. For region II, however, with its origins deeply rooted in transport mechanisms, geometrical factors must play some role. Such effects have been noted in fracture mechanics specimens, where the crack velocity plateau becomes a function of specimen width.[16,20] Our results suggest that crack *shape* is an even more important factor than crack *size*. Thus, in the present instance with axisymmetric contact loading the crack system always has a surface trace in direct contact with the environment, so transport effects are apparent only in the subsurface propagation; region II effects are then manifested as a constraint on the surface expansion by the more slowly moving inner crack portions.

The heptane results in Fig. 2 seem to indicate that higher regions in the crack velocity function are unlikely to influence fatigue properties strongly, particularly in longer-term tests, where the crack spends nearly all its growth time in region I. This is not altogether unexpected, bearing in mind the smoothing effect of integrating over the crack velocity function in the failure mechanics. Nevertheless, care should be taken in extrapolating fatigue data to long lifetime domains which lie well outside the data range. Fortunately, the conventional linear extrapolation procedure (i.e. without due regard to the curvature in the fatigue plot caused by higher regions) will tend to underestimate lifetimes, in line with the requirements of conservative design.

Finally, we should point out that the insensitivity to region II effects discussed here may not extend to all strength-test procedures. In proof testing, the position and slope of region II have been shown to significantly affect subsequent strength distributions. The difference between proof testing and dynamic fatigue is that, in the latter, the failure stress is controlled more by the lower end of the crack velocity spectrum through which the flaw grows, whereas in the former it is only the higher end which controls. A detailed description of proof testing in this context will be given elsewhere.[21]

APPENDIX

In this Appendix a summary is given of the derivation of dynamic fatigue equations from the crack velocity function for flaws with residual contact stress. Reference is made to earlier papers for more detailed formulations.[6,11,14]

The analysis begins with the assumption that the crack velocity v relates to the stress intensity factor K via a power law,

$$v = v_0(K/K_c)^n \tag{A-1}$$

where n and v_0 are empirical exponent and coefficient, respectively, for a given material/environment system and K_c is the material toughness. For cracks of characteristic dimension c produced at a peak indentation load P and subjected to subsequent tensile stress σ_a, the stress intensity factor has the form

$$K = \chi P/c^{3/2} + \psi\sigma_a c^{1/2} \tag{A-2}$$

where χ and ψ are dimensionless constants; the first term in Eq. (A-2) represents the residual contact field and the second represents the applied field. In dynamic fatigue testing the stressing rate is held constant as a function of time t, i.e.

$$\sigma_a = \dot{\sigma}_a t \qquad (\dot{\sigma}_a = \text{constant}) \tag{A-3}$$

Combining the above three equations gives

$$dc/dt = v_0(\chi P/K_c c^{1/2} + \psi\dot{\sigma}_a c^{1/2} t/K_c)^n \tag{A-4}$$

which serves as a master differential equation. Solution of this equation involves computation of the time-to-failure, t_f, i.e. the time for the crack to grow from its original size to a critical instability configuration ($K = K_c$, $dK/dc > 0$), thereby defining the failure strength, $\sigma_f = \dot{\sigma}_a t_f$.

Solutions of *analytical* form are obtainable from Eq. (A-4) only for single-region crack velocity functions. For the case where P is used as a test variable, these solutions are of power-law form[11,14]

$$\sigma_f P^{1/3} = (\lambda_P' \dot{\sigma}_a P)^{1/(n'+1)} \tag{A-5}$$

with exponent and coefficient which relate to the crack velocity parameters in Eq. (A-1) via the "transformation equations"[14]

$$n = 4n'/3 - 2/3 \tag{A-6a}$$

$$v_0 = (2\pi n')^{1/2}(\sigma_m P^{1/3})^{n'}(c_m/P^{2/3})/\lambda_P' \tag{A-6b}$$

The quantities labeled with subscript m in Eq. (A-6b) refer to the conditions under *equilibrium* crack growth, i.e. with $K = K_c$, $dK/dc = 0$ in Eq. (A-2), whence

$$\sigma_m P^{1/3} = 3K_c^{4/3}/4^{4/3}\psi(\chi P)^{1/3} \tag{A-7a}$$

$$c_m/P^{2/3} = (4\chi P/K_c)^{2/3} \tag{A-7b}$$

These instability conditions are measurable as the strength and corresponding crack size in inert environments.[6,7] Thus from Eq. (A-5) we see that a plot of $\log(\sigma_f P^{1/3})$ vs $\log(\dot{\sigma}_a P)$ should be universally linear for all contact loads.

For multiregion crack velocity functions no such analytical solutions are available. It is then necessary to integrate Eq. (A-4) *numerically* over the crack velocity range.[6]

Acknowledgments: The authors thank E. R. Fuller and S. M. Wiederhorn for discussions and T. P. Dabbs and A. C. Gonzalez for collecting some of the data.

References

[1] S. M. Wiederhorn; pp. 613–46 in Fracture Mechanics of Ceramics, Vol. 2. Edited by R. C. Bradt, D. P. H. Hasselman, and F. F. Lange. Plenum, New York, 1974.
[2] S. M. Wiederhorn and J. E. Ritter; pp. 202–14 in Fracture Mechanics Applied to Brittle Materials. Edited by S. W. Freiman. *ASTM Spec. Tech. Publ.*, No. 678, 1979.
[3] S. M. Wiederhorn, "Influence of Water Vapor on Crack Propagation in Soda-Lime Glass," *J. Am. Ceram. Soc.*, **50** [8] 407–14 (1967).
[4] S. M. Wiederhorn, S. W. Freiman, E. R. Fuller, Jr., and C. J. Simmons, "Effects of Water and Other Dielectrics on Crack Growth," *J. Mater. Sci.*, **17** [12] 3460–78 (1982).
[5] H. C. Chandan, R. C. Bradt, and G. E. Rindone, "Dynamic Fatigue of Float Glass," *J. Am. Ceram. Soc.*, **61** [5–6] 207–10 (1978).
[6] B. R. Lawn, D. B. Marshall, G. R. Anstis, and T. P. Dabbs, "Fatigue Analysis of Brittle Materials Using Indentation Flaws: I," *J. Mater. Sci.*, **16** [10] 2846–54 (1981).
[7] R. F. Cook, B. R. Lawn, and G. R. Anstis, "Fatigue Analysis of Brittle Materials Using Indentation Flaws: II," *J. Mater. Sci.*, **17** [4] 1108–16 (1982).
[8] D. B. Marshall and B. R. Lawn, "Flaw Characteristics in Dynamic Fatigue: The Influence of Residual Contact Stresses," *J. Am. Ceram. Soc.*, **63** [9–10] 532–36 (1980).
[9] P. Chantikul, B. R. Lawn, and D. B. Marshall, "Micromechanics of Flaw Growth in Static Fatigue: Influence of Residual Contact Stresses," *J. Am. Ceram. Soc.*, **64** [6] 322–25 (1981).
[10] B. R. Lawn, A. G. Evans, and D. B. Marshall, "Elastic/Plastic Indentation Damage in Ceramics: The Median/Radial Crack System," *J. Am. Ceram. Soc.*, **63** [9–10] 574–81 (1980).
[11] T. P. Dabbs, B. R. Lawn, and P. L. Kelly, "A Dynamic Fatigue Study of Soda-Lime Silicate and Boroaillicate Glasses Using Small Scale Indentation Flaws," *Phys. Chem. Glasses*, **23** [2] 58–66 (1982).
[12] D. B. Marshall and B. R. Lawn, "Residual Stress Effects in Sharp Contact Cracking: I," *J. Mater. Sci.*, **14** [8] 2001–12 (1979).
[13] D. B. Marshall, B. R. Lawn, and P. Chantikul, "Residual Stress Effects in Sharp Contact Cracking: II," *J. Mater. Sci.*, **14** [9] 2225–35 (1979).
[14] E. R. Fuller, B. R. Lawn, and R. F. Cook, "Theory of Fatigue for Brittle Flaws Originating from Residual Stress Concentrations," *J. Am. Ceram. Soc.*, **66** [5] 314–21 (1983).
[15] F. Kerkhof; pp. 303–21 in Linear Fracture Mechanics. Edited by G. C. Sih, R. P. Wei, and F. Erdogan. Envo Publishing Co., Lehigh Valley, PA, 1974.
[16] H. Richter; pp. 447–57 in Proceedings of Eleventh International Congress on Glass, Vol. 2. Edited by J. Gotz. C. V. T. S., Prague, 1977.
[17] T. A. Michalske, V. D. Frechette, and R. Hudson; pp. 1091–97 in Advances in Fracture Research, Vol. 2. Edited by D. Francis. Pergamon, New York, 1981.
[18] S. W. Freiman, D. R. Mulville, and P. W. Mast, "Crack Propagation Studies in Brittle Materials," *J. Mater. Sci.*, **8** [11] 1527–33 (1973).
[19] S. W. Freiman, "Effect of Straight-Chain Alkanes on Crack Propagation in Glass," *J. Am. Ceram. Soc.*, **58** [7–8] 339–40 (1975).
[20] C. L. Quackenbush and V. D. Frechette, "Crack-Front Curvature and Glass Slow Fracture," *J. Am. Ceram. Soc.*, **61** [9–10] 402–406 (1978).
[21] S. M. Wiederhorn, S. W. Freiman, E. R. Fuller, Jr., and H. Richter, "Effect of Multiregion Crack Growth on Proof Testing"; unpublished work.

To be published in J. Geophys. Research, 1984.

EFFECTS OF CHEMICAL ENVIRONMENTS ON SLOW CRACK GROWTH IN GLASSES AND CERAMICS

S. W. Freiman
Inorganic Materials Division
National Bureau of Standards
Washington, DC 20234

ABSTRACT

This paper presents a review of our current understanding of environmentally induced slow crack growth in glasses, single crystals and polycrystalline ceramics. It is shown that the rate of crack growth is controlled by the chemical activity of the active species in the environment as well as by the stress intensity at the crack tip. A recently developed molecular model of stress induced chemical reaction between vitreous silica and water is described. The implications of this model for the effects of other chemical species on crack growth are discussed. Finally, the complications introduced by the presence of grain boundaries in polycrystalline ceramics are pointed out.

EFFECTS OF CHEMICAL ENVIRONMENTS ON SLOW CRACK GROWTH IN GLASSES AND CERAMICS

S. W. Freiman
Inorganic Materials Division
National Bureau of Standards
Washington, DC 20234

INTRODUCTION

The objective of this paper is to provide a current view of the mechanisms of environmentally influenced, subcritical, crack growth in both glasses and ceramics. This review will concentrate on various aspects of the stress aided chemical reaction which governs the crack process. Particular attention will be paid to recent models for stress assisted physical and chemical processes which appear to govern crack growth.

Before discussing crack growth in glasses and ceramics, it should be said that all of these materials will be considered to be ideally brittle, i.e. that there are no zones of plastic deformation at propagating crack tips. This assumption has been shown to be valid in MgO and aluminum oxide [Lawn et al., 1980]. Even for "softer" materials such as MgF_2, where dislocations are known to be generated around advancing crack tips, fracture is still governed by bond breaking mechanisms.

Most of the crack growth data reported herein was taken using double cantilever beam specimens in which a constant load or bending moment is applied to the specimen and crack extension measured optically as a function of time. Crack velocities from 10^{-10} to 10^{-2} m/sec can be obtained in this

way. The data are usually plotted as log V versus K_I*, where K_I is the stress intensity factor at the crack tip and is calculated from the load and specimen dimensions.

GENERAL CRACK GROWTH BEHAVIOR

V-K_I plots for glasses, single crystals and polycrystalline ceramics can be quite complex in shape (Figure 1). Each segment can, however, be described by a different rate controlling mechanism. Because they are isotropic and homogeneous, most of the work in determining these mechanisms has been performed on silicate glasses. These mechanisms can be synopsized as follows:

Region I.

Because slowly growing cracks spend most of their growth period in this regime, it is of primary importance. Slopes of curves range from n = 11 for some binary glasses to n > 100 for some polycrystalline ceramics. Wiederhorn [1967] showed that crack velocity is controlled by the rate of reaction of the active ingredient in the environment with the chemical bonds of the solid at the crack tip. This reaction may or may not involve the formation of corrosion products.

---

*For engineering purposes and ease of mathematical manipulation crack growth data is often expressed as $V = A K_I^n$ where A and n are constants which depend on material and environment. While this expression is easily integrated to calculate times to failure, its theoretical basis is much weaker than an expression of the form, $V = V_o \exp(bK_I)$. Because of its common usage, however, this paper will use n as a measure of the slope.

While reductions in surface energy due to the attachment of surface groups to SiO_2 can be considered as the driving force for the stress enhanced reaction at a crack tip, as suggested by Orowan [1944] and more recently by Parks [1983], the crack growth rate is determined by the kinetics of the chemical process.

Reaction rate theory can be used to derive a model for stress assisted crack propagation in glasses and ceramics. Such a derivation for the SiO_2-H_2O reaction (the specific molecular chemistry is described in the next section) is shown in summary as follows:*

A general expression for H_2O reacting with an Si-O bond is given by:

$$[\text{Si-O-Si}] + H_2O \rightleftharpoons \chi \longrightarrow 2\,[\text{SiOH}] \qquad (1)$$

where χ is the activated complex. As in most reaction rate theory [Laidler, 1965], the decomposition of the activated complex to the products is assumed to very rapid compared to the reverse reaction.

$$\text{Rate} = \kappa \frac{kT}{h} \exp\left(-\Delta G^{\neq}/RT\right) \frac{a(H_2O)}{f} \qquad (2)$$

where κ is the transmission coefficient (for most reactions assumed equal to 1, meaning every activated complex becomes a product); k is the Boltzman constant; T is temperature; h is Plancks constant; $\Delta G^{\neq}$ is the Gibbs free

*For a more detailed derivation see Wiederhorn et al. [1982].

energy of activation, and $a(H_2O)$ is the activity of the water and f is the activity coefficient for the activated complex.

Combining terms and assuming that the crack velocity is directly proportional to the reaction rate, we obtain:

$$V = V_o \, a(H_2O) \exp (-\Delta G^{*}/RT) \qquad (3)$$

There are at least two important aspects to equation (3). First, note that the reaction rate, and therefore the crack velocity, is proportional to the activity rather than the concentration of water in solution in the liquid or gas. If water vapor is assumed to behave as an ideal gas, then

$$a_i = \frac{P_i}{P_o} \qquad (4)$$

where P_o is the vapor pressure of pure water at the temperature of the experiment. In a gaseous environment, P_i is the vapor pressure of water and P_i/P_o is the relative humidity. For water dissolved in non-aqueous liquids, P_i is the equilibrium vapor pressure of water over the solution and P_i/P_o is the relative humidity of the gaseous atmosphere over the solution. Given these definitions and the relationship expressed in equation 3, it becomes clear why the data of Wiederhorn [1967] and Freiman [1974] obey a simple $V \simeq$ r.h. relationship (Figure 2). The fact that crack velocity is dependent on relative humidity rather than concentration has important implications for predictions of structural reliability. It means that liquids such as silicone oil and fluoronated hydrocarbons cannot be considered inert because their solubility for water is small. Second, this expression provides a fundamental

basis for plotting crack velocity data as lnV vs. K_I rather lnV vs. $\ln K_I$ as noted earlier.

The stress dependence of the reaction is contained in the $\Delta G^{\ddagger}$ term. It has been shown (Wiederhorn et al. 1980) that this term can be expanded as follows:

$$\Delta G^{\ddagger} = - T\Delta S^{\ddagger} + \Delta E^{\ddagger} - (\pi d)^{-1/2} K_I \Delta V^{\ddagger} - (\gamma V^{\ddagger} - \gamma V)/\rho \qquad (5)$$

where $\Delta S^{\ddagger}$, $\Delta E^{\ddagger}$ and $\Delta V^{\ddagger}$ are the activation entropy, activation energy and activation volume respectively; d is a dimensional parameter depending on the structure of the crack tip.* The last term is included following the approach of Charles and Hillig [1962] and accounts for changes in the surface energy of the crack tip during the reaction. The effect of stress on the crack tip reaction rate is included in the $(\pi d)^{1/2} K_I \Delta V^{\ddagger}$ term. d must have units of $(\text{dimension})^2$ so that $d^{-1/2} K_I$ has units of stress. The use of the activation volume in this context assumes that the tensile stress dependence of the reaction rate can be expressed as the negative of the pressure dependence. Equations 3 and 5 can be combined to yield

$$V = V_o \exp [(-E^{\ddagger} + b K_I)/RT] \qquad (6)$$

where all of the non-stress dependent terms are included in $E^{\ddagger}$.

---

*Wiederhorn et al. (1982) use the crack tip radius, ρ, but for values of ρ approximately that of the network spacing in the solid, this term probably has little meaning.

The previous derivation of the kinetics of crack growth was completely general. No details of the chemical reaction between the environment and the glass were discussed. One important question is why H_2O is such an effective crack growth agent for all silicate glasses, when the corrosion rate of a material such as vitreous SiO_2 is extremely low?

Michalske and Freiman [1983] have described a specific chemical mechanism by which strained Si-O bonds in vitreous silica react with molecules of a gas or liquid. This model for the H_2O-SiO_2 reaction is shown in Figure 3 as a three step process:

Step 1. An H_2O molecule orients itself with respect to an Si-O-Si bond at the crack tip such that the lone electron pair orbitals on the oxygen of the water molecule are aligned toward the silicon, and hydrogen bonding occurs between the O_{silica} and the hydrogen. The strain (as much as 20%) on the bridging Si-O bond clearly enhances the tendency to react at this site.

Step 2. Electron transfer from the O_{water} to the Si occurs simultaneous with proton transfer to the O_{silica}. Two new bonds are formed, $Si\text{-}O_{water}$ and $H\text{-}O_{silica}$.

Step 3. Rupture of the weak hydrogen bond between O_{water} and the transferred hydrogen occurs to yield Si-OH surface groups on each fracture surface.

Note that the model does not require prior dissociation of the water molecule, nor must reaction products be removed from the solid. Wiederhorn and Johnson [1973] observed definite effects of hydrogen ion activity on crack growth in silica and other glasses suggesting that OH^- and H^+ ions may show a different stress dependent reaction rate than H_2O. These effects need further study, however.

The above model suggests that other environments should also enhance crack growth in silica if the species has structural and bonding features similar to water, namely, proton donor sites on one part of the molecule, and lone pair orbitals on another. It is likely that there are size limitations as well since the Si-O bond distance is only 1.63 Å. It is interesting to note the similarity of this model to that of Griggs and Blacic [1965] for the hydrolytic weakening of quartz.

Figure 4 shows crack growth curves for amorphous silica in water, ammonia (NH_3), hydrazine (N_2H_4), formamide ($HCONH_2$) and N_2 gas. As will be discussed later, the plateau in the N_2 gas curve occurs when crack growth is controlled by the rate of diffusion to the crack tip of the small quantity of dissolved water. The absence of this plateau in the curves for ammonia, hydrazine and formamide leads to the conclusion that their reaction with the crack tip bonds governs crack growth rates in preference to the reaction of the water present in these environments. Based on the plateau in the crack growth curves obtained in environments such as carbon monoxide (CO), acetonitrile (CH_3CN) and nitrobenzene ($C_6H_5NO_2$), these did not control crack growth, as would be predicted by the above model, since each of these

molecules does not meet all of the required bonding specifications. Although each contains lone pair orbitals, none can donate protons. It should also be noted that no direct correlations were found to exist between dielectric constant or dipole moment alone and an environment's ability to cause crack growth in preference to water.

Recent crack growth data obtained on a commercial soda-lime-silica glass shows the same trends as that described for silica [Freiman and White, 1982]. There was no obvious participation of the Na^+ ions in the crack growth process. However, preliminary data suggest that when the Na content is increased significantly as in a binary 33% Na - 67% SiO_2 glass, variations in the crack growth mechanisms appear.

Regions IA and IB.

The mechanism of crack growth in the steeper IA regime in a number of glass seems to be similar to that in region I, but there is some evidence that there are accompanying changes in crack tip geometry. Work by Michalske [1982] has demonstrated the occurrence of crack blunting and a stress corrosion limit in soda-lime-silica glass in water, but except for some data in borosilicate glasses [Wiederhorn and Johnson, 1973, Simmons and Freiman, 1980], determination of a definite crack limit have not been extended to other glasses or ceramics. For instance, no evidence for a region of increased slope has been observed for vitreous SiO_2 at velocities as low as 10^{-11} m/sec.

A Region IB plateau in the velocity range of 10^{-10} to 10^{-8} m/sec has been observed only in binary alkali-silicate glasses tested in aqueous solutions [Simmons and Freiman, 1981]. The authors hypothesize that, because of the

great solubility of these glasses in water at lower K_I's, cracks grow at a rate approximating that of the SiO_2 dissolution rate. A very small stress is apparently sufficient to remove corrosion products at the crack tip and accelerate the dissolution process there, in preference to the sides of the crack. However, effects of stresses generated due to a H^+ for Na^+ exchange cannot be ruled out.

Region II.

This plateau appears when crack growth occurs in an environment in which the minor constituent in the liquid or gas controls the crack tip reaction. As the crack proceeds, the species in the environment which reacts with the chemical bonds at the crack tip, e.g. H_2O, is depleted in the vicinity of the tip, thereby creating a concentration gradient. As noted earlier, in Region I the rate is controlled by the reaction rate at the tip, but as the crack velocity increases, the size of the H_2O depleted zone, δ, grows. At some crack velocity the rate at which the active species can diffuse through this zone to the tip becomes slower than the reaction rate, and hence becomes the controlling step in determining rates of growth. Based on the use of the Stokes-Einstein expression for the diffusivity of a molecule in a liquid, it was shown that this velocity is given by: [Wiederhorn et al., 1982]

$$V_{plateau} = \frac{0.0275\ kT}{6\ \pi r\ \delta}\left(\frac{C_o}{\eta}\right) \qquad (7)$$

where k is the Boltzman constant, T is temperature, r is the size of the diffusing species, C_o is the bulk concentration of this diffusing species, and η is the viscosity of the solution. Experimental data for alcohol-water

solutions has verified the applicability of Equation (7) (Figure 5). Because diffusion can also take place in from the faces of a double cantilever beam specimen for instance, the Region II velocity is also crack front length dependent and can show a small stress intensity dependence, i.e. a slope = 2 to 6.

Region III.

Crack growth curves in Region III are quite steep, n > 100. Wiederhorn [1967] showed that crack growth rates in Region III for soda-lime glass are independent of water concentration. Freiman [1974], showed that while crack growth rates in Region III are not affected by water in the environment, in agreement with Wiederhorn, there are effects of the liquid in which the water was dissolved, e.g. the chain length of an alcohol. Similar data was subsequently reported by Richter [1977]. A model explaining Region III crack growth based on an electrostrictive interaction between the solid and the fluid at the crack tip has recently been proposed by Wiederhorn et al. [1982]. Their model is synopsized as follows:

If we assume that the slope of the V-K_I curve in Region III (or in Region I) is determined by the stress dependence of a reaction rate at the crack tip, then the activation volume, $\Delta V^{\neq}$, can be taken as a measure of the stress dependent process. From a physical point of view $\Delta V^{\neq}$ represents the difference in volume between the reactants and the activated complex. It is assumed that the formation of charges during the rupture of a strained Si-O bond at crack tip has a significant effect on $\Delta V^{\neq}$, suggesting that environments which can alter the magnitude of these charges will influence $\Delta V^{\neq}$ and therefore the slope of the V-K_I curve.

Wiederhorn et al. derived the following expression for $\Delta V^{\neq}$ in a solid-solvent system in which the electrostatic contributions are of primary importance:

$$\Delta V_{ES} = \frac{N_a e^2}{r} (3B)^{-1} (\varepsilon_1 + \varepsilon_2)^{-1} - (\varepsilon_1 + \varepsilon_2)^{-2} \frac{\delta \varepsilon_2}{\delta P} \qquad (8)$$

where N_a is Avogadro's number, e is the unit of charge, r is the atomic radius, (contributions due to Si and O are calculated separately) B is the bulk modulus of the solid and ε_1 and ε_2 are the dielectric constants of the liquid and solid respectively. One can see that the second term on the right contains the partial derivative of the solid dielectric constant with respect to presssure, i.e. the stress contribution. A plot of log (velocity) versus K_I, should have a slope proportional to ΔV. Figure 6 is a plot of ΔV_{ES} calculated from Equation (8) compared to the ΔV_{total} determined from the slope of the V-K_I curve.* The correlation between the calculated and measured values suggests the general validity of the above approach.

EFFECTS OF CHEMICAL BONDING AND MICROSTRUCTURE

Most ceramic materials are susceptible to crack growth in the presence of water. What is surprising is that these materials include such diverse chemical compositions as Al_2O_3, MgF_2, ZnSe, and graphite, as well as many others. Is the mechanism of subcritical crack growth the same as that

*A value of d of 0.5 nm was assumed for this calculation. While there is clearly uncertainty in this number, it should be correct within at least an order of magnitude.

described for SiO_2? What are the effects of changing the ratio of covalent to ionic bonding in the solid? What are the effects of strain on the bond character? Complete answers to these questions are not known at present. However, recent data obtained on Al_2O_3 (sapphire) [Michalske et al., 1982] suggests that this material behaves identically to amorphous SiO_2 in that the same environments that governed crack growth in the latter also control in Al_2O_3 and to the same relative degree. In the more ionically bonded MgF_2, however, the above authors found that ammonia no longer controls crack growth in Region I, while acetonitrile (CH_3CN) is an effective crack growth environment even though it has no proton donating capability. This behavior suggests that individual atom solvation may play a part in the fracture of ionic solids. There may be a pure electrostatic bonding of the solvent molecules to the Mg and F atoms. The seeming lack of any measurable subcritical crack growth in silicon, a completly covalent solid, indicates the needs for some degree of charge separation during stressing.

Very little detailed crack growth data exists for polycrystalline ceramics. There are several general observations that can be made, however. First, it is apparent that grain boundary structure and chemistry becomes a significant factor in determing crack growth rates. One can show, for instance, that MgO, which does not appear to be subject to subcritical crack growth in single crystal form, does undergo delayed failure when prepared in polycrystalline form [Freiman, 1976]. Fracture occurs almost exclusively along grain boundaries. Other polycrystalline ceramics in which subcritical crack growth is observed also exhibit primarily intergranular failure over the regime in which the crack is growing slowly, even in cases where these is no obvious grain boundary phase [Mecholsky and Freiman, 1981]. A transition from

an intergranular to a transgranular failure mode is frequently observed at the critical flaw boundary in these materials. Whether this kind of behavior is due to chemical effects or to changes in the ability of the crack front to change directions at different velocities is not known. In addition, there are effects of grain size on the slope of the V-K_I curve which are not understood.

SUMMARY

An overall picture of the complex relationship between crack velocity and stress intensity factor has been presented. It has been shown that chemical reaction kinetics can be used to explain the dependence of crack growth rates on the activity of a given environment. Mechanisms of subcritical crack growth in glasses and ceramics have been described in terms of models for the stress induced reactions of environments with crack tip bonds. It has been shown that the tendency of a given substance to participate in such a reaction can be predicted from knowledge of the molecular chemistry of the environment and the bonding in the solid. While only limited crack growth data exist for polycrystalline ceramics, it is clear that processes in these materials are dominated by grain boundary chemistry and structure.

In closing, it is perhaps worthwhile to point out that no mention was made in this paper of the possible effects of zeta potential on crack growth even though other authors in this conference discuss it rather extensively, i.e. Westwood [1983], Dunning [1983]. It is our observation that no clear correlation has been made between zeta or surface potential and the rates of subcritical crack growth. There is serious question whether zeta potentials

measured on bulk solids or powders will be similar in any way to those within the small confines of a crack tip. In addition, these measurements suggest what has happened to a surface after reaction with an environment, while we are interested in the kinetics of the interaction process.

ACKNOWLEDGEMENTS

I thank S.M. Wiederhorn and G.S. White for their time and effort in their numerous discussions with me on this subject.

REFERENCES

Charles, R.J. and Hillig, W.B., Symposium on Mechanical Strength of Glass and Ways of Improving It, p. 511, Union Scientifique Continentale du Verre, Charleroi, Belgium, 1962.

Dunning, J.M., Effects of Aqueous Chemical Environments on Crack Propagation in Quartz, this volume.

Freiman, S.W., Effect of Alcohols on Crack Propagation in Glass, J. Am. Ceram. Soc. 57, 350-353, 1974.

Freiman, S.W., Effect of Environment on Fracture of Ceramics, Ceramurgia, 2, 111-118, 1976.

Freiman, S.W. and White, G.S., Effects of Chemical Environments on Crack Growth in Soda-Lime Glass, Bull. Am. Ceram. Soc. 61, 414, 1982.

Griggs, D.T. and Blacic, J.O., Quartz: Anomalous Weakness of Synthetic Crystals, Science, 147, 292-295, 1965.

Laidler, K.J., Chemical Kinetics, McGraw Hill, New York, 1965.

Lawn, B.R., Hockey, B.J., and S.M. Wiederhorn, Atomically Sharp Cracks in Brittle Solids. An Electron Microscopy Study, J. Mat. Sci. 15, 1207, 1980.

Mecholsky, J.J. and Freiman, S.W., Fractographic Analysis of Delayed Failure in Ceramics, ASTM STP 733, Fractography and Materials Science, 246-258, 1981.

Michalske, T. A., Crack Arrest in Glass: The Blunt Truth, to be published in Fracture Mechanics of Ceramics, V-VI, 1982.

Michalske, T.A. and Freiman, S.W., A Molecular Interpretation of Stress Corrosion in Silica, Nature, 295, 511-12, 1982.

Michalske, T.A., Freiman, S.W., and Bunker, B., A Chemical Approach to Predicting Stress Corrosion Behavior of Brittle Materials, Bull. Am. Ceram. Soc., 61, 414, 1982.

Orowan, E., The Fatigue of Glass under Stress, Nature, 154, 341-343, 1944.

Parks, G.A., The Surface and Interfacial Free Energies of Quartz, this volume.

Richter, H., The Effect of Different Liquids on the Transition from Slow to Fast Crack Propagation in Soda-Lime Glass, Physics of Non-Crystalline Solids, Ed. by G.H. Frischat, Trans. Tech. Pub., Aedermannsdorf, Switzerland, 1977.

Simmons, C.J. and Freiman, S.W., Effects of Phase Separation on Crack Growth in Borosilicate Glass, J. Non. Cryst. Solids, 38-39, 503-508, 1980.

Simmons, C.J. and Freiman, S.W., Effect of Corrosion Processes on Subcritical Crack Growth in Glass, J. Am. Ceram. Soc. 64, 683-686, 1981.

Westwood, A.M., Aquamechanical Effects in Non-metals, this volume.

Wiederhorn, S.M., Influence of Water Vapor on Crack Propagation in Soda-Lime Glass, J. Am. Ceram. Soc. 50, 407-414, 1967.

Wiederhorn, S.M., and Johnson, H., Effect of Electrolyte pH on Crack Propagation in Glass, J. Am. Ceram. Soc. 56, 192-197, 1973.

Wiederhorn, S.M., Fuller, E.R. Jr., and Thomson, R., Micromechanisms of Crack Growth in Ceramics and Glasses in Corrosive Environments, Metal Science, 14, 450-458, 1980.

Wiederhorn, S.M., Freiman, S.W., Fuller, E.R. Jr., and Simmons, C.J., Effects of Water and Other Dielectrics on Crack Growth, accepted for publication in Journal of Materials Science.

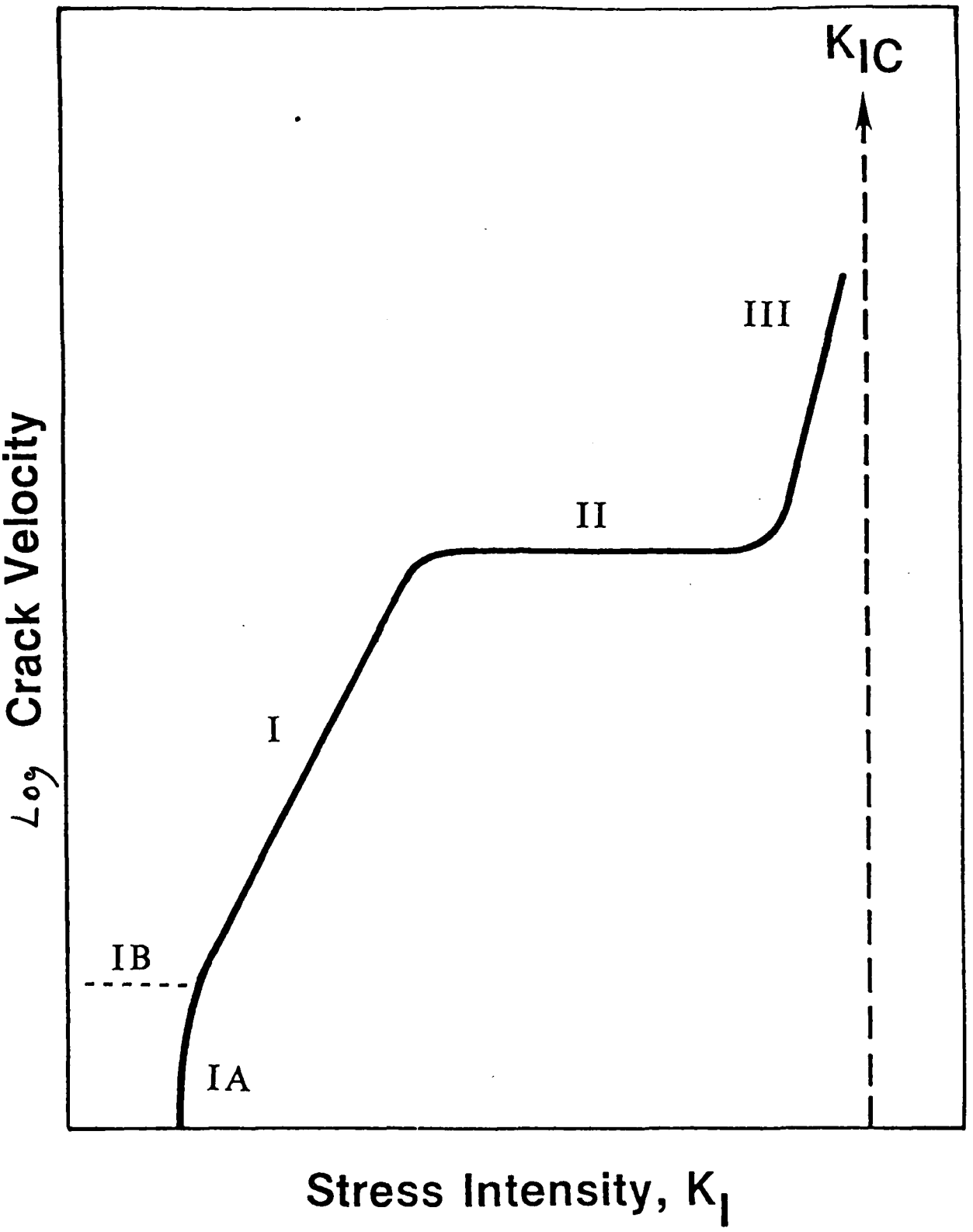

Figure 1. Schematic of the different regions of a typical crack growth curve for glasses and ceramics tested in air for instance.

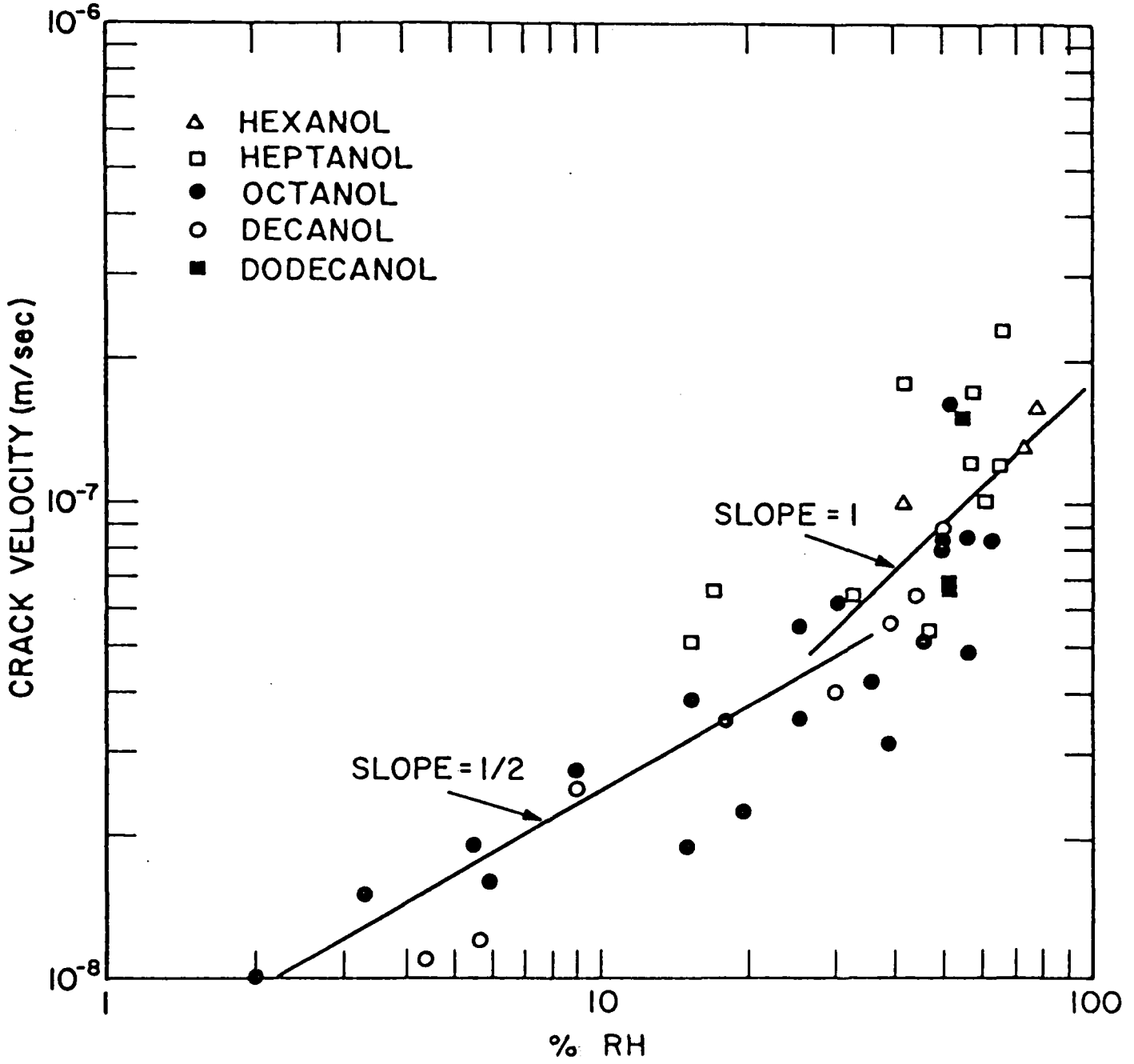

Figure 2. Crack velocity in soda-lime silica glass at a K_I - 0.45 $MPaM^{1/2}$ as a function of the relative humidity i.e. activity of water, in various straight chain alcohols. (After Freiman [1974]).

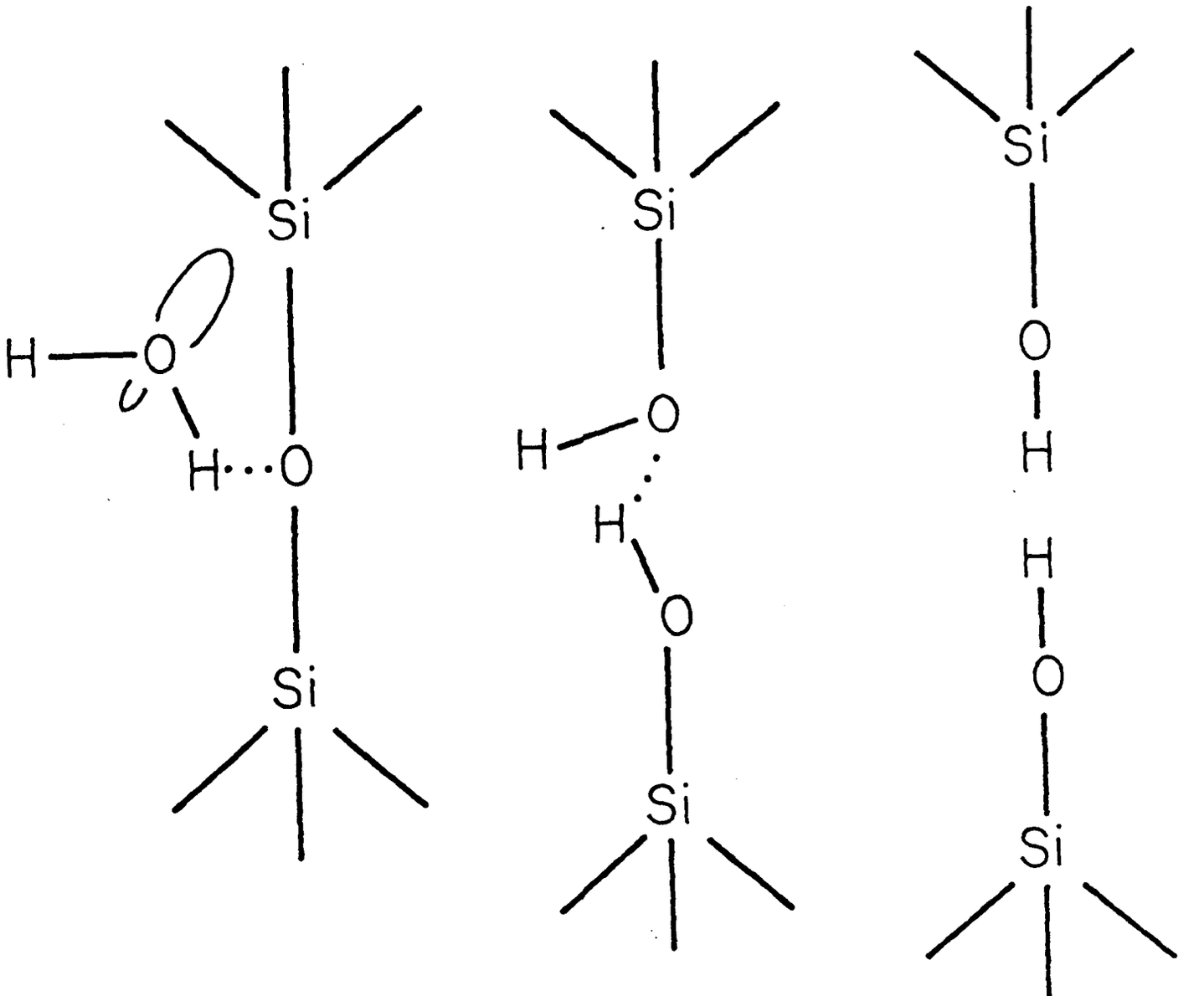

Figure 3. Model for the stress induced chemical reaction of H_2O with amorphous silica. (After Michalske and Freiman [1982]).

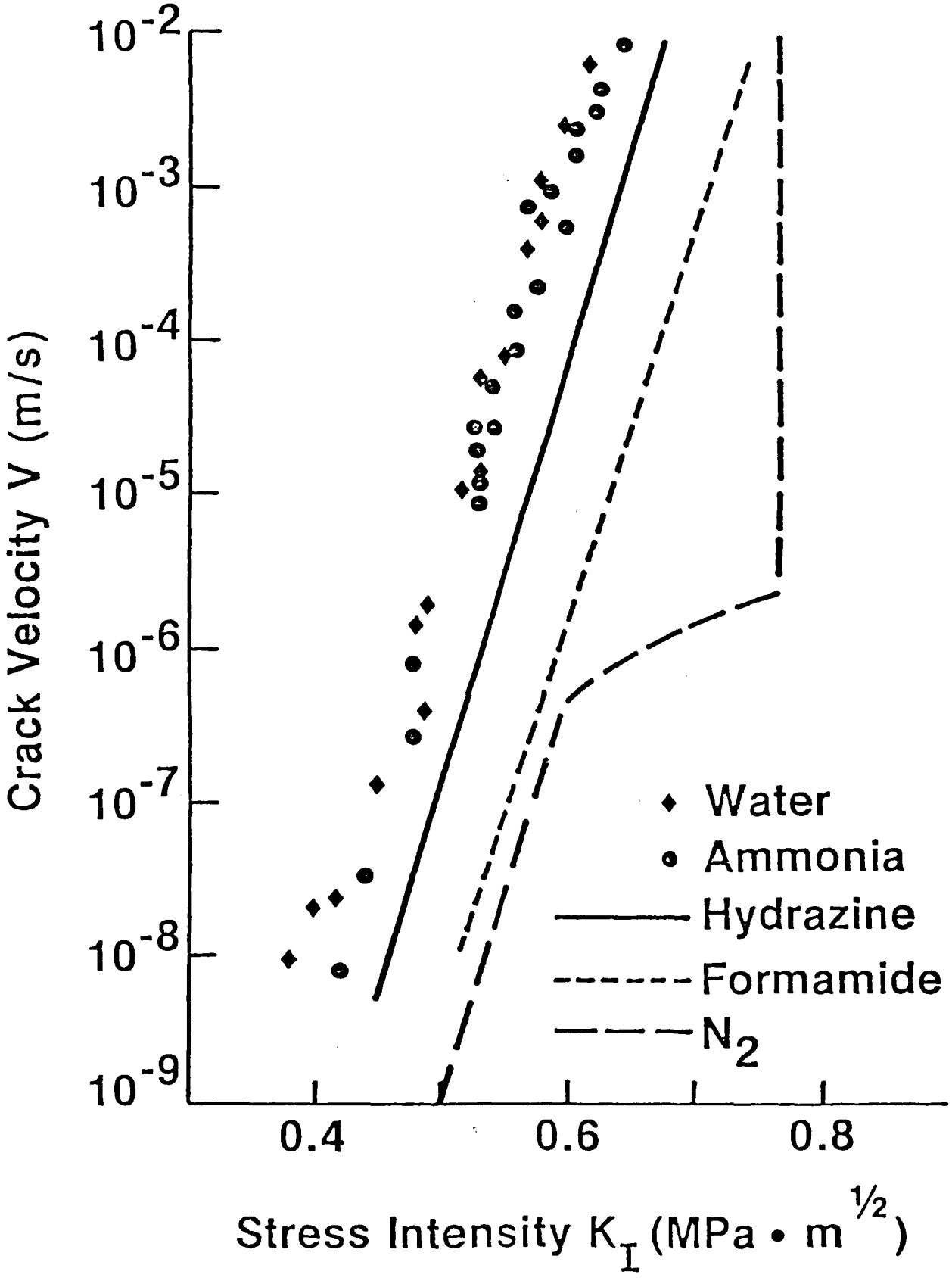

Figure 4. Crack growth curves for amorphous silica tested in environments whose molecular structure should be favorable to cause stress induced reactions. (After Michalske and Freiman [1982]).

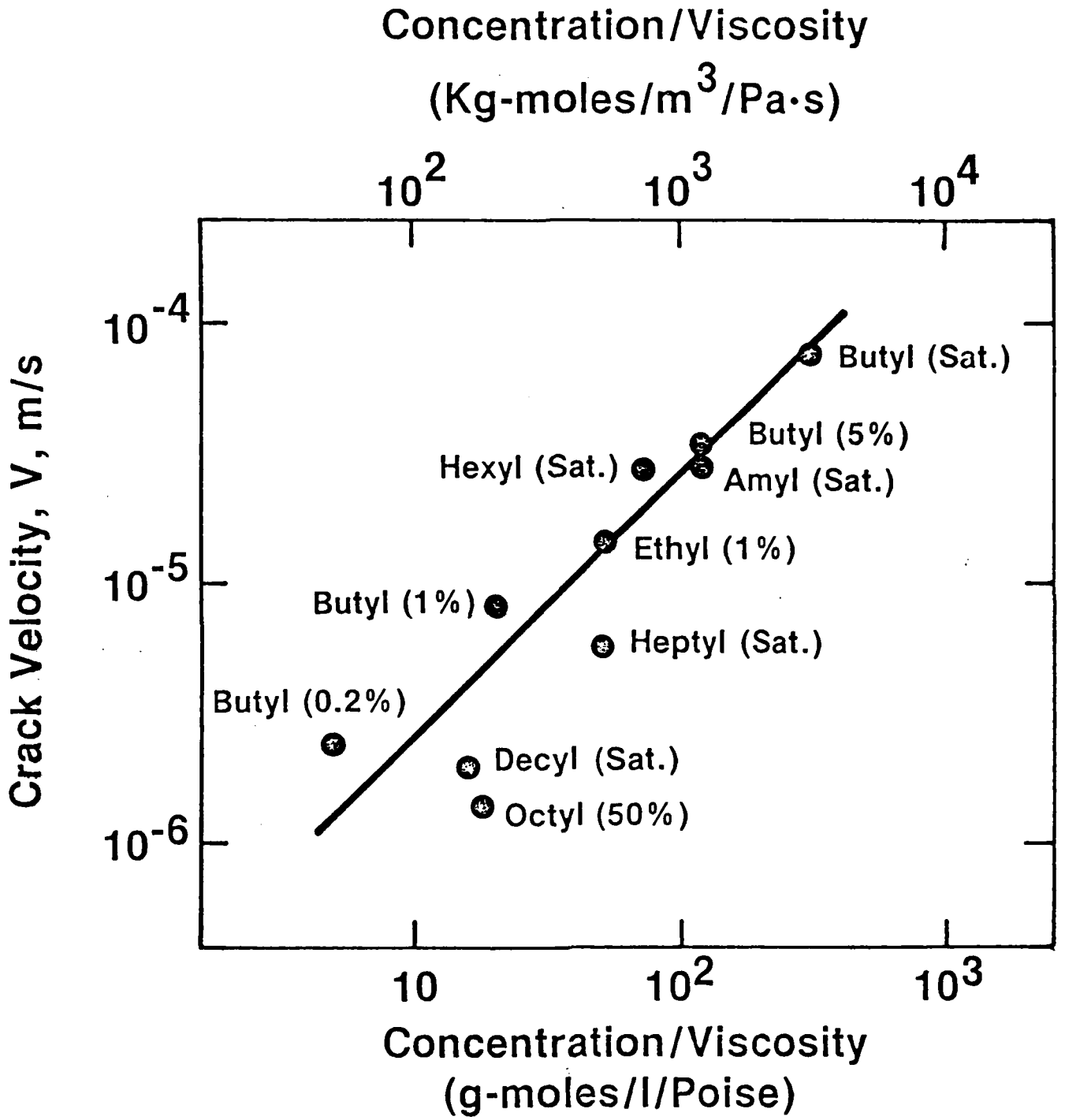

Figure 5. Crack velocity in Region 2 as a function of (concentration/viscosity), as suggested by Equation 1. Data is for soda-lime silica glass tested in straight chain alcohols containing various amounts of water. (After Wiederhorn et al. [1982]).

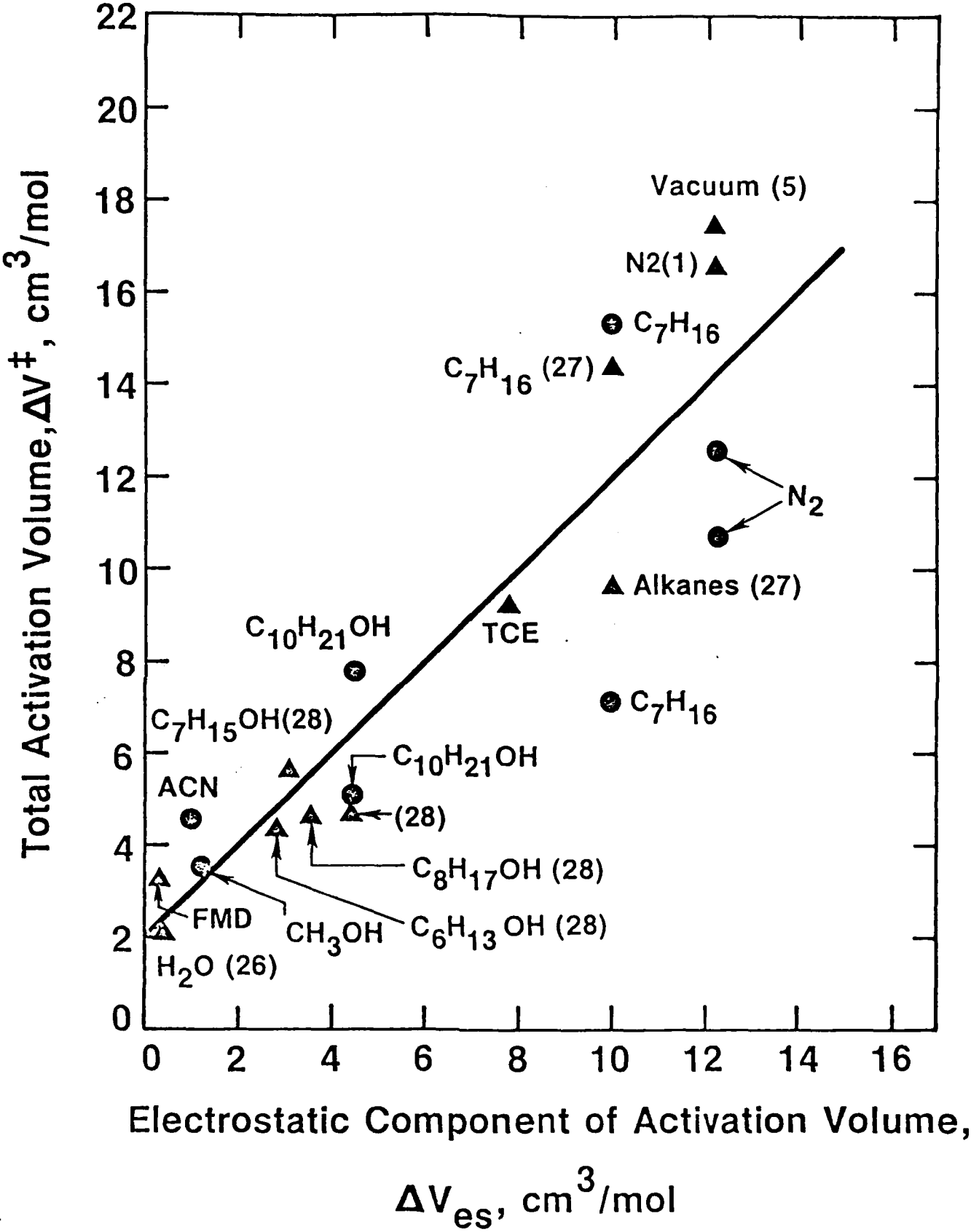

Figure 6. Activation volume, ΔV_{total}, determined from the slope of the V-K_I curve for soda-lime silica glass tested in environments whose dielectric constant varies from 1 (vacuum) to 78 (H_2O plotted against the ΔV_{es} calculated from Equation 8. (After Wiederhorn et al. [1982]).

J. Materials Science, 17, 3460-3478 (1982)

Effects of Water and other Dielectrics on Crack Growth

S. M. Wiederhorn, S. W. Freiman, E. R. Fuller, Jr.
and C. J. Simmons
National Bureau of Standards
Washington, D.C. 20234

ABSTRACT

The effect of water and a variety of organic liquids on the crack growth rate in soda lime silica glass was investigated. When water is present in organic liquids, it is usually the principal agent that promotes subcritical crack growth in glass. In region I, subcritical crack growth is controlled primarily by the chemical potential of the water in the liquid; whereas in region II, crack growth is controlled by the concentration of water and the viscosity of the solution formed by the water and the organic liquid. In region III, where water does not affect crack growth, the slope of the crack growth curves can be correlated with the dielectric constant of the liquid. It is suggested that these latter results can be explained by electrostatic interactions between the environment and charges that form during the rupture of Si-O bonds.

Effects of Water and other Dielectric Fluids on Crack Growth

S. M. Wiederhorn, S. W. Freiman, E. R. Fuller, Jr.

and C. J. Simmons

National Bureau of Standards

Washington, D.C. 20234

1. Introduction:

Subcritical crack growth in glasses is believed to result primarily from a stress-enhanced chemical reaction between a chemical environment, usually water, and the Si-O bonds of the glass. The reaction occurs preferentially at crack tips where stresses are high. Prior investigations of subcritical crack growth in glass have indicated a rather complex dependence of crack velocity on the applied stress intensity factor and on the amount of water in the environment. If crack velocity is plotted as either an exponential, or power function of applied stress intensity factor, a trimodal curve is obtained, Figure 1; each of the three regions of the curve results from a different mechanism of crack growth.[1,2]

Region I crack growth behavior is characterized by a dependence of crack velocity on stress intensity factor, K_I, and on the partial pressure of water in the environment.[1] If either of these two quantities are increased, the crack velocity is observed to increase. Crack growth studies conducted in either nitrogen gas[1] or in alcohols[3,4] suggest that

the crack velocity is reaction rate limited in region I, and therefore, is controlled by the chemical potential of water in the environment at any level of applied stress intensity. Hence, identical crack growth behavior should be obtained in environments in which the chemical potential of water is the same.

Region II crack growth behavior is also characterized by a dependence of crack velocity on the amount of water in the environment. In contrast to region I behavior, however, the crack velocity in region II does not depend strongly on the applied stress intensity factor. Theoretical interpretations of region II crack growth behavior lead to the conclusion that the crack velocity is controlled by the rate of transport of water from the environment to the crack tip.[1,2,5] Although it is recognized that crack growth in region II is limited by factors that affect transport processes, experimental data to quantify this relation have not yet been obtained.

Region III crack growth behavior is characterized by a strong dependence of crack growth rate on stress intensity factor, and by a complete absence of any dependence of crack growth rate on water in the environment. Of the three regions of crack growth, region III behavior is the least understood. Region III crack growth has been observed in vacuum for a variety of commercial silicate glasses, but not for glasses that have a high concentration (>90 percent) of silica.[6] Because of these observations it has been suggested that region III crack growth is controlled by fracture mechanisms that do not depend on environment.

Studies of region III crack growth in normal alcohols, however, conflict with this view.[3,4] In normal alcohols, it has been shown by Freiman[3] that the slope of the crack growth curves is not as steep as that obtained in vacuum, or in dry nitrogen. Furthermore Freiman[3] and Richter[4] have demonstrated that the positions of the crack growth curves depend on the chain length of the alcohol. Hence, in some cases an environmental dependence of region III crack growth is apparent.

This paper provides additional experimental data to clarify our understanding of subcritical crack growth in glass. Crack growth data obtained in alcohols confirm the proposed role of chemical potential in controlling the crack growth rate in region I. In region II, however, water concentration, rather than chemical potential, will be shown to control the rate of crack growth. A model for diffusion controlled crack growth is developed to show that fluid viscosity is also a parameter of importance. Finally, data is presented to confirm the fact that crack growth behavior in region III is affected by the chemical composition of the test media. Crack growth in region III is influenced by an electrostatic interaction between the environment and charges that develop at the crack tip during the fracture process.

2. Experimental Procedure

Crack propagation studies were conducted on soda lime silica glass in normal alcohols, heptane, formamide, trichloroethylene and acetonitrile. The alcohols were selected as test media because the

solubility of water in alcohols decreases with increasing alcohol chain length, so that it is possible to produce solutions of water and alcohol that have equal chemical potentials even though they contain different concentrations of water. These solutions were used to elucidate the effect of water concentration on region II crack growth behavior. Where possible, the partial pressure of water in the solutions was determined by direct analysis with an immersible hygrometer. The amount of water in solution, (i.e. the concentration) was determined by the Karl-Fisher technique. This procedure permitted us to make independent comparisons of effects of chemical composition and chemical potential on crack growth in region II. A set of ethyl and butyl alcohol solutions, used primarily for the study of region I crack growth, was made by adding predetermined amounts of water to the "pure" alcohols. The chemical potential of these solutions were then determined by reference to phase equilibrium diagrams for these solutions.[7,8] The viscosities of solutions used for region II crack growth studies were determined by direct analysis using a Cannon-Fenske viscosimeter (Table 1).

Crack growth studies in region I, II and III were conducted on soda-lime-silica glass microscope slides using both the double cantilever beam technique and the double torsion technique.[9,10] Region I studies were conducted using double cantilever beam specimens, 7 x 25 x 2 mm, with a 0.5 mm deep groove along the midplane on both sides of the specimen to control the direction of crack growth. Double torsion specimens, (ungrooved) 75 x 25 x 1 mm, were used for crack growth measurements in regions I, II and III. In regions I and II the load relaxation method

was used to collect crack growth data, whereas in region III, both load relaxation and constant displacement techniques were used.

Studies in region II were made in saturated alcohols prepared by mixing excess water with the alcohols and agitating the liquids several times a week for six months. A chemical analysis of the water in solution and a measurement of the partial pressure of the water in the alcohol are presented in Table 1. With the exception of the octyl alcohol, all of the alcohols were found to be saturated with water. We were somewhat surprised by the observation that the octyl alcohol used in our study was not fully saturated, and have no explanation for this result. However, crack growth studies (region II) to be discussed below are consistent with this observation.

The double torsion technique was also used to investigate crack growth behavior in region III. To determine if the position of the crack velocity curve in alcohol differed significantly from that in dry nitrogen, crack propagation data were obtained by the relaxation method on the same specimen, first in dry nitrogen, then in alcohol. Three crack velocity curves were first obtained in nitrogen gas. Without disturbing the specimen, either methyl, amyl, or decyl alcohol were added to the test chamber and three more crack velocity curves were obtained. This procedure enabled us to reduce systematic variations and thus obtain crack propagation curves that accurately reflect the positions of the crack growth curves in alcohol, relative to those in dry nitrogen gas.

In a second study of region III crack growth, the constant displacement rate technique was used to obtain crack growth data in dry nitrogen gas, methyl alcohol, decyl alcohol, acetonitrile and heptane. At least 10 experimental runs were made at each displacement rate in order to reduce systematic error that resulted in variations in measured K_I. The mean value and standard deviation of K_I were obtained for each displacement rate measurement, and at least three displacement rates were used to determine the position and slope of each crack velocity curve. Displacement rates used in these studies were selected so that the velocities were in region III. The velocities had to be low enough, however, to assure that cavitation of the fluid at the crack tip did not occur.[11] Some experimental results in region III were also obtained on vitreous silica (C7940) in octyl alcohol using the applied moment, double cantilever beam technique.[12] Since silica glass normally does not exhibit subcritical crack growth in region III,[6] the demonstration of subcritical crack growth in octyl alcohol is a clear indication of an interaction between glass and alcohol.

3. Results

The crack propagation data for soda-lime-silica glass in ethyl and butyl alcohols are shown in Figures 2,3. The shapes and positions of these curves are similar to those obtained earlier on this glass tested in nitrogen gas[1] and in other alcohols[3,4]. In regions I and II, crack velocity is observed to decrease as the amount of water in the alcohols is decreased. In region III, the data for the butyl alcohol appears to

approach a common curve, as it does for nitrogen gas[1]. Hence the mechanisms for fracture of soda lime silica glass in ethyl and butyl alcohols are probably identical to those observed in nitrogen gas and in long chain alcohols studied earlier by Freiman[3] and Richter[4].

The crack growth data from region I of the present paper (Figures 2 and 3) can be compared with earlier data collected in nitrogen gas[1] by plotting the logarithm of the crack velocity as a function of the logarithm of the relative humidity of the water in the alcohol. To do this, crack velocities were taken from Figures 2 and 3 for an applied stress intensity factor of 0.563 MPa-$m^{\frac{1}{2}}$, which is the same value of K_I used in the earlier study.* The relative humidities were determined from the concentrations of water in the alcohols, using experimental phase diagrams[7,8]. The resultant plot, Figure 4, indicates a relationship between crack velocity and relative humidity that is roughly linear over the range of relative humidities studied. Furthermore, the alcohol data are found to lie relatively close to the earlier data collected in nitrogen gas. Since the scatter of crack growth curves obtained by the double cantilever beam technique can be as much as a factor of ~2 along the velocity axis, the difference between the three sets of data can be attributed to experimental scatter. A comparison of the

---

* This procedure necessitated a linear extrapolation of the region I v-K_I data for the butyl alcohol (Figure 3) slightly beyond the range of the data in region I.

ethyl and butyl alcohol data with crack growth data collected by Freiman[3] on long chain alcohols was also made; agreement between the two sets of data was similar to that shown in Figure 4. These results confirm earlier conclusion that crack growth in region I is controlled by the relative humidity (i.e. partial pressure) of the environment in contact with the crack tip.[1,3] As will be discussed in section 4.1, such behavior is consistent with reaction rate theory, in which the effect of environment on the crack growth rate depends on the chemical potential or activity of the water in the alcohol.

In contrast to the results presented above, crack growth in region II does not appear to be controlled directly by the relative humidity of the water in the alcohol. This conclusion is supported by plotting the region II crack growth data presented in Figures 2 and 3 as a function of relative humidity of water in the alcohol. Data plotted in this manner are compared in Figure 5 with similar data obtained by Freiman from studies of crack growth in octyl alcohol[3]. To assure ourselves that the two sets of data were consistent, new crack growth data were collected in nominally saturated octyl alcohol. The crack velocity in region II for the octyl alcohol was found to be in line with the earlier data by Freiman. A comparison of the data collected in ethyl alcohol and butyl alcohol with the data collected in octyl alcohol shows that the ethyl and butyl alcohol data lie far from the curve obtained for the octyl alcohol. Since the separation of the data is much greater than can be explained by experimental scatter, we conclude that factors other than the relative humidity of water control crack growth in region II.

The conclusion stated above is supported by the double torsion studies (relaxation method) conducted in saturated alcohols, Figure 6. With the exception of the octyl alcohol, which was not fully saturated, the crack velocity in region II is observed to decrease as the chain length of the alcohol is increased. This decrease in velocity correlates directly with the concentration of water in these alcohols, and inversely with the viscosity of the alcohols. Since the alcohols used to obtain Figure 6 were fully saturated (with the exception of the octyl alcohol), they had the same relative humidity of water as the water with which they were in contact. The change of crack velocity of approximately 1.5 orders of magnitude in region II, therefore, cannot be explained by a variation in the relative humidity of the water in the alcohol solutions. A model will be presented in Section 4.3 of this paper, which explains region II crack growth behavior in terms of water concentrations and viscosity of the water-alcohol solution.

The data obtained in region III by the double torsion technique (relaxation method) is presented in Figure 7, for methyl, amyl and decyl alcohol. In agreement with other studies[3,4], our data shows a small, but systematic shift of the crack propagation curve to higher values of K_I as the length of the alcohol chain is increased. Furthermore, regardless of alcohol chain length, the curves obtained in alcohol had slopes that were less than those obtained in dry nitrogen gas.

The most surprising aspect of the data shown in Figure 7 has to do with the position of the crack growth curve obtained in decyl alcohol.

Three separate runs using this alcohol resulted in data that were similar to that shown in Figure 7. In all cases, the crack growth curve in decyl alcohol crossed the curve obtained in nitrogen gas, suggesting that at higher crack growth rates, decyl alcohol was retarding the crack growth. This finding, and the observation of a systematic shift and a lower slope of the crack growth data in the alcohols suggests that the alcohols are involved in some intimate way with the fracture process in region III. To further check the possibility of an intimate interaction between organic fluids and the silica network of the glass, experimental data were collected on silica glass in octyl alcohol. The results of this study are shown in Figure 8. If silica were tested in nitrogen gas, it would not have been possible to obtain crack growth data in region III since fracture occurs abruptly in vitreous silica once the crack has passed from region II.[6] The fact that region III crack growth was obtained in octyl alcohol supports our contention of a direct effect of the alcohol on the fracture process of glass.

To substantiate the data shown in Figure 7, data were obtained using the double torsion technique, constant displacement rate method. The data obtained in this way (Figure 9) support the data shown in Figure 7; the slope of the curve obtained in dry nitrogen, or in decyl alcohol is greater than that obtained in methyl alcohol. Furthermore, the data for decyl alcohol and nitrogen gas fall in a significantly higher range of K_I than the data for methyl alcohol. It is interesting to note that the data for decyl alcohol also falls in a higher range of K_I than that for nitrogen gas, a finding that is consistent with the

data in Figure 7. However, because of the experimental scatter in both the nitrogen gas and decyl alcohol curves this difference in location cannot be construed as being significant from this figure alone. Finally, data obtained in acetonitrile also had a slope that was significantly lower than that obtained in nitrogen gas, whereas the slope of the curve obtained in heptane was similar to that of nitrogen gas.

4.0 Discussion of Results

4.1 Reaction Rate Theory

The results presented in this paper can be understood in terms of chemical reaction rate theory, which has been used recently by Wiederhorn, Fuller and Thomson[13] to derive a model for crack growth in ceramics and glasses. To ease our discussion of the present set of data, a brief review of the model is presented in this section, giving the underlying theory and the equations that are pertinent to the results. In Section 4.4, the model is extended to account for electrostatic interactions that are believed to occur between the environment and charges that form during rupture of Si-O bonds at the crack tip.

Consider a chemical reaction of the general type:

$$a\,A + b\,B + \ldots \rightarrow X^{\ddagger} \rightarrow l\,L + m\,M + \ldots \qquad (1)$$

If the reverse reaction is negligible, the rate of reaction is given by:

$$\text{Rate} = k_r [A]^a [B]^b \ldots \quad (2)$$

where [A], [B], . . . are the concentrations of the reactants. The order of the reaction with regard to each component is given by the exponents in equation 2 (i.e. the order with regard to A is a), and the overall order of the reaction is given by the sum $a + b + \ldots$. The reaction rate constant, k_r, can be determined by transition rate theory and is given by the following relation:[14,15]

$$k_r = \kappa \, (kT/h) \exp(-\Delta G_o^{\ddagger}/RT) \, (f_A^a \, f_B^b \ldots / f^{\ddagger}) \quad (3)$$

where κ is the transmission coefficient and is usually assumed equal to 1; $\Delta G_o^{\ddagger}$ is the Gibbs free energy of activation; and f_A, f_B, . . . , $f^{\ddagger}$ are the activity coefficients for the reactants and for the activated state. The Gibbs free energy of activation is the standard Gibbs free energy change associated with the activation process, and can be related to the standard chemical potentials of the reactants and the activated complex.[14,15,16]

$$\Delta G_o^{\ddagger} = \mu_o^{\ddagger} - \mu_{Ao}^a - \mu_{Bo}^b - \ldots \quad (4)$$

By combining equations 2 and 3, and by using the definition of chemical activity ($a_A = [A] f_A$), the rate of chemical reaction can be

expressed in terms of the chemical activity of the reactants:

$$\text{Rate} = (\kappa/f^{\ddagger})\ (kT/h)\ a_A^a\ a_B^b\ \ldots\ \exp\ (-\Delta G_o^{\ddagger}/RT) \qquad (5)$$

where a_A, a_B, . . . are the chemical activities of reactants A, B, etc.

Equation 5 can also be expressed in terms of the chemical potential, μ_A, μ_B, . . . , of the reactants:

$$\text{Rate} = (\kappa/f^{\ddagger})\ (kT/h)\ \exp\ (a\mu_A + b\mu_B + \ldots - \mu_o^{\ddagger})/RT \qquad (6)$$

where the chemical potentials of the reactants, μ_A, μ_B, etc., are given by the following type of relation: $\mu_A = \mu_{Ao} + RT \ln a_A$. The free energy change in the exponent of equation 6 includes effects of chemical composition on reaction rate. By contrast, compositional effects on reaction rate are included in the activities of equation 5.

For purposes of this paper, the crack growth rate is assumed to be proportional to the rate of chemical reaction of the crack tip, and the reaction is assumed to be first order with respect to the water in solution.* For these conditions, equations 5 or 6 can be written as:

---

* The assumption of a first order reaction may not be valid for very low activities of water. In an earlier study[1], it was noted that the slight curvature of the data for nitrogen shown in Figure 4 suggested a change in the order of the chemical reaction from first order at high relative humidities to one-half order at low relative humidities. This observation was later substantiated for long chain alcohols by Freiman.[3] At the high humidities used in the present paper, the data for ethyl and butyl alcohols can be represented by a first order reaction of the water in solution with the glass.

$$v = v_o\, a_s \exp\,(\mu_{so} + \mu_g - \mu_o^{\ddagger})/RT \qquad (7)$$

where a_s is the activity of the water in solution, and where μ_{so}, μ_g and $\mu_o^{\ddagger}$ refer respectively to the water in solution, the reactive species in the glass (presumably Si-O bonds) and the activated complex. The standard state for the water is taken as pure water in the liquid state at 1 atmosphere pressure and a temperature of 25° C, a convention that follows the practice used in references 7 and 8. The frequency factor, kT/h, the transmission coefficient, κ, the activity coefficient, $f^{\ddagger}$, and geometric factors relating the number of bonds broken to the crack velocity are all incorporated into v_o of equation 7. It is worth noting that the dependence of crack velocity on the amount of water in the environment is all contained in the activity a_A, whereas the dependence of crack velocity on stress is all contained within the exponent of equation 7.

Although the free energy of activation in equation 7 contains three terms ($\Delta G^{\ddagger} = \mu_o^{\ddagger} - \mu_g - \mu_{so}$), these terms are not all equivalent with regard to water enhanced crack growth. The chemical potentials of both the glass, μ_g, and the activated state, $\mu_o^{\ddagger}$, depend on the state of stress at the crack tip, and hence, are the prime determinants of the slope of the v-K_I curves shown in Figures 1-3. As the stress applied to the crack tip is increased, $\mu_o^{\ddagger} - \mu_g$ must decrease to account for an increase in the rate of crack growth. The slope of the v-K_I curve depends on the sensitivity of $\mu_o^{\ddagger} - \mu_g$ to the applied stress, the greater the sensitivity, the steeper the slope of the v-K_I plot. By contrast

the chemical potential of the water does not depend on the state of stress at the crack tip, and hence, has no effect on the slope of the v-K_I curve. It is for this reason that all of the curves in region I of Figures 1-3 have approximately the same slope.

A quantitative treatment of the dependence of applied stress on $\Delta G^{\ddagger}$ has been developed by modelling the crack tip as an elliptical slit in a continuum.[13] The chemical reaction is assumed to occur at the tip of the slit and the individual bonds at the crack tip are assumed to be acted upon by stresses calculated from the Inglis relation.[17] The following expression is obtained for the free energy of activation:[13]

$$\Delta G^{\ddagger} = - T\Delta S^{\ddagger} + \Delta E^{\ddagger} - [2 K_I/(\pi\rho)^{\frac{1}{2}}] \Delta V^{\ddagger} - (\gamma^{\ddagger} V^{\ddagger} - \gamma V)/\rho \qquad (8)$$

where $\Delta S^{\ddagger}$, $\Delta E^{\ddagger}$ and $\Delta V^{\ddagger}$ are, respectively, the activation entropy, the activation energy and the activation volume. The parameter ρ is the radius of curvature of the crack tip, and is assumed to be of the order of the lattice, or network spacing in the solid: 0.5 nm for glass.*

The term containing K_I on the right hand side of the equation is the stress to which the reacting species at the crack tip are subjected. This portion of the activation free energy determines the stress dependence of crack growth rate. More specifically, if crack growth data are fitted to the following empirical relation:

---

* A curved crack tip is assumed primarily to estimate the stress level at the crack tip. The nature and structure of real crack tips in glass are, at present, not fully understood.

$v = v_o \exp(-E^* + bK_I)/RT$, then the slope of the v-K_I data, b, can be used to determine the activation volume for crack growth. Equating b to the coefficient of K_I in equation 8, the following relation is obtained for $\Delta V^{\ddagger}$:

$$\Delta V^{\ddagger} = (b/2)\ (\pi\rho)^{\frac{1}{2}} \tag{9}$$

This expression will be used later in the paper to relate the crack growth data (i.e. the slope b) to a variable calculated from an electrostatic model of environmental interactions at crack tips.

The last term on the right hand side of equation 8 is included to account for the fact that surface curvature can modify the chemical potential of the reacting species.[13] The parameters γ and V are the surface tension and molar volume of the reacting species (the strained Si-O bonds of glass for example) before reaction, while $\gamma^{\ddagger}$ and $V^{\ddagger}$ are these same quantities for the activated complex on surface during reaction. The inclusion of this surface energy term follows the approach first taken by Charles and Hillig[18] in their dissolution model of static fatigue.

4.2 Region I Crack Growth

The crack growth data collected in the present paper can best be compared with equation 7 of the theory presented in Section 4.1. Since v_o and the chemical potentials μ_{so}, μ_g and $\mu_o^{\ddagger}$ are constants for a given temperature and state of stress, the equation implies that at a constant applied stress intensity factor, the crack velocity will depend only on

the activity, a_s, of water in the alcohol solution. If the standard state of the chemical potential of the water in the alcohol is taken as pure water, then the chemical activity of the fully saturated alcohols used in the present studies is $\sim$1, at saturation, (i.e. the chemical potentials of the water are almost the same for all of the alcohols). Furthermore, if water vapor at room temperature is assumed to behave as a perfect gas, then the activity of the water is given by the ratio of the partial pressure, p_s, of water over the solution to that, p_{so}, over pure water: $a_s = p_s/p_{so}$.[16] Since p_s/p_{so} is defined as the relative humidity, the crack velocity is predicted to be proportional to the relative humidity of the water, as is observed experimentally (Figure 4). Hence we conclude that the chemical activity, or what is equivalent, the chemical potential of water in solution is the prime driving force for crack growth in region I.

The above observation has rather broad implications with regard to the effect of water on the lifetime of structural ceramics. As long as the chemical potential of water is the same in two solutions, the response of cracks in structural ceramics to stress will be identical with regard to region I crack growth. Since the lifetime of ceramics is controlled mainly by region I (i.e. slow) crack growth, the chemical potential of water in solution is the prime environmental determinant of structural reliability. Although several investigations of the effect of relative humidity on component lifetime are consistent with this prediction,[19,20] this subject has not been studied systematically and certainly warrants further investigation.

4.3 Region II Crack Growth

The mechanism described in Section 4.1 will control crack growth as long as the number of water molecules reaching the crack tip maintains the activity of water at the crack tip constant. When the velocity is fast enough, the water will be used up at a rate faster than can be supplied by diffusion from the environment. When this happens, the rate of transport will control the rate of crack motion.

Using a one dimensional model of diffusive transport of water to a crack tip it has been shown that the rate of crack growth in region II can given by:[1]

$$v = 0.0275\ D\ X_o/n\delta \qquad (10)$$

where D is the diffusivity of water in the alcohol, δ is the diffusive boundary layer thickness in front of the crack tip, X_o is the molar concentration of the water in the solution and n is the order of the chemical reaction.* For relative humidities >0.1, the parameter n has been shown to be 1 for water reactions in nitrogen gas and will be assumed to be equal to 1 for the alcohols.

---

* The constant 0.0275 is appropriate when all variables in equation 10 are expressed in SI units.

The diffusivity, D, of water in alcohols has been measured in only a few of the shorter chain length alcohols.[21] Hence in order to compare the data with equation 4, it is necessary to use a theoretical expression for the diffusion coefficient. For this purpose we use the Stokes-Einstein relation:[22]

$$D = (kT)/(6\pi r\eta) \tag{11}$$

where η is the fluid viscosity, r is the radius of the diffusing molecule and k is the Boltzman constant. Substituting equation 11 into equation 10, the following equation is obtained for the crack velocity in region II:

$$v = (0.0275\ kT/(6\pi r\delta))(X_o/\eta) \tag{12}$$

If the form of equation 12 is correct, then the crack velocity in region II should be proportional to X_o/η (i.e. the ratio of the molar concentration of water in the alcohol to the viscosity of the alcohol). The data plotted in this manner (Figure 10) scatters about a line of slope 1, as would be expected from the theory. Much of the scatter in Figure 10 can be attributed to the uncertainty in selection of the characteristic velocity of region II. As can be seen from examination of Figure 6, the error in estimating the crack velocity in region II can be as much as a factor of 2. Furthermore, the fact that crack velocity in region II exhibits a small but significant dependence on applied stress intensity factor contributes to the uncertainty in selecting

characteristic velocities. Considering these sources of scatter in the experimental data, the correlation between the variables shown in Figure 10 lends credence to our model of diffusion controlled crack growth.

The data shown in Figure 10 can be used to obtain an estimate of the diffusive boundary layer, δ, at the crack tip. The intercept on Figure 10 is approximately 2.5×10^{-8} m/s; substituting this value of crack velocity into equation 12 and assuming T = 300 K and r (the molecular radius of H_2O) = 0.3 nm a value of δ = 0.8 μm is obtained. This value is approximately one-third that obtained in earlier studies of crack growth in nitrogen gas. Since the collision distances in liquids ($\sim$.5 nm) are less than the collision distances in gases ($\sim$50 nm at standard temperature and pressure), the boundary layer, δ, in a liquid is expected to be less than that in a gas. The thickness of the boundary is likely to vary from one type of liquid to another, depending on the nature of the interactions that occur between the liquid and the water that is dissolved in it.

4.4 Region III Crack Growth

The data presented in this paper and in the papers by Freiman[3] and Richter[4] suggest that alcohols and other organic liquids affect crack growth in Region III. The influence of these environments is indicated by small shifts in the position of the crack propagation curves and by small decreases in the slopes of these curves when compared to the

position and the slope of the curve obtained in nitrogen gas. Two possible mechanisms were considered to explain our experimental observations. The first involves viscous drag of the liquid on the freshly formed fracture surfaces, which would retard crack growth, causing small shifts in the crack velocity curves. If viscous drag were an important mechanism, then the crack growth curve would be expected to shift to higher values of K_I as the viscosity of the liquid increased. This type of shift in the position of the crack growth curve is in fact observed for the alcohols. The possibility of a viscous drag contribution to the crack growth behavior was, however, rejected for two reasons: (1) the shape of the crack growth curves obtained experimentally differs from that predicted from fluid dynamic equations; (2) viscous drag cannot explain the experimental crack growth behavior at low velocities, since all of the crack growth curves would be expected to join up with the nitrogen curve as the viscous drag effects vanished. To support these conclusions, detailed discussion of viscous drag is given in Appendix A.

The second mechanism considered to explain our experimental findings involves electrostrictive interactions between the glass and the fluid at the crack tip. If one accepts the chemical interaction model of subcritical crack growth in ceramic materials, then the slope of the crack propagation curves in regions I or III is determined by the activation volume, $\Delta V^{\ddagger}$, of the chemical reaction that occurs at the crack tip.[13] When fracture is caused by the reaction of water with glass, $\Delta V^{\ddagger}$ represents the difference in molar volume between the

reactants and the chemical complex in the activated state. If fracture occurs in the absence of water, ΔV^* then represents the change in volume that occurs as the strained Si-O bonds move into an activated state. Referred to as a fission reaction in the chemical literature, this is the type of reaction of primary interest in fracture processes.

When a fission reaction occurs in a liquid environment, it has been shown that the activation volume normally consists of two parts: one part relates to the stretching of the bond that is being broken; the second part relates to volume changes in the fluid surrounding the reacting molecule.[15,23-25] The second part is usually attributable to electric charge formation or destruction during the chemical reaction, which results in a localized electrostriction, and hence a change in volume in the fluid surrounding the reacting species. This change in volume must be included as part of the activation volume because the volume change is concomitant with the fission reaction. For normal chemical reactions, charge formation or destruction results in rather large contributions to the activation volume. In fact, the electrostatic portion of the activation volume is usually 3 to 10 times that due to changes in bond length alone. Hence, if charges are either formed or destroyed during the rupture of a silicon-oxygen bond in glass, electrostatic effects in the glass during crack growth will have to be considered.

In order to model the effect of environment on a fission reaction in glass, a procedure similar to that used by Wiederhorn, Fuller and Thomson[13] is employed. The procedure models the crack tip as an ellipse and uses the stress at the major axis of the ellipse, calculated from the Inglis relation,[17] as the driving force for the chemical reaction. The crack tip stress then replaces pressure as the thermodynamic parameter usually used to discuss chemical reactions. The crack tip stress is of course a negative pressure. The effect of charge formation is then treated by elementary solvation theory:[16,22] the charged atoms or molecules formed during the reaction being approximated by charged conducting spheres; the medium surrounding the reacting species being treated as a continuum with a dielectric constant, ε. For the fission of a silicon-oxygen bond during crack growth in glass, positive and negative charges are assumed to form on the silicon and oxygen atoms respectively as they are separated. This assumption that a full unit of charge develops during the activated state is based on the work of Akmed et al.,[24] who reported charge formation on silicon and oxygen atoms during the crushing of silica glass. Suggestions of charge formation during fracture were also made in earlier glass literature.[27,28]

The procedure used in the present paper to estimate the electrostatic component of the activation volume differs somewhat from that used by Wiederhorn, Fuller and Thomson,[13] in that the reacting species (the oxygen and the silicon) are assumed to lie at a stressed surface of the glass. This assumption is necessary in order to evaluate the effect of environment on the reacting species. Furthermore, we assume

that the electrostatic component of the activation volume (or activation free energy) is entirely the result of charging the oxygen and silicon atoms during the fission process. Finally, we assume that the reaction is sufficiently slow that the static component of the dielectric constants can be used to estimate the electrostrictive processes at the crack tip, and that both the glass and the environment at the crack tip can be treated as a continuum. These last two assumptions are usually made to treat the kinetics of chemical reactions in liquids.[15,23-24]

A schematic diagram of the model used in the present paper to account for the electrostatic component of the activation volume is given in Figure 11. Charges are assumed to form at a flat interface during the reaction. Each Si and O atom in the activated state is assumed to react independently with the glass and the surrounding environment during the fission reaction. This assumption is often made in evaluating the electrostatic component of the activation volume and tends to neglect dipole or quadrupole effects on reaction rate. The configuration shown in Figure 11 was chosen because electrostatic effects of the dielectric fluid on the rupture process are easily estimated from this model. The model does not take into account effects that result from curvature of the crack near the crack tip or stearic hinderance due to limits in the dimensions of the crack near its tip. It is assumed that the change in free energy, ΔG_{es}, when a charge forms at the interface can be estimated by the energy required to charge conducting spheres of radius, r_{Si} and r_O, equal to the radius of the silicon and oxygen atoms (0.04 and 0.14 nm) respectively. Each atom is assumed to develop a full unit of charge as rupture occurs,

a positive charge for the silicon atom and a negative charge for the oxygen atom. The free energy of formation of each charged atom, ΔG_{es}, is given by:*

$$\Delta G_{es} = (N_a e^2/r)/(\varepsilon_1+\varepsilon_2) \qquad (13)$$

per mole of charge formed for each ion. N_a is Avogadro's constant, and ε_1 and ε_2 are the dielectric constants of the glass and the liquid respectively.

The electrostatic component of the activation volume for the reaction is determined from equation 13, using the relation, $\Delta V_{es} = \partial \Delta G_{es}/\partial P$, where P is the pressure that constrains the chemical reaction. When the reaction occurs at the surface of the glass, this pressure is equal to the negative of the crack tip stress. Hence for a chemical reaction constrained by a pressure, P, the activation volume ΔV_{es} is given by:

$$\Delta V_{es} = (N_a e^2/r)\,[-(\varepsilon_1+\varepsilon_2)^{-1}\,\partial \ln r/\partial P - (\varepsilon_1+\varepsilon_2)^{-2}\partial\varepsilon_1/\partial P] \qquad (14)$$

for each ion. The derivation of equation (14) is based on the assumption that the pressure is applied only to the glass, hence the partial derivative is taken only with regard to ε_1. Equation 14 can be written in terms of the bulk modulus B:

$$\Delta V_{es} = (N_a e^2/r)[(3B)^{-1}(\varepsilon_1+\varepsilon_2)^{-1} - (\varepsilon_1+\varepsilon_2)^{-2}\partial\varepsilon_1/\partial P] \qquad (15)$$

*This equation is derived in Appendix B.

From equation 15, we note that the electrostatic contribution to the activation volume depends on four parameters: the size of the electrostatic charge formed during the reaction; the value of the bulk modulus; the value of the dielectric constants (ε_1 and ε_2) and the partial derivative of the dielectric constant with regard to the applied pressure. As already mentioned, equation 15 neglects any dipole, or quadrupole contributions to ΔV_{es}. The partial derivative of ε_1 with regard to P is usually negative for solids; however, some positive values have been measured.[29,30] When $\partial\varepsilon_1/\partial P$ is negative, then the activation volume is positive. However when $\partial\varepsilon_1/\partial P$ is positive, the activation volume, ΔV_{es} , can be positive or negative depending on the size of the two terms in the square brackets. Finally, the dependence of ΔV_{es} on environment depends primarily on the dielectric constant, ε_2, of the environment.

Crack growth data can be compared with the electrostrictive model for crack growth by plotting $\Delta V^{\ddagger}$, the total activation volume (equation 9), as a function of ΔV_{es}, the electrostatic portion of the activation volume. It is worth noting that $\Delta V^{\ddagger}$ determined from equation 9 contains both the stretching and the electrostatic components of the activation volume. For crack growth studies conducted on soda-lime-silica glass in different environments, ΔV_{es} is expected to depend primarily on ε_2, the dielectric constant of the fluid at the crack tip. For fluids that have a high dielectric constant (i.e. water, formamide) ΔV_{es} is expected to be small, and as a consequence, the value obtained for $\Delta V^{\ddagger}$ will be due primarily to stretching of the Si-O bonds by the applied forces. For

environments that have low dielectric constants (i.e. alkanes, vacuum) ΔV_{es} will be large and $\Delta V^{\ddagger}$ will contain components due both to electrostatic interactions and to stretching. Figure 12 presents a plot of $\Delta V^{\ddagger}$ as a function of ΔV_{es}.* Despite the experimental scatter, a correlation between $\Delta V^{\ddagger}$ and ΔV_{es} is apparent from the figure. The figure demonstrates a definite dependence of crack growth data on the dielectric constant of the test media, and as such lends support to the idea that electrostatic interactions between the environment and the highly strained bonds at the crack tip influence crack growth. The scatter of the data in Figure 12, illustrates the difficulty of obtaining accurate values of the slope of the v-K_I data in region III, especially when the slopes are high, as they are in alkanes, nitrogen gas, and vacuum. Further confirmation of the theory will require the development of more accurate methods of determining the slope of crack growth curves. These techniques should then be applied to crack growth

---

* The authors could find no values of $\partial\varepsilon_1/\partial\rho$ in the literature for soda-lime-silica glass. The value of $\partial\varepsilon_1/\partial P$ (-9.72×10^{-11} Pa^{-1}) used for Figure 12 was obtained by Colwell[30] on an alkali containing glass made at the National Bureau of Standards. The fluid dielectric constants ε_2 and the slopes, b, of the crack growth curves used for Figure 12 are given in Table 2.

studies in low dielectric constant liquids, <8, where electrostatic effects are expected to be greatest. Furthermore, a variety of glasses and single phase ceramics should be studied to evaluate the effect of $\partial\varepsilon_1/\partial P$ on crack growth data.

5. Summary

This paper presents the results of a series of studies to determine the effect of water and a variety of organic liquids on crack growth in soda-lime-silica glass. Throughout the paper the crack growth process is viewed as a chemical reaction and the data are interpreted in terms of chemical reaction rate theory. In the presence of a chemically active environment, rupture of the Si-O bonds of the glass network is viewed as a fission reaction in which Si-O bonds, strained by the crack tip stresses, are cleaved by the chemical environment. In the absence of a chemical reaction between the glass and the environment the fission reaction occurs as a result of a stress induced cleavage of the Si-O bonds of the glass network structure. The three regions of crack growth, observed in crack growth studies are interpreted in terms of reaction rate theory.

In region I, crack growth in organic liquids is the result of a chemical reaction between the active component in the environment (usually H_2O) and the glass; the rate of growth is controlled by the chemical potential of the active component. This finding confirms those of earlier studies and is consistent with the chemical reaction rate

theory of crack growth. In region II the rate of crack growth is determined by diffusion of the reactant to the crack tip. We show that crack growth in region II is not controlled by the chemical potential of the reactant, but by its concentration. Using the Stokes-Einstein relation for the diffusivity, a linear relation is obtained between the crack velocity and the ratio of the concentration of water to the viscosity of the organic fluid. Finally in our discussion of crack growth in region III, we introduce the idea that electrostrictive effects at crack tips can influence the crack growth behavior of solids. The concept of an electrostatic component to the activation volume is commonly used by physical chemists to explain the effects of solvents on rates of chemical reactions. In this paper, a model was developed to quantify the effect of dielectric media on crack growth rate in glass. The model follows classical chemical lines and has the virtue of providing a relation between the slope of $v\text{-}K_I$ data and the dielectric constants of the glass and the test medium. A plot of the total activation volume obtained from the slope of crack growth data versus the electrostatic component of the activation volume calculated from theory, lends support to the model and suggests that electrostrictive effects influence the growth of cracks in glass. Despite this agreement, the approximate nature of the model should be recognized. Further studies may show that some variables neglected in the model are in fact important to our understanding of region III crack growth. Clearly, additional data is needed to fully evaluate the theory presented in this paper.

Acknowledgment: This work was supported by the Office of Naval Research, Metallurgy and Ceramics Program. The authors are grateful for the technical assistance of A.C. Gonzalez, D. Kravitz, and G.S. White. Helpful discussions with R. M. Thomson, J. W. Cahn, B. R. Lawn and H. Richter are also gratefully acknowledged.

REFERENCES

1. S. M. Wiederhorn, "Influence of Water Vapor on Crack Propagation in Soda-Lime Glass", J. Am. Ceram. Soc., 59, 407-414 (1967).

2. K. Schonert, H. Umhauer and W. Klemm, "The Influence of Temperature and Environment on the Slow Crack Propagation in Glass", pp 474-482 in Proc. 2nd Int. Conf. on Fracture, Biyhten, 1969, Chapman and Hall, London (1970).

3. S. W. Freiman, "Effect of Alcohols on Crack Propagation in Glass," J. Am. Ceram. Soc. 57, 350-353 (1974).

4. H. Richter, "The Effect of Different Liquids on the Transition from Slow to Fast Crack Propagation in Soda-Lime-Glass," pp 618-624 in The Physics of Non-Crystalline Solids, G. H. Frischat, ed., Trans. Tech. Publications, CH-4711 Aedermannsdorf, Switzerland (1977).

5. C. L. Quackenbush and V. D. Frechette, "Crack-Front Curvature and Glass Slow Fracture," J. Am. Ceram. Soc. 61, 402-406 (1978).

6. S. M. Wiederhorn, H. Johnson, A. M. Diness and A. H. Heuer, "Fracture of Glass in Vacuum," J. Am. Ceram. Soc., 57, 336-341 (1974).

7. M. Randall and H. P. Weber, "The Activity of the Constituents in Mixtures of n-butyl Alcohol and Water at 30 ^{o}C," J. Phys. Chem. 44, 917-920 (1940).

8. H. R. Null, Phase Equilibrium in Process Design, Wiley-Interscience, New York (1970).

9. S. M. Wiederhorn, "Subcritical Crack Growth," pp 613-646 in Fracture Mechanics of Ceramics, 2, Microstructure Materials and Applications," R. C. Bradt, D. P. H. Hasselman, and F. F. Lange, eds., Plenum Press, New York (1974).

10. B. J. Pletka, E. R. Fuller, Jr., and B. G. Koepke, "An Evaluation of Double-Torsion Testing-Experimental," pp 19-37 in Fracture Mechanics Applied to Brittle Materials, ASTM STP 678, S. W. Freiman, ed., American Society for Testing and Materials (1979).

11. T. A. Michalske and V. D. Frechette, "Dynamic Effects of Liquids on Crack Growth Leading to Catastrophic Failure in Glass," J. Am. Ceram. Soc., 63, 603-609 (1980).

12. S. W. Freiman, D. R. Mulville, and P. W. Mast, "Crack Propagation Studies in Brittle Materials", J. Mat. Sci. 8, 1527-33 (1973).

13. S. M. Wiederhorn, E. R. Fuller, Jr., and R. Thomson, "Micromechanisms of Crack Growth in Ceramics and Glasses in Corrosive Environments," Metal Science 14, 450-458 (1980).

14. S. Glasstone, K. J. Laidler, and H. Eyring, Theory of Rate Processes, McGraw-Hill, New York, 1941.

15. G. Kohnstam, "The Kinetic Effects of Pressure," pp 355-408 in Progress in Reaction Kinetics, G. Porter, ed., Pergamon Press, London (1970).

16. W. J. Moore, Physical Chemistry, Prentice-Hall Inc., Englewood Cliffs, N.J. (1972).

17. C. E. Inglis, "Stresses in a Plate due to the Presence of Cracks and Sharp Corners," Trans. Inst. Naval Archit. 55, 219- (1913).

18. R. J. Charles and W. B. Hillig, pp 511-27 in Symposium on Mechanical Strength of Glass and Ways of Improving It. Florence, Italy, September 25-29, 1961. Union Scientifique Continentale du Verre, Charleroi, Belgium, 1962.

19. R. E. Mould, "Strength and Static Fatigue of Abraded Glass under Controlled Ambient Conditions: IV. Effect of Surrounding Medium," J. Am. Ceram. Soc. 44, 481-91 (1961).

20. J. E. Ritter, Jr., and C. L. Sherburne, "Dynamic and Static Fatigue of Silicate Glasses," J. Am. Ceram. Soc. 54, 601-605 (1971).

21. P. A. Johnson and A. L. Babb, "Liquid Diffusion of Non-Electrolytes," Chem. Rev. 56, 387-453 (1956).

22. J. O'M. Bockris and A. K. N. Reddy, Modern Electrochemistry, vol. 1, Plenum Press, New York (1970).

23. S. D. Hamann, "Chemical Kinetics," pp 163-207 in High Pressure Physics and Chemistry, vol. 2, R. S. Bradley, ed., Academic Press, New York (1963).

24. E. Whalley, "Use of Volumes of Activation for Determining Reaction Mechanisms," Advan. Phys. Org. Chem. 2, 93-162 (1964).

25. C. A. Eckert, "High Pressure Kinetics in Solution," Ann. Rev. Phys. Chem. 23, 239-264 (1972).

26. K. A. Akhmed-zade, V. V. Baptizmanskii, V. A. Zakrevskii, and E. E. Tomashevskii, "Paramagnetic Centers Produced by Mechanical Destruction of Silica," Soviet Physics-Solid State, 14, 351-354 (1972).

27. R. E. Benson and J. E. Castle, "Reactions of Freshly Formed Surfaces of Silica," J. Phys. Chem. 62, 840-843 (1958).

28. W. A. Weyl, "Crystal Chemical Considerations of the Surface Chemistry of Silica," Research 3, 230-235 (1950).

29. R. S. Bradley, "Other Miscellaneous Effects of Pressure," pp 325-337 in High Pressure Physics and Chemistry, vol. 2, R. S. Bradley, ed., Academic Press, New York (1963).

30. J. H. Colwell, "Stable Pressure Transducer," National Bureau of Standards Report, NBSIR 76-1116, July 1976.

31. S. M. Wiederhorn and L. H. Bolz, "Stress Corrosion and Static Fatigue of Glass," J. Am. Ceram. Soc. 53, 543-548 (1970).

32. S. W. Freiman, "Effect of Straight-Chain Alkanes on Crack Propagation," J. Am. Ceram. Soc. 58, 339-340 (1975).

33. S. W. Freiman, "Temperature Dependence of Crack Propagation in Glass in Alcohols," J. Am. Ceram. Soc. 58, 340-341 (1975).

34. P. C. Paris and G. C. Sih, "Stress Analysis of Cracks" in Fracture Toughness Testing and Its Applications, ASTM STP 381 (1965), pp 80-81.

35. G. I. Barenblatt, "The Mathematical Theory of Equilibrium Cracks in Brittle Fracture," Adv. Appl. Mech. 7, 55-126 (1962).

36. G. K. Batchelor, An Introduction to Fluid Dynamics, Cambridge University Press, Cambridge (1967).

37. I. S. Gradshteyn and I. M. Ryzhik, Table of Integrals, Series, and Products (Academic Press, New York, 1980), p. 527 (formula 4.224.11).

38. J. D. Jackson, Classical Electrodynamics (John Wiley & Sons, Inc. New York, 1962).

APPENDIX A

The Effect of Viscous Flow on Crack Motion

In an earlier section of this paper, the idea that the position of the v-K_I curves in alcohol could be explained by viscosity effects was rejected. In this section we develop equations that relate the crack motion to the viscosity of the fluid at the crack tip and show why the idea was rejected.

Assume that the crack can be represented by a parabola that intersects an external surface, Figure 1A. The parabola is selected because the crack has the shape of a parabola near its crack tip in the linear elastic approximation. The crack length is equal to c, the y-coordinate is perpendicular to the plane of the crack and the x coordinate lies in the plane of the crack. As the crack moves along, it sucks fluid into the crack opening, which is exposed to an infinite reservoir of fluid at an ambient pressure, P_a. In order for the fluid to flow to the crack tip, the fluid pressure decreases from the crack opening to the crack tip. Therefore the fluid within the crack is at a negative pressure relative to the ambient pressure, P_a. The negative pressure loads the surface of the crack in such a way as to tend close the crack. Thus, the closing force on the crack surface produces a negative stress intensity factor, K_p which opposes the positive, applied stress intensity factor, K_a, that is driving the crack to propagate.

To calculate the decrease in pressure from the crack opening to the crack tip, and to estimate the negative stress intensity factor, we assume that the coordinate system is fixed to the crack tip. Then the crack surface appears to recede from the crack tip at a velocity v_o, which is also the velocity of the crack. The half width of the crack, y_o, is determined by the standard (plane strain) fracture mechanics relation for the displacement in the vicinity of a crack that is subject to a stress intensity factor K_I (see, for example, Ref. 34)

$$y_o^2 = [2K_I(1-\nu)/G]^2(x/2\pi) \tag{1A}$$

where G is the shear modulus of the solid and ν is Poisson's ratio. The stress intensity factor, K_I, therefore describes the stresses and displacements at the crack tip and has to be equal to the sum of K_a and K_p: $K_I = K_a + K_p$. This approach to the crack tip stresses is similar to the approach used by Barenblatt[35] in his discussion of crack tip forces.

At any distance, x, from the crack tip, the pressure drop across a section, dx, of the crack is given by the Poiseille flow equation for a parallel sided channel:

$$v_o = (1/3\eta)\,(dP/dx)\,y_o^2 \tag{2A}$$

where η is the viscosity of the fluid in the crack. As noted by Batchelor,[36] this approximation is valid provided the slope of the

walls of the channel change slowly with distance along the channel. Substituting equation 1A into equation 2A and integrating the pressure drop from a point within the crack to the crack mouth, the following equation is obtained for the pressure, P, at any point within the channel:

$$P = P_a + 6\pi v_o \eta \, [G/2K_I(1-\nu)]^2 \ln (x/c) \qquad (3A)$$

Note that as the position x approaches the crack tip (i.e. $x \to o$), large negative pressures occur within the fluid.

The negative stress intensity factor, K_p, that results from the reduction of pressure within the crack can be calculated from a standard equation for a two dimensional crack within a solid that is subject to an applied stress $\sigma(x)$: [34]

$$K_p = 2 \, (c/\pi)^{1/2} \int_o^c \sigma(x') \, dx' / [c^2 - (x')^2]^{1/2} \qquad (4A)$$

where $x' = c-x$ measures the distance from the crack mouth.

The stress $\sigma(x')$ at any point on the crack surface is determined from the difference between the pressure within the crack and the external pressure: $\sigma(x') = P - P_a$. Note from 3A that $\sigma(x')$ is a negative quantity, as it should be for a closing force on the crack tip. Substituting the equation for $\sigma(x')$ into equation 4A and integrating,[36] the following equation is obtained for K_p:

$$K_p = -1.5\ (\pi \ln 2 + 4C)\ v_o \eta\ [G/K_I(1-\nu)]^2\ (\pi c)^{1/2}$$

$$= -8.76\ v_o \eta\ [G/K_I(1-\nu)]^2\ (\pi c)^{1/2} \qquad (5A)$$

where $C = 0.915966$ is Catalan's constant.

For a constant crack length, c, K_p depends only on the crack velocity, v_o, and the crack tip stress intensity factor, K_I; since K_I is a slowly varying function of v_o for ceramic materials, K_p depends primarily on v_o.

Normally when a v-K_I curve is determined experimentally, it is K_a that is measured and presented as a plotting parameter. As long as K_p is small, the v-K_I curve and the v-K_a curve will be indistinguishable. However when K_p becomes large relative to K_a, the experimental curve will diverge from the "true" v-K_I curve. This occurs when part of the applied load is transferred from the specimen to the fluid within the crack. The range of velocities over which this occurs can be calculated by evaluating equation 5A and comparing it with crack tip stress intensity factor. As shown in Table 1A, where $P-P_a$ and K_p are calculated as a function of velocity for water, the transition range over which these viscous effects are important occur over a relatively narrow range of crack velocities. The data in Table 1A are plotted in Figure 2A to give a predicted v-K_a curve. We note that the curve bends over rather

sharply, over a velocity range of about two orders of magnitude. Behavior of this type has been observed for water by Schönert et al.[2] and by Michalske and Frechette for water and for methyl alcohol.[12] Since the shape of the curves observed in the present paper are not similar to those obtained for the alcohols in region III, we conclude that viscous effects of the crack tip fluid played little if any role in the present experiments, thus justifying our statements in section 4.3.

APPENDIX B

Electrostatic Energy of a Charged Sphere on a Dielectric Interface

The model used in section 4.3 to describe the region III crack growth behavior relates the change in free energy during the crack-tip fission reaction to the electrostatic energy required to charge a conducting sphere embedded on a dielectric interface (see Figure 12). In this appendix we derive an expression for this electrostatic energy.

In a linear dielectric medium, the electrostatic energy of a system of charges is related to the electric field E that they produce by the relation:[38]

$$W_{es} = \frac{1}{8\pi} \int \varepsilon \, |E|^2 \, d^3R \qquad (1B)$$

where ε is the dielectric constant and the volume integral is over all space. Accordingly, the problem reduces to finding the electric field E, or its scalar potential Φ, since then $E = -\nabla\Phi$, and integrating the results according to Eq. (1B).

The electrostatic potential Φ is determined as a solution of Poisson's equation:

$$\nabla^2\Phi = -4\pi\chi \qquad (2B)$$

where χ is the charge density. The boundary conditions for the present problem require: (1) that the surface of the conducting sphere is at a constant potential; (2) that the displacement field, εE, normal to the sphere is equal to 4π times the surface charge density; (3) that the surface charge density integrated over the surface of the sphere is Q; and (4) that the tangential components of E is continuous across all boundaries. Rather than solve Eq. (2B) directly, we note that a solution of Poisson's equation is unique when the potential is specified on all closed conducting surfaces (Dirchlet boundary conditions), as in the present problem. Thus, if we obtain a solution by any means, we have the unique solution.

A solution to the present problem is obtained from the electrostatic potential of a point charge Q embedded on a planar interface between to two semi-infinite dielectrics. This solution:[38]

$$\Phi(R) = \frac{2Q}{(\varepsilon_2 + \varepsilon_1)R} \tag{3B}$$

has spherical equipotential surfaces and hence gives the proper form of the solution for distance greater than the radius r of the conducting sphere (i.e., R>r). Inside the sphere the potential is constant:

$$\Phi = \frac{2Q}{(\varepsilon_2 + \varepsilon_1)r} \text{ , for } R \leq r \tag{4B}$$

The electric field vector is given by the negative of the gradient of the potential, and only has a radial component E_R since the potential is spherically symmetric:

$$E_R = \begin{cases} 0 & , \text{ for } R<r \\ \dfrac{2Q}{(\epsilon_2 + \epsilon_1)R^2} & , \text{ for } r<R \end{cases} \qquad (5B)$$

It is easy to verify that this solution satisfies the remaining boundary conditions.

The electrostatic energy required to charge the conducting sphere is obtained by integrating Eq. (5B) in Eq. (1B):

$$W_{es} = \frac{1}{8\pi}\int_{\text{dielectric 2}} \epsilon_2 E_R^2 \, d^3R + \frac{1}{8\pi}\int_{\text{dielectric 1}} \epsilon_1 E_R^2 \, d^3R$$

$$= \frac{Q^2}{(\epsilon_2 + \epsilon_1)r} \qquad (6B)$$

In section 4.3 the charge Q is taken to be a full unit of electronic charge, $Q = e$.

Table 1: Viscosity, Water Concentration and Relative Humidity of Alcohols used in Region II Crack Growth Study.

Alcohol	Viscosity (Pa•s)	Water Concentration (mol/liter)	Percent Relation Humidity
Butyl	3.13×10^{-3}	9.2	100
Amyl	3.46×10^{-3}	4.08	100
Hexyl	3.95×10^{-3}	3.04	100
Heptyl	5.16×10^{-3}	2.52	100
Octyl	6.31×10^{-3}	1.13	50
Decyl	10.99×10^{-3}	1.68	100
Ethyl (1%)	1.1×10^{-3}*	0.555	7
Butyl (0.2%)	2.95×10^{-3}*	0.111	5
Butyl (1%)	2.95×10^{-3}*	0.555	21
Butyl (5%)	2.95×10^{-3}*	2.78	70

* The viscosities of the partially saturated ethyl and butyl alcohols were assumed to be equal to the pure alcohols at 20 °C.

Table 2: A comparison of the slopes, b, of crack growth data with the dielectric constant, ε_1, of the test medium. All crack growth measurements were made on soda-lime-silica glass; slopes were determined from an empirical fit to the equation: $v = v_o \exp bK_I/RT$.

Test Medium	Dielectric Constant, ε_1	Slope, b MKS units	Test Method
Formamide	109	0.168	D.C.B.
Water	78	0.111	D.C.B., ref. 31
Acetonitrile	39	0.232	Double Torsion
Methanol	33	0.182	Double Torsion
		0.169	Double Torsion
Hexanol	13.3	0.223	D.C.B., ref. 33
Heptanol	12.2	0.283	D.C.B., ref. 33
Octanol	10.3	0.228	D.C.B., ref. 33
Decanol	8.0	0.240	D.C.B., ref. 33
		0.252	Double Torsion
		0.391	Double Torsion
Trichloroethylene	3.4	0.463	D.C.B.
Alkanes	2	0.488	D.C.B., ref. 32
Heptane	2	0.361	Double Torsion
		0.772	Double Torsion
		0.724	D.C.B., ref. 32
Nitrogen	1	0.636	Double Torsion
		0.542	Double Torsion
		0.823	D.C.B., ref. 1
Vacuum	1	0.88	D.C.B., ref. 6

Table 1A. Effect of viscous forces on crack motion calculated from equations 3A and 5A. The pressure is calculated for a 1 mm crack at a distance of 1 μm from the crack tip. (G = 28 GPa, ν = 0.24 and η = 1 mPa·s)

Crack Velocity (m/s)	K_I (mPa·m$^{1/2}$)	$P - P_a$ (mPa)	K_p (mPa·m$^{1/2}$)
1.00×10^{-1}	0.570	-13.6	-0.205
5.72×10^{-2}	0.560	- 8.1	-0.122
2.63×10^{-2}	0.543	- 3.9	-0.059
1.20×10^{-2}	0.530	- 1.9	-0.028
5.25×10^{-3}	0.505	- 0.91	-0.014
2.40×10^{-3}	0.490	- 0.44	-0.007
1.00×10^{-3}	0.470	-0.20	-0.003

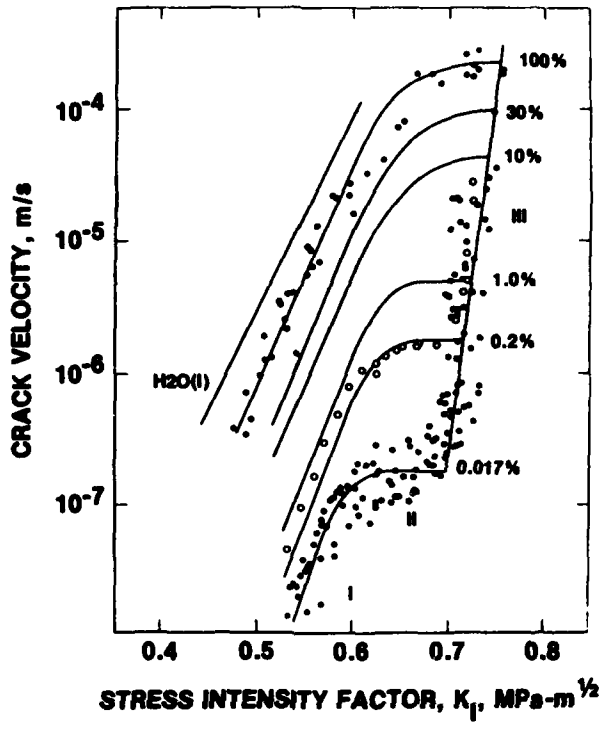

Figure 1. Effect of relative humidity on crack growth in soda-lime-silica glass (ref. 1).

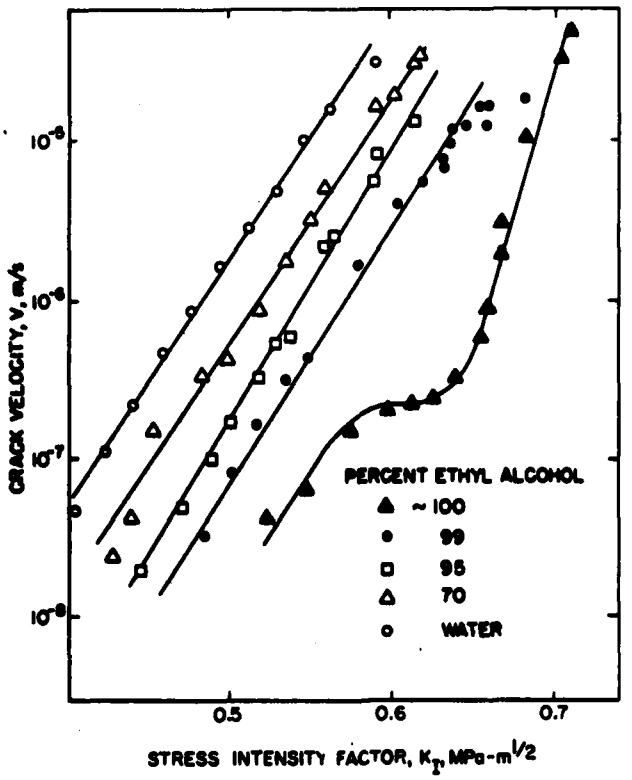

Figure 2. Crack propagation in ethyl alcohol containing water. The concentration of water is expressed in volume percent.

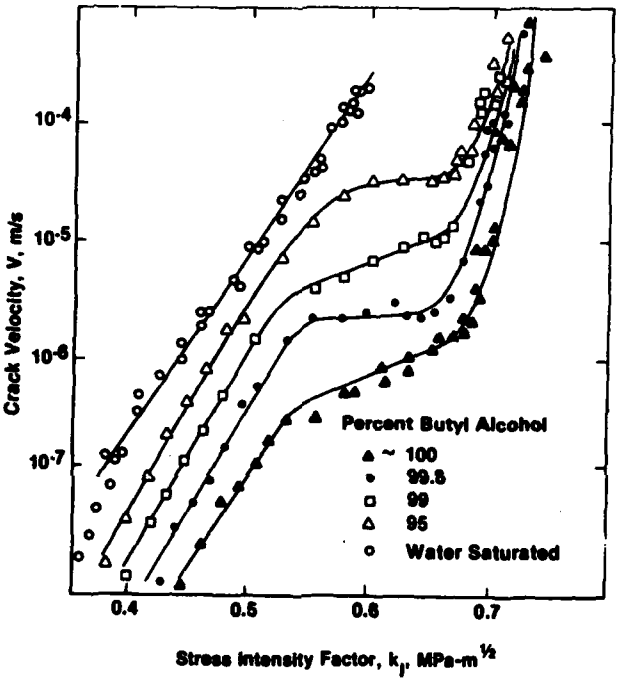

Figure 3. Crack propagation in butyl alcohol containing water. The concentration of water is expressed in volume percent.

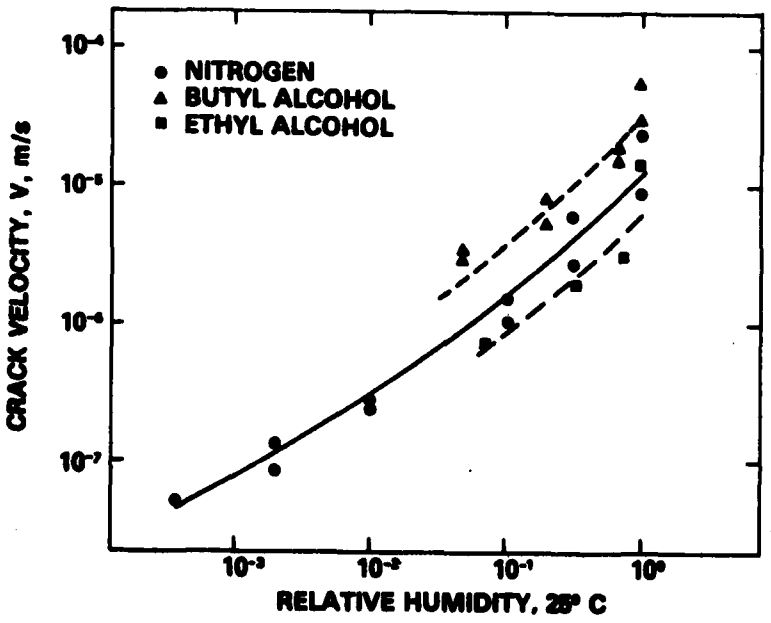

Figure 4. Crack growth rate in region I as a function of relative humidity. Data are taken from figures 2 and 3 at an applied stress intensity factor of 0.563 MPa-$m^{\frac{1}{2}}$.

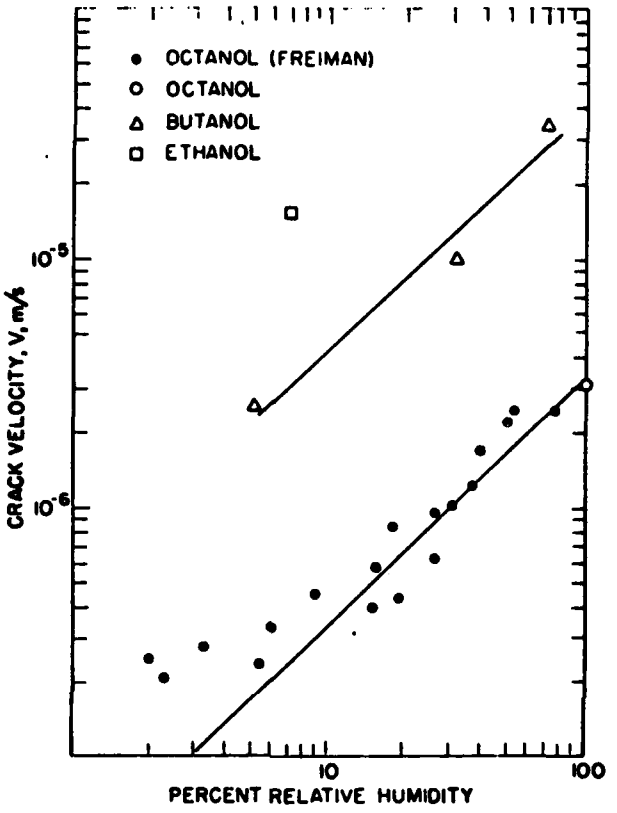

Figure 5. Crack growth rate in region II as a function of relative humidity. The data was taken from figures 2 and 3 using the plateau values of the velocity and relative humidities calculated from the concentration using thermodynamic data reported in references 7 and 8.

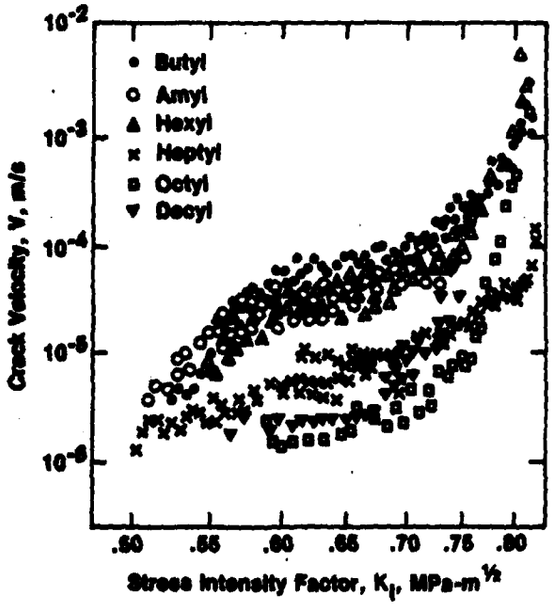

Figure 6. Crack growth data on soda-lime-silica glass collected by the double torsion technique (relaxation method) in alcohols. With the exception of the octyl alcohol, all alcohols were fully saturated. The octyl alcohol was ∿50 percent saturated.

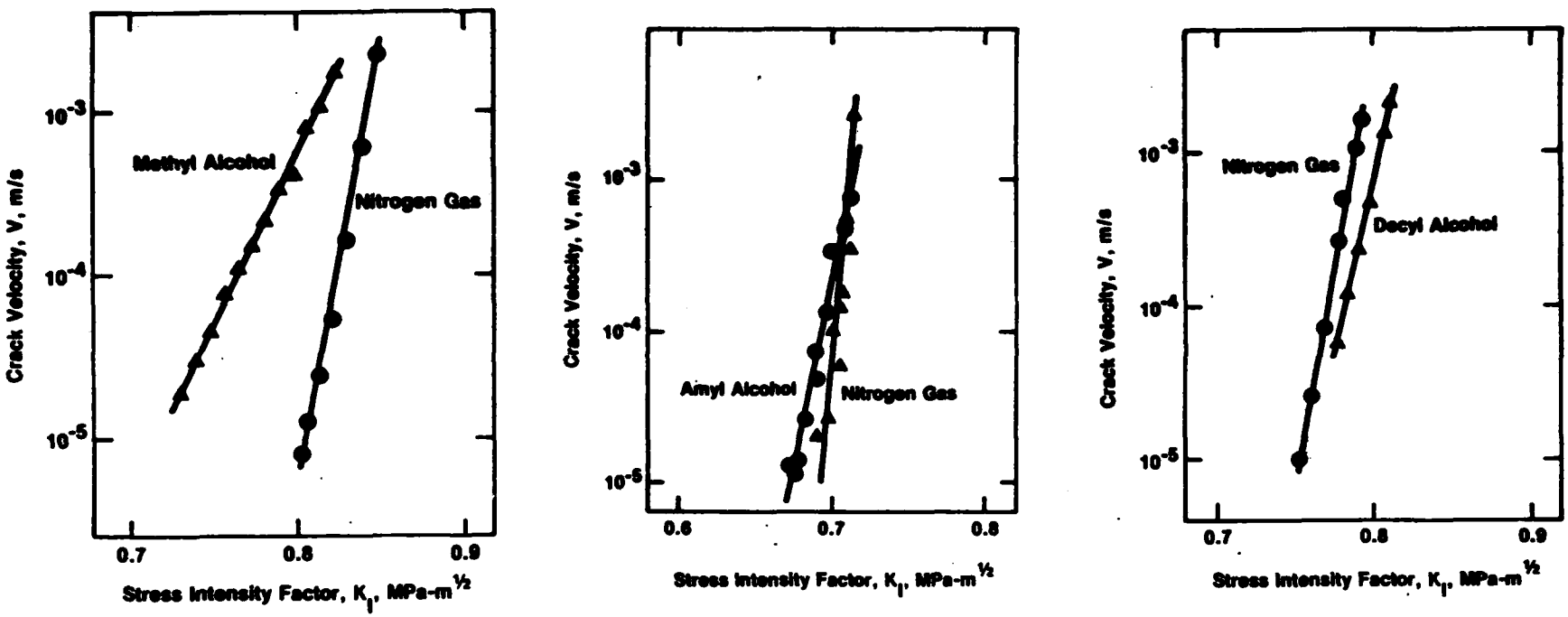

Figure 7. Region III crack growth data collected on soda-lime-silica glass by the double torsion technique (relaxation method) in dry nitrogen gas, and in methyl, amyl and decyl alcohols. Note the shift in the curve to higher values of K_I and the increase in the slope of the crack growth curve as the chain length of the alcohol is increased.

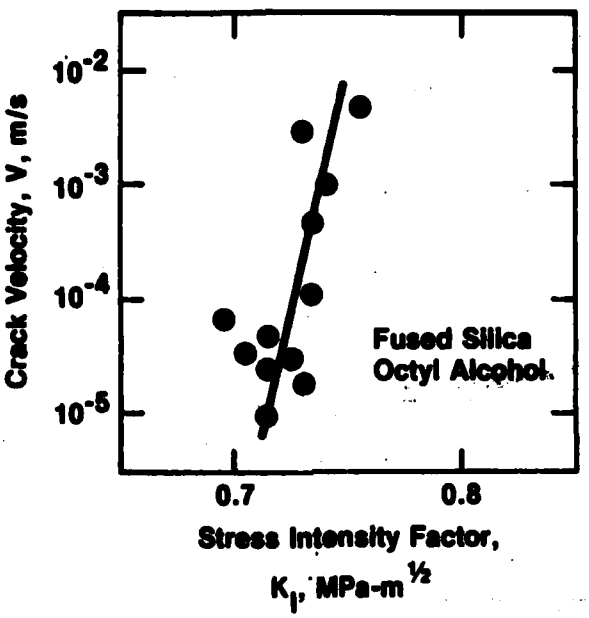

Figure 8. Region III crack growth data collected on silica glass (C7940) by the double cantilever beam technique (constant moment method).

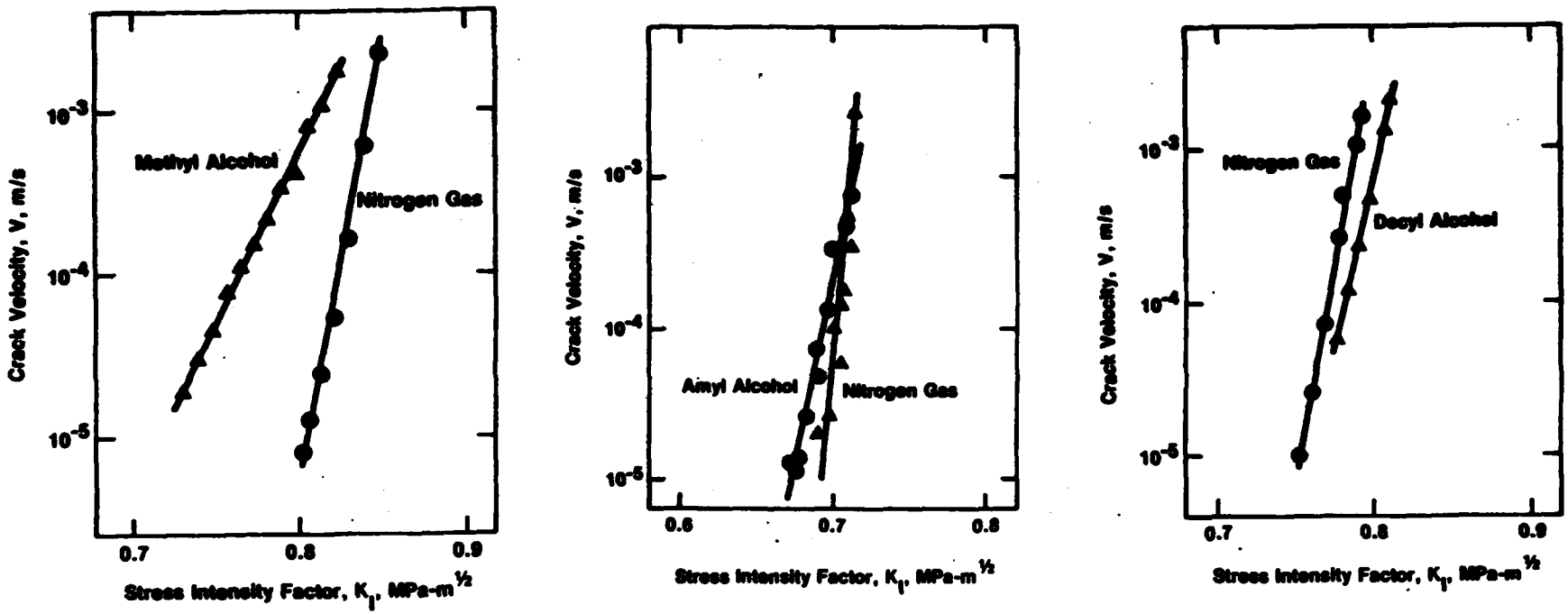

Figure 7. Region III crack growth data collected on soda-lime-silica glass by the double torsion technique (relaxation method) in dry nitrogen gas, and in methyl, amyl and decyl alcohols. Note the shift in the curve to higher values of K_I and the increase in the slope of the crack growth curve as the chain length of the alcohol is increased.

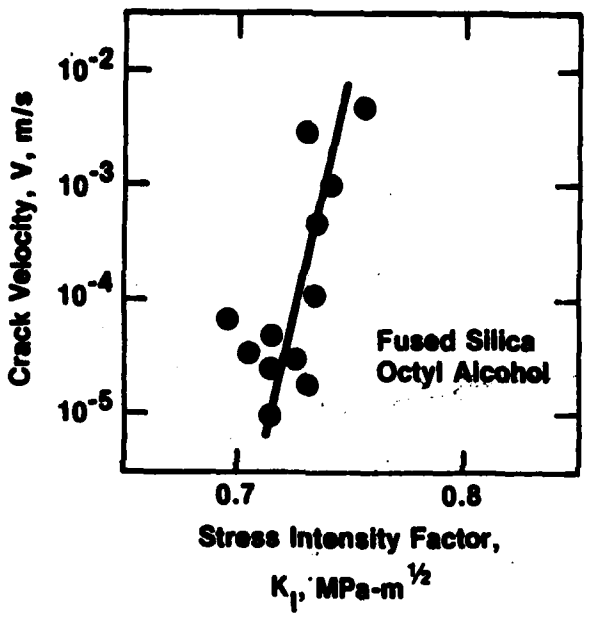

Figure 8. Region III crack growth data collected on silica glass (C7940) by the double cantilever beam technique (constant moment method).

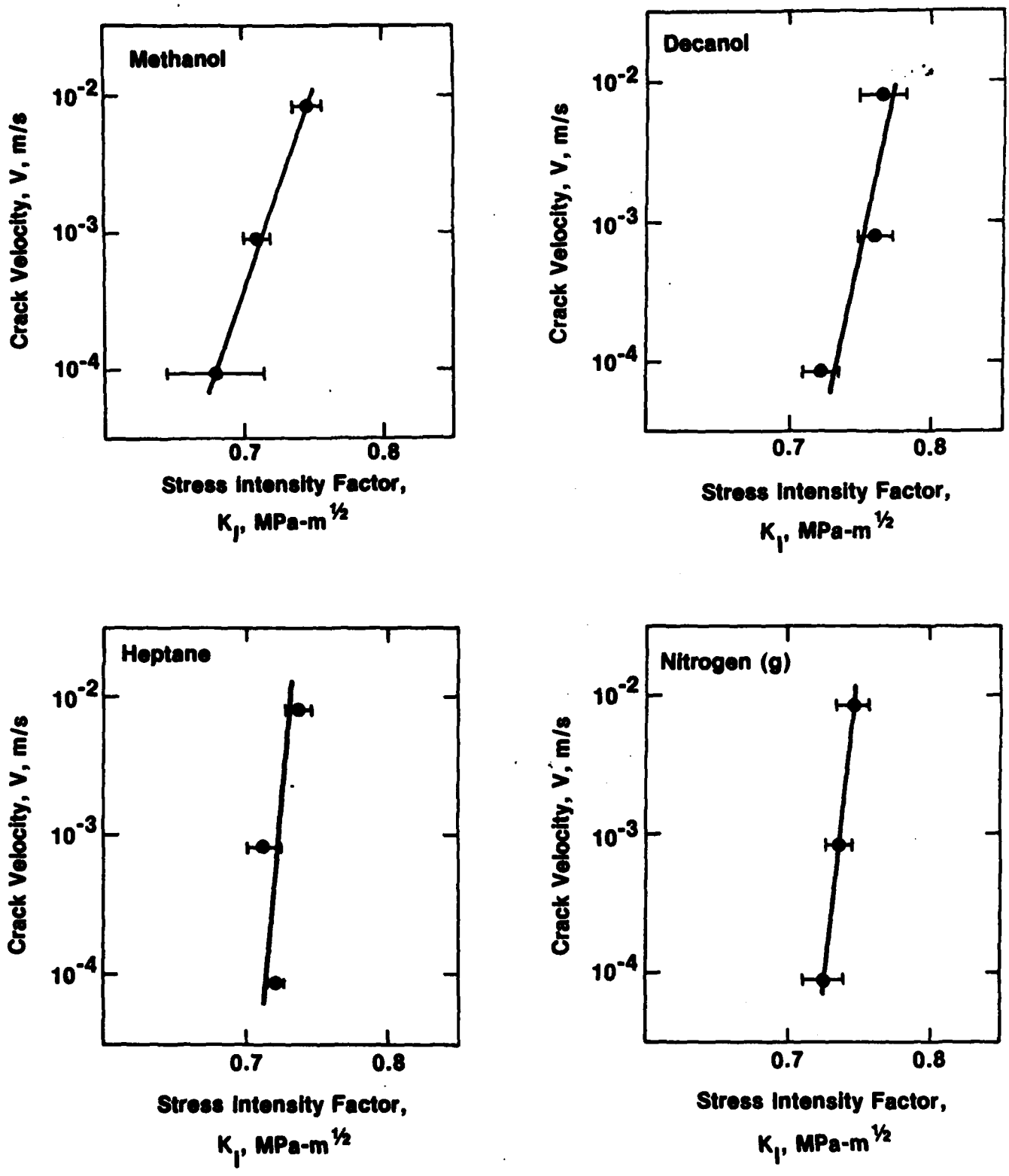

Figure 9. Region III crack growth data collected on soda-lime-silica glass by the double torsion technique (plateau method) in dry nitrogen gas and in methyl alcohol, decyl alcohol and heptane.

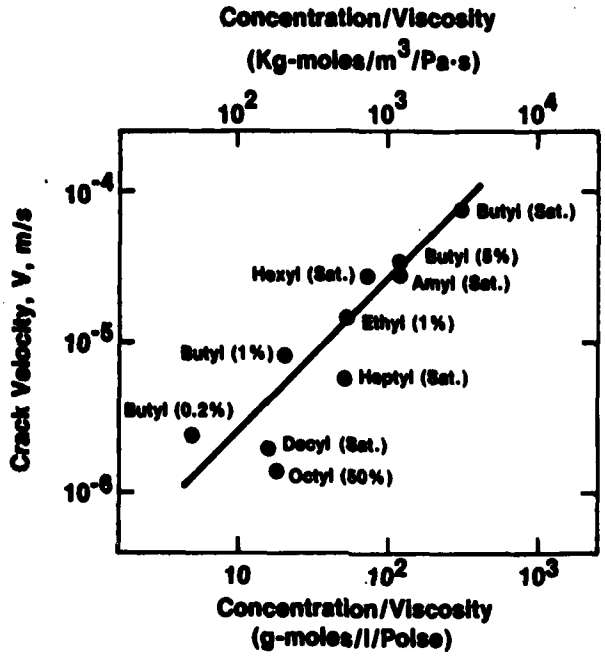

Figure 10. Plot of the crack velocity in region II as a function of the ratio of the molar concentration to the viscosity. Crack growth data on the alcohols taken from figures 2, 3 and 6.

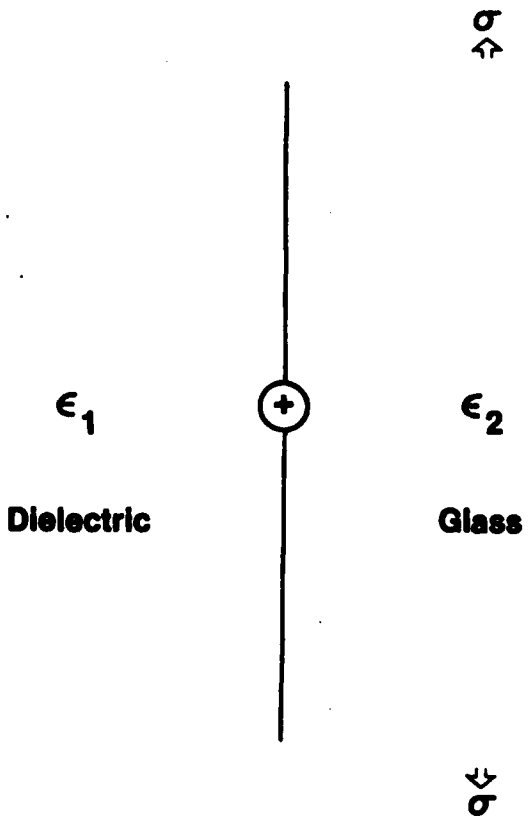

Figure 11. Schematic of model used to determine the electrostatic component of the activation volume.

AD-A136 729 STRESS CORROSION OF CERAMIC MATERIALS(U) NATIONAL BUREAU OF STANDARDS WASHINGTON D C INORGANIC MATERIALS DIV* S W FREIMAN ET AL. 01 NOV 83 N00014-79-F-0030 2/2

UNCLASSIFIED F/G 11/2 NL

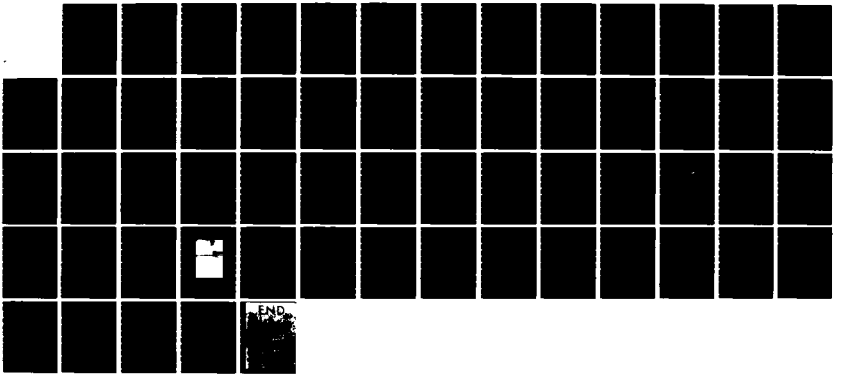

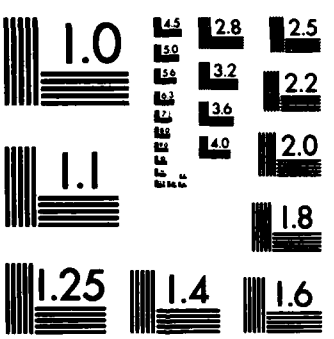

MICROCOPY RESOLUTION TEST CHART
NATIONAL BUREAU OF STANDARDS-1963-A

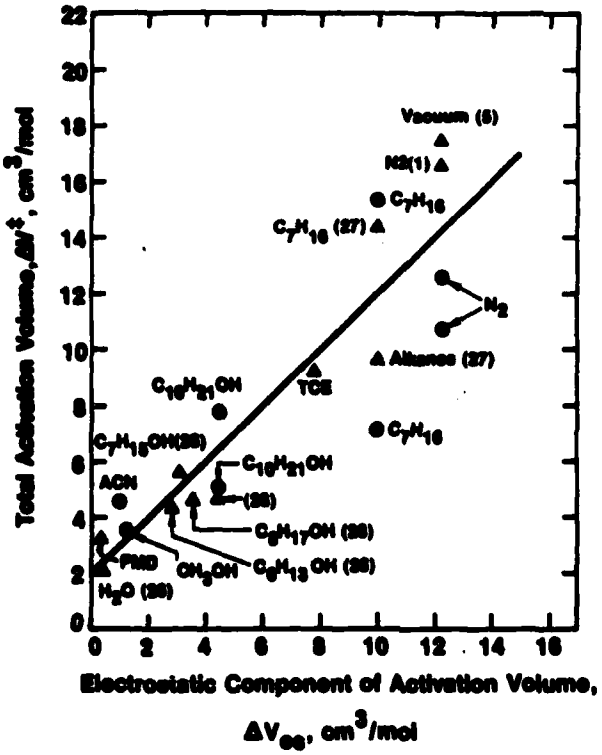

Figure 12. Plot of the total activation volume (eq. 9) as a function of the electrostatic component of the activation volume (eq. 15). The value of $\partial\varepsilon_1/\partial P$ (-9.72×10^{-11} Pa^{-1}) was taken from data by Colwell[30] collected on an alkali containing glass made at NBS. Double cantilever beam data are indicated by circles, double torsion data by triangles. Data taken from the literature are identified by reference numbers on the figure. ACN is an abreviation for acetonitrile; FMD is an abbreviation for formamide; TCE is an abbreviation for trichlorethylene. The other chemical symbols are standard chemical designations.

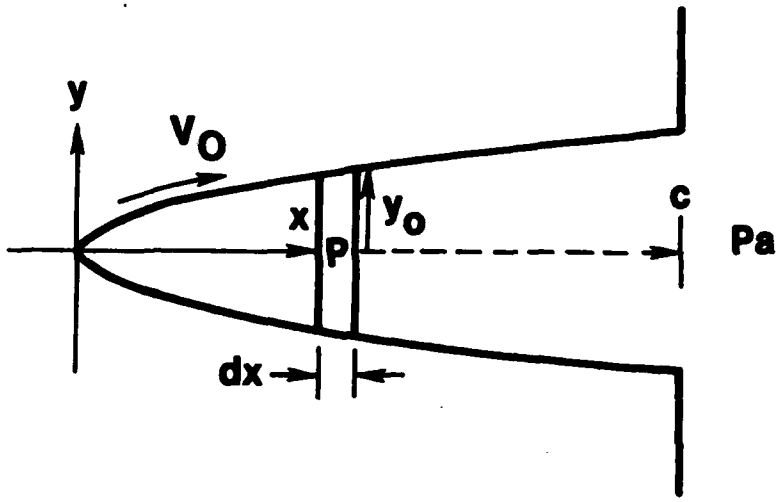

Figure 1A: Schematic diagram of parabolic shaped surface crack.

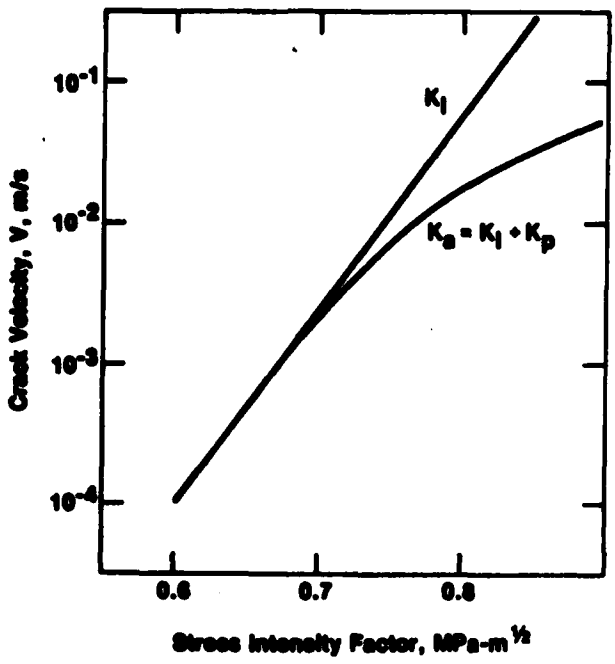

Figure 2A: Calculated effect of fluid viscosity on v-K_I curve: soda-lime-silica glass in water. The K_I portion of the curve is linear extrapolation of data collected at velocities less than 10^{-3} m/s.

To be published in ASTM STP XXX, "Methods for Assessing the Structural Reliability of Brittle Materials," 1984.

EFFECT OF MULTIREGION CRACK GROWTH ON PROOF TESTING

S.M. Wiederhorn
S.W. Freiman
E.R. Fuller, Jr.
National Bureau of Standards

H. Richter
Fraunhofer-Institut fur Werkstoffmechanik

ABSTRACT

The effect of subcritical crack growth on proof testing is examined. Crack velocity curves obtained by fracture mechanics techniques are used to predict theoretical strength distributions for specimens that survive proof testing. These theoretical distributions are then compared with experimental distributions obtained on soda-lime silica glass slides. The comparison reveals a strong sensitivity of the proof test results to the exact position and shape of the crack growth curve. Minor changes in the crack growth curve result in major shifts in position and shape of the strength distribution curves after proof testing. The importance of crack geometry and specimen configuration to crack growth behavior, and hence to the strength distribution, is emphasized.

1. INTRODUCTION

In order to improve the reliability of ceramic materials in structural applications, proof testing is often used as a method of controlling the strength distribution. Weak components are broken by the proof stress leaving a population of components with a minimum value of the strength, which in the absence of subcritical crack growth, is equal to the stress used during the proof test. Thus, proof testing truncates the strength distribution, and guarantees that all components will be at least as strong as the minimum value. Because of its simplicity, proof testing has been used successfully as a basis of design in many structural applications.[1-10]

Potential problems in the application of proof testing occur when subcritical crack growth accompanies proof testing. An example of this is seen in a recent study on soda-lime silica glass tested in air or water.[11] It was shown that, for certain test conditions, the proof test did not truncate the strength distribution. Furthermore, test results did not fully agree with the theory that was used to explain them.[12] The study suggested the need for additional research on the effect of multiregion crack growth on proof testing. It is because of this need that the present study was conducted. The study is similar to one recently completed by Ritter et al.[13], and the results are complementary to those obtained by those authors.

2. EXPERIMENTAL PROCEDURE

Heptane was chosen as a test medium for this study because of its low affinity for water. At normal temperatures and pressures heptane contains only ~ 50 ppm water, which corresponds to a partial pressure of water equal to 30% relative humidity. The net effect of the low concentration of water is to suppress region II crack growth behavior to a velocity of ~ 10^{-6} m/s, but to leave the curve for region I crack growth virtually unchanged. The range of

the crack growth curve in region II, 0.5 MPa-$m^{1/2}$ to 0.7 MPa-$m^{1/2}$, is greater than that obtained in most other environments, and therefore, is expected to enhance the effect of multiregion crack growth on proof testing.

Proof-test specimens were unannealed microscope slides with dimensions of 75 x 25 x 1 mm. Test conditions and the number of specimens used in each test are given in Table 1. All specimens were loaded to the proof load in four-point bending at a rate of 33 MPa/s. As the equipment was automated to reduce the load as soon as the proof test load was reached, the hold time at the proof test load was less than 0.1 s and is assumed to be zero in the present study. Based on crack growth data reported in reference 14, and preliminary strength measurements in heptane, the unloading rates were selected to yield the maximum range of predicted effects of proof testing on the strength distribution curve after proof testing. Following the proof test, specimens were loaded to failure at a loading rate of 33 MPa/s without changing their position in the test fixture. Thus, the stress distribution within the test specimen was the same when the strength was measured as it was during the proof test.

Crack velocity data were obtained using two fracture mechanics configurations. Applied-moment, double cantilever beam specimens (75 x 25 x 1 mm) were used to collect crack velocity data over the velocity range 10^{-10} to 10^{-3} m/s; crack velocities were measured by direct observation of the crack tip as a function of time[15]. Single-edge, notched tensile specimens (130 x 25 x 2 mm)[16] were used to collect data over the velocity range 10^{-9} to 100 m/s. In the velocity range 10^{-9} to 10^{-7} m/s, velocities were measured by monitoring the crack tip visually. Higher velocity measurements were made by the use of an acoustic pulse technique described in detail elsewhere.[17] A sonic pulse was used to mark the fracture surface so

that the position of the crack front was established as a function of time. Velocities were then determined after completion of the experiment by microscopic examination of the crack surface.

To compare the crack velocity data with the strength data a computer code was designed to calculate the breaking stress of the specimens after the proof test. The computer code is a modified version of the one discussed in reference 12. Input data for the code are: (1) the Weibull parameters S_o and m obtained in the test environment (heptane); (2) a $v\text{-}K_I$ plot expressed as a piecewise power-law fit to the $v\text{-}K_I$ data; (3) the fracture mechanics parameters K_{Ic}, K_{Iscc} and Y (Y is defined by the equation $K_I = Y\sigma\sqrt{a}$ where a is the characteristic crack size, σ the applied stress and K_I the stress intensity factor)*; and (4) the proof test parameters (stressing rate during loading and unloading, proof stress, and the hold time which is assumed to be zero in the present experiment).

The computer code first calculates the initial distribution of strength from the initial distribution obtained in heptane and the input data enumerated above.** This procedure provides a common basis for comparing

---

* The value of K_{Ic} used in the present study was 0.75 MPa-$m^{1/2}$. The reason for selecting this value is discussed in the Appendix.

** The initial values of m and S_o determined in this study are listed in Table 1a of the Appendix. This calculation is needed because subcritical crack growth occurs during the strength tests. The initial distribution, calculated from the computer code, is an idealized distribution that would be determined if strength measurements could be made without the occurrence of subcritical crack growth.

crack growth data and proof test data, and was used by Ritter et al.[13] in their study. After the initial distribution has been determined, the computer code determines the effect of the proof test cycle on this distribution, by first calculating the degree of strength degradation (i.e. the amount of crack growth) during the proof test cycle, and then by calculating the breaking stress in heptane of the specimens that survived the proof test cycle. The results of this analysis can then be compared directly with experimental strength distribution data obtained in heptane. The main output of the computer code is a graphical representation in which Weibull probability coordinates are used to display the strength distribution after proof testing. On command, the computer code was capable of plotting the initial strength distribution in heptane, the calculated initial distribution, and the distribution after proof testing.

The value of Y (1.5) used in the present paper is representative of the maximum stress intensity factor at a semi-elliptical surface crack with a minor to major axis ratio of ~ 0.6.[18] This ratio was observed in the present study for indentation cracks in glass surfaces (see fig. 7, below). We assume that Y remains constant as the surface crack increases in size. This assumption permits us to use a one-dimensional model to determine the strength distribution after proof testing. For real cracks, the shape of the crack, and consequently, the value of Y probably changes during crack growth. Although this aspect of crack growth is important, the more simple treatment adopted here should permit us to identify the principal factors that influence strength degradation during proof testing.

3. RESULTS

Crack Growth Data

The results of the crack velocity measurements are given in figure 1a. Approximately 100 data points were collected by each of the two techniques. Data for the single-edge, notched (SEN) specimens were spread evenly over the velocity range 10^{-7} to 10^{2} m/s; the double cantilever beam (DCB) data were spread evenly over the velocity range 10^{-10} to 10^{-3} m/s*. Thus, the data from the single edge notched specimens are concentrated in a higher range of crack velocities than the data from the double cantilever beam specimens. Only 5 data points were obtained on single edge notched specimens at velocities of $< 10^{-7}$ m/s.

Because the two sets of velocity data overlap over much of the data range, differences between the data are shown more clearly by fitting each set of data piecewise with straight lines, figure 1b**. When this is done, the crack growth data obtained by the single-edge, notch technique appear to lie at slightly higher values of K_I than the data obtained by the double cantilever beam technique. A small lateral translation of the two sets of data by approximately 0.05 MPa-$m^{1/2}$ brings them into close coincidence, and for practical purposes, makes the two sets of data indistinguishable over most of the data range.

---

* The abbreviation SEN and DCB are changed to SE(T) and DB(Mx) in the E616-82 Standard Terminology Relating to Fracture Testing. A discussion of the terminology will be found in the 1983 Annual Book of ASTM Standards.

** A summary of the piecewise linear fit to the crack growth data is given in Table 2a of the Appendix.

The difference between the two sets of data in region II possibly results from the difference in thickness of the specimens used in the two techniques. The greater thickness of the SEN specimens increases the diffusion path for water from the bulk to the crack tip environment and suppresses the region II data to lower crack velocities. This type of data has been reported earlier by Richter.[17]

At velocities that exceed ~ 10^{-4} m/s, the slope of the v-K_I curve is observed to decrease, almost as if there were a second region II behavior. At K_I ~ 0.93 MPa-$m^{1/2}$ the crack velocity is observed to increase precipitously by about one to two orders of magnitude. This sudden increase in velocity has been attributed to cavitation of the fluid near the crack tip,[19] whereas the decrease in slope of the v-K_I curve at velocities that exceed ~ 10^{-4} m/s is probably due to viscous drag of the fluid on the fracture surfaces.[20]

Strength Data

The initial strength distribution obtained by breaking 628 microscopic slides in heptane is shown in figure 2. Expressed as a two parameter Weibull distribution, the parameters for the regression line are S_o = 112 MPa for the intercept, and m = 7 for the slope. Despite the large number of specimens tested, the curve still exhibits experimental scatter about the regression line. The applicability of the strength distribution to the specimens subjected to the proof test can be checked qualitatively by comparing the number of specimens broken during the loading portion of the proof test cycle with those predicted from figure 2. This procedure is permissible since the loading rate was the same for all 4-point bend tests in this study. As can be seen from Table 2, the measured and predicted number of failures differ by 1 percent for the medium and slow unloading rates. The difference of 7 percent (34 versus 1 perc failures) for the rapid unloading rate can be

accounted for by a four percent error in either the proof test level, or S_o for the proof tested specimens. In view of this small difference in strength, we feel justified in using the Weibull parameters determined from figure 2 to describe the underlying strength distributions.

Results of the proof test study (figure 3) indicate the occurrence of a large number of failures below the proof stress for all three unloading rates. For the medium unloading rate approximately 42 percent of the specimens failed below the proof stress when they were reloaded to failure. For the rapid and slow unloading rates 16 percent of the survivors failed below the proof stress upon reloading to failure. This decrease in strength is consistent with theoretical expectations, since subcritical crack growth is expected to weaken all specimens that survive the proof test. Specimens that are weakened most by the proof test are those with strengths that lie closest to the proof test stress prior to testing. The weakest specimen after testing had strengths of 74, 61 and 50 percent of the proof-stress for the rapid, medium and slow unloading rates respectively. This finding agrees with that reported by Ritter et al.[13] who noted that the strength degradation of specimens just passing the proof test is greater as the unloading rate is decreased.

The strength distribution curves shown in figure 3 give little indication that the proof test truncated the distribution curves. Only the fastest unloading rate gave evidence of truncation. However for this curve, a large number of specimens broke at strengths that were less than the proof-stress. Strength distribution curves for the medium and slow unloading rates differ only slightly from the initial strength distribution. Because of the large number of specimens tested, however, we believe that the small changes in shape and position of strength distribution curves shown in figure 3 are statistically significant. As will be shown, these changes in shape and

position can be explained by the occurrence of subcritical crack growth during the proof-test.

4. COMPARISON OF CRACK VELOCITY DATA WITH PROOF TEST DATA

Strength Distribution Curves

A comparison of the strength distribution curves with the curves calculated from the v-K_I data are given in figure 4. The straight lines in this figure represent the initial distribution of specimen strengths obtained in heptane. The data points were selected from figure 3 to indicate the location of the data; not all of the data points are given. The curves in figure 4 are the theoretical estimates of the strength distribution after proof testing, determined from the crack velocity data in figure 1b.

For the rapid unloading-rate, the two theoretical curves predict sharply truncated, strength distributions. Considering this prediction, few strengths should have been measured with values of less than ~ 100 MPa. However, in contrast to this expectation, the experimental curve was not sharply truncated; approximately 16 percent of the specimens broke at stresses less than 100 MPa. Although the experimental data fall along the theoretical curves at strength levels greater than 100 MPa, there is a low-strength "tail" in the data that is not explained by either theoretical curve. This "tail" was also observed by Ritter et al.[13] in their recent study of soda-lime silica glass proof tested in heptane.

The strength distribution for the rapid unloading rate (figure 4) differs considerably from the distribution obtained in an earlier study in which the proof testing was conducted in dry nitrogen gas.[11] In the earlier study, the experimental data closely approximated the theoretical curve. The difference in results between studies is probably not attributable to water in the environment. In both studies the unloading rate was sufficiently fast that

the strength degradation during the proof test should have been controlled by the "water free" portions of the crack growth curves. It is possible that the difference in results is due to physical rather than chemical aspects of the two environments. Viscosity, for example, is much greater for liquids than for gases; therefore viscous drag by the liquid on the crack surfaces could retard the motion of the crack and permit some specimens to survive which would otherwise have failed during the proof test. Clearly, additional studies are needed to confirm this possibility, and more generally, to explore differences in the effect of liquids and gases on the strength of materials. From a practical point of view, however, results from the present study in heptane and the earlier one in nitrogen gas suggest that proof testing in liquids may not be a wise procedure, because the strength distribution curve may not be sharply truncated when the test is performed in a liquid.

In the case of the medium and slow unloading rates (figure 4) the theoretical curves depart significantly from the experimental data: the departure is much greater than would be expected from the scatter of the experimental data. Furthermore, the two theoretical curves in these figures show a divergence that is surprisingly large considering the small difference between the crack velocity curves in figure 1. These differences between the experimental data and the theoretical curve on the one hand and the two theoretical curves on the other, suggest that the strength distribution curves after proof testing are extremely sensitive to the exact location of the curves that describe crack motion. As can be seen by comparing figure 1 with the medium and slow unloading rate curves of figure 4, small changes in the position of the $v\text{-}K_I$ curve result in very large differences in the predicted position of the strength distribution curve after proof testing. This extreme sensitivity of the strength distribution to the crack velocity also explains

the differences between the experimental and theoretical strength distribution curves in figure 4.

Maximum Crack Velocity During Proof Testing

The sensitivity of the strength distribution curves to the exact shape and position of the crack velocity curves can be understood in terms of the maximum velocity achieved by the critical flaw in the course of the proof test. During a proof test, strength loss occurs at all levels of applied stress (above the fatigue limit) as a consequence of subcritical crack growth. The strength loss is most severe where the crack velocity is highest. Thus, the high velocity regime of the $v\text{-}K_I$ diagram is most important for determining the distribution of strengths after proof testing. In fact, because most crack growth occurs at the maximum crack velocity, strength degradation should be related to the maximum velocity achieved in the course of the proof test: the higher the velocity the greater the amount of strength degradation.

To examine the relation between the maximum crack velocity during proof testing and the strength distribution curve, the maximum crack velocity was calculated for each of the points used to plot the theoretical curves shown in figure 4. The maximum velocity was determined and then printed next to each point on the theoretical curve to indicate the maximum velocity during the proof test. An example of the type of data generated is shown in figure 5 for the slow unloading rate (results for the fast and medium unloading rates are similar to figure 5, and are not discussed here). As can be seen from figure 5 the range of maximum velocities was relatively narrow for both sets of curves, covering approximately two orders of magnitude (10^{-6} to 10^{-8} m/s) for the SEN specimens and one order of magnitude (10^{-7} to 10^{-8} m/s) for the DCB specimens. Regardless of the unloading rate, or the $v\text{-}K_I$ data, the narrow velocity range was common to each of the strength distribution curves obtained

in the present study. Thus only a small portion of the $v\text{-}K_I$ plot is effective in establishing the position and shape of the strength degradation curve after proof testing. This point is illustrated in figure 6 which shows the range of crack velocities that was effective in establishing the strength degradation curves shown in figure 5. Moving the $v\text{-}K_I$ plot by a small amount dramatically changes the portion of the $v\text{-}K_I$ curve that determines the strength distribution after proof testing. For example, in figure 5 the shape of the DCB curve is determined primarily by region I crack growth behavior. Lowering the region II portion of the $v\text{-}K_I$ curve slightly, as has been done for the SEN specimen, permits a large fraction of the specimens to achieve velocities that are characteristic of region II crack growth behavior. Because the slope of the strength distribution curve depends on the slope of the crack growth curve[12], this change in crack growth behavior dramatically alters the shape of the strength distribution curve after proof testing.

The general shape and appearance of the strength distribution curves in figure 5 are a direct consequence of the fact that these curves were calculated from the crack velocity data in figure 1. Both the crack growth and strength curves are multi-regioned. Because of the importance of the maximum velocity as a determinant for strength, each segment of the strength distribution curve is related to a segment of the crack growth curve. However, the two curves are inverted relative to one another: the high velocity region of the crack growth curve maps onto the low probability region of the strength distribution curve and vice versa. Furthermore, the slopes of corresponding segments of the two curves are also related: the slope, m, of the strength distribution curve is given by n-2 where n is the slope of the crack velocity curve.[12] This one-to-one relation between the two curves plays an important role in determining the sensitivity of the strength distribution

the differences between the experimental and theoretical strength distribution curves in figure 4.

Maximum Crack Velocity During Proof Testing

The sensitivity of the strength distribution curves to the exact shape and position of the crack velocity curves can be understood in terms of the maximum velocity achieved by the critical flaw in the course of the proof test. During a proof test, strength loss occurs at all levels of applied stress (above the fatigue limit) as a consequence of subcritical crack growth. The strength loss is most severe where the crack velocity is highest. Thus, the high velocity regime of the v-K_I diagram is most important for determining the distribution of strengths after proof testing. In fact, because most crack growth occurs at the maximum crack velocity, strength degradation should be related to the maximum velocity achieved in the course of the proof test: the higher the velocity the greater the amount of strength degradation.

To examine the relation between the maximum crack velocity during proof testing and the strength distribution curve, the maximum crack velocity was calculated for each of the points used to plot the theoretical curves shown in figure 4. The maximum velocity was determined and then printed next to each point on the theoretical curve to indicate the maximum velocity during the proof test. An example of the type of data generated is shown in figure 5 for the slow unloading rate (results for the fast and medium unloading rates are similar to figure 5, and are not discussed here). As can be seen from figure 5 the range of maximum velocities was relatively narrow for both sets of curves, covering approximately two orders of magnitude (10^{-6} to 10^{-8} m/s) for the SEN specimens and one order of magnitude (10^{-7} to 10^{-8} m/s) for the DCB specimens. Regardless of the unloading rate, or the v-K_I data, the narrow velocity range was common to each of the strength distribution curves obtained

in the present study. Thus only a small portion of the v-K_I plot is effective in establishing the position and shape of the strength degradation curve after proof testing. This point is illustrated in figure 6 which shows the range of crack velocities that was effective in establishing the strength degradation curves shown in figure 5. Moving the v-K_I plot by a small amount dramatically changes the portion of the v-K_I curve that determines the strength distribution after proof testing. For example, in figure 5 the shape of the DCB curve is determined primarily by region I crack growth behavior. Lowering the region II portion of the v-K_I curve slightly, as has been done for the SEN specimen, permits a large fraction of the specimens to achieve velocities that are characteristic of region II crack growth behavior. Because the slope of the strength distribution curve depends on the slope of the crack growth curve[12], this change in crack growth behavior dramatically alters the shape of the strength distribution curve after proof testing.

The general shape and appearance of the strength distribution curves in figure 5 are a direct consequence of the fact that these curves were calculated from the crack velocity data in figure 1. Both the crack growth and strength curves are multi-regioned. Because of the importance of the maximum velocity as a determinant for strength, each segment of the strength distribution curve is related to a segment of the crack growth curve. However, the two curves are inverted relative to one another: the high velocity region of the crack growth curve maps onto the low probability region of the strength distribution curve and vice versa. Furthermore, the slopes of corresponding segments of the two curves are also related: the slope, m, of the strength distribution curve is given by n-2 where n is the slope of the crack velocity curve.[12] This one-to-one relation between the two curves plays an important role in determining the sensitivity of the strength distribution

curve to the crack velocity curve, especially when only a narrow range of crack velocity data is relevant to the strength distribution curve, as is the case in the present study.

5. CORRELATION BETWEEN THEORY AND EXPERIMENT

In view of the above discussion, the lack of correlation between the experimental and theoretical strength distributions can be understood in terms of the high sensitivity of the strength distribution curve to the exact shape and position of the crack growth curve. Any physical or chemical process that disturbs the position of this $v\text{-}K_I$ curve, or prevents an accurate determination of the curve can affect the position and shape of the strength distribution curve, and thus result in a lack of agreement between the theoretical and experimental strength distribution curves. Some of the causes of poor agreement between the theoretical and experimental distribution curves will now be discussed. As will be seen, the causes are of two types: experimental errors that prevent an accurate determination of the "true" $v\text{-}K_I$ curve; and physical or chemical effects that alter the behavior of small surface cracks in such a way that their response to applied stress is significantly different from that obtained on large macroscopic cracks. Of the two causes, the latter are more fundamental to our understanding of crack growth and strength degradation. However, in practice both can be equally important for the determination of accurate strength distribution curves.

Experimental Uncertainty

The experimental uncertainty to be associated with the crack growth data is illustrated in figure 1, by the small difference in position of the two $v\text{-}K_I$ curves and by the random scatter of the data of each curve. The difference between the two curves (figure 1a) represents a systematic uncertainty in measurement that has its origin in the technique used to make

the measurement. This type of error can be reduced only by more thorough theoretical and experimental investigations of the two crack velocity techniques to trace the origin of the measurement difference. The random error in figure 1 is given by the scatter of data about their mean value for any given value of K_I or v. As can be seen from this figure the scatter in K_I ranges from ~ 3 to 10 percent of K_I, whereas the error in v ranges from ~ 0.2 to ~ 1 order of magnitude in crack velocity, depending on the value of v and K_I and the technique used to determine the v-K_I plot. These errors are typical of those that have been reported previously in the literature for crack velocity studies on glass.

With regard to the present experiment, the experimental scatter of the data in figure 1 is sufficient to preclude a determination of the "true" v-K_I curve with sufficient accuracy to predict the position and shape of the strength distribution curve after testing. As a consequence of this finding, it is suggested that more accurate measurement techniques are needed to determine crack growth behavior. Without more accurate methods of measurement, one should be wary of using crack growth data to predict proof testing results. However, even with better measurement techniques there may be more basic reasons that strength distribution curves cannot be determined accurately from crack growth data. These reasons relate to the equivalence of crack growth data from large and small cracks.

Large versus Small Cracks

Although it is usual to assume that the growth of microscopic size cracks in ceramic materials is described by crack growth data obtained by macroscopic, fracture-mechanics techniques, there are good physical reasons why this assumption may not be valid. In other words, small cracks that control the strength of glass may not behave in the same way as large cracks

used in fracture mechanics studies. Three factors that may contribute to the difference in crack growth behavior are: (1) residual stresses due to plastic deformation at the origin of surface cracks; (2) blunting of small cracks due to stress corrosion; and (3) differences in the v-K_I curve resulting from geometric differences between large and small cracks.

Residual Stresses

The effect of residual stresses on the strength of glass was first discussed by Marshall and Lawn[21,22]. The effect results from the fact that surface cracks in glass are usually formed by mechanical damage during the grinding and polishing of glass, or by mechanical contact with hard substances after the glass has been produced. Residual stress fields always form at points of mechanical contact as a consequence of micro-plastic deformation at contact asperities. Unless the residual stresses are relieved by annealing, they contribute to the stress field that forces cracks to grow during a proof test. Therefore, these stresses should be taken into account to determine the strength distribution after proof testing. As the crack grows, the effect of residual stresses gradually becomes less important; the effect is least for the weakest specimens that survive the proof test. Hence, the effect of residual stresses on the strength distribution is expected to be most pronounced for the high probability portion of the stress distribution. In this paper it is assumed that residual stresses played little role in the strength degradation process. This assumption is supported by the fact that the proof test results in figure 3 are very similar to those obtained by Ritter et al. on annealed specimens[13]. However, to fully understand the role of residual stresses on proof testing, additional studies are clearly needed.

Crack Blunting

By applying transition rate theory to ceramic materials, Charles and Hillig[23] suggested the existence of a static fatigue limit caused by crack tip blunting in materials such as glass. At stresses above the fatigue limit, surface flaws sharpen and grow, whereas at stresses below the fatigue limit, crack tip blunting and crack arrest occurs. The Charles-Hillig theory is consistent with all known experimental data on the strength of glass. Recently, Michalske, using fracture mechanics techniques, has demonstrated a fatigue limit in soda-lime silica glass at a value of $K_I \sim 0.25$ MPa-$m^{1/2}$.[24] The fatigue limit was identified by a hysteresis in the crack velocity curve, and by microstructural features that were left on the face of a crack that was repropagated after having been blunted by stress corrosion. Resharpening of cracks in soda-lime silica glass occurs almost instantaneously when the stress-intensity factor exceeds 0.425 MPa-$m^{1/2}$. If the stress intensity for resharpening falls within the range of K_I that is effective in determining the strength distribution after proof testing, then crack blunting can have a significant effect on the shape of the strength distribution curve after proof testing. Our studies on this point are quite limited; however, they do show that crack blunting is more important for proof tests that were conducted using slow unloading rates rather than fast ones. In addition our studies show that the strongest specimens are not affected at all by the proof test, whereas the weakest ones suffer the same degree of strength degradation as would occur if there were no static fatigue limit. Additional studies to clarify the role of crack blunting on proof testing should include the establishment of resharpening kinetics and the incorporation of these kinetics into the strength treatment.

Crack Geometry

Effects of environment on both the strength and the crack growth rate have been studied by a number of investigators. Studies on soda-lime-silica glass indicate relatively good agreement between strength measurements and crack growth measurements, when measurements are conducted either in water where region I crack growth is dominant, or in an inert environment such as dry nitrogen, where region III crack growth is dominant. For both techniques the stress corrosion susceptibility, n, was found to be similar regardless of the technique used to make the measurement.* Therefore it is unlikely that the behavior of large cracks differs significantly from small ones when only region I or region III crack growth is involved in degrading the strength.[25] The same conclusion, however, may not be valid when region II crack growth occurs.

Crack growth in region II has been studied by a number of investigators. Wiederhorn[26] and Schönert et al.[27], were the first to attribute region II crack growth to an environment limited transport of water to the crack tip. Schönert et al. demonstrated that the crack front changed its shape as the crack moved from region I to region II, and again when it moved from region II to region III. When studies are conducted with through cracks in flat specimens (edge-notched or double cantilever beam specimens), the portion of the crack front in the center of the specimen always leads the portion of the

*When residual stresses effect the crack growth behavior, a correction must be made for the effect of these stresses on the stress corrosion susceptibility, n. However, even in this case, the value of n for crack growth can be related to that obtained from fatigue data.[22,23]

crack front that intersects the specimen surface in region I or III. In region II, however, the reverse is true: the portion of the crack front near the surface always leads that in the center.

Quackenbush and Frechette[28] and Richter[29] confirmed the findings of Schonert et al. and attributed crack growth in region II to a combined effect of region I and region III crack growth behavior. Since water is freely available at the specimen surface, crack motion is enhanced by water; whereas, away from the specimen surface the crack tip is starved for water because of the longer diffusion path, and crack motion is retarded. In specimens with through cracks, the cracks move as a unit in region II, the center portion of the crack being pulled along by portions near the surface. As the applied stress-intensity factor in region II is increased, the crack velocity is observed to increase, but not as rapidly as in regions I or III. Furthermore as K_I is increased, more of the crack perimeter behaves as if it were depleted of water, and finally when the outer portion of the crack is completely depleted of water, it too enters region III and the crack perimeter regains its normal shape. Thus, region II represents a transition in crack growth behavior between regions I and III; depending on the availability of water at the crack tip, different portions of the crack front behave somewhat independently as the crack moves.*

---

* In an earlier paper, Varner and Frechette[30] suggest that crack arrest occurs periodically in the central portion of the crack in region II (for studies conducted in nitrogen gas). A later study by Richter[29] (conducted in air) and by Quackenbush and Frechette[28] (conducted in decane) gave no indication of crack arrest in region II. The results of the present study on indentation crack also give no indication of crack arrest in region II.

The effects just described also occur for surface cracks that are responsible for the failure of strength specimens. The effect is shown in figure 7 which illustrates successive positions of a surface crack that was propagated to failure in normal heptane. The crack was formed by the use of a diamond pyramidal indenter; the velocity was measured by the use of a sonic pulse generator. The crack position is indicated by ripple marks on the fracture surface, each set of marks indicating successive positions of the crack as it grows larger. In figure 7a the ripple marks closest to the indentation (half-way between the two arrows) represent region I crack growth, whereas those furthest from the indentation represent region III crack growth. The arrows mark the transition between region II and region III crack growth. As can be seen from figure 7b, the shape of the crack in region II differs from the normal semi-elliptical shape that is characteristic of region I or region III crack motion. As in the case of the through cracks discussed above, the change in shape can be attributed primarily to water depletion at portions of the crack that are distant from the surface. Because of water depletion, these portions of the crack move slower than those near surface where the water is plentiful. Thus, the shape of the surface crack is modified by the water content of the environment near the crack perimeter. Because of the difference in geometry between small surface cracks and the large cracks that are typical of fracture mechanics specimens, physical constraints on the crack front are different for the two types of cracks*. Therefore, crack growth in region II will probably not be the same for the two types of cracks even though crack growth in region II represents a

*For example, K_I for an elliptical crack can vary by as much as 50 percent along the crack perimeter.

transition in behavior between regions I and III for both crack types. The differences between the theoretical and experimental strength distribution curves in figure 4 may be the result of these geometric considerations. Substantiation of this belief, however, will require the solution of three dimensional elasticity/diffusion boundary value problems to determine exactly how crack growth occurs for surface cracks. This task is beyond the scope of the present paper.

6. SUMMARY

This paper presents a critical analysis of the applicability of crack growth data to proof testing as a means of improving the reliability of structural ceramic materials. In particular, the paper deals with the question of predicting strength distribution curves from crack growth data obtained by standard fracture-mechanics techniques. To deal with this question, both strength data and crack growth data were obtained on soda-lime-silica glass specimens that were tested in liquid heptane. Crack growth data were obtained by the applied-moment, double-cantilever beam (DCB) technique, and by the single-edge, notch tension (SEN) technique. Although there were systematic differences between the two sets of crack velocity data, a partial overlap of the data was observed over most of the data range. Considering that two different test techniques were used to collect the data, the two sets of crack growth data were considered to be consistent with the degree of scatter that has been reported for crack growth data.

Proof-test experiments were conducted on soda-lime silica glass microscope slides that were subjected to 4-point bending. Strength distribution curves after proof testing were obtained using three different unloading rates during the proof test cycle. Truncation of the strength data was obtained only for specimens subjected to a rapid (165 MPa/s) rate of

unloading. Specimens that were subjected to either slow (0.33 MPa/s), or medium (3.3 MPa/s) rates of unloading gave curves that hardly differed from the initial strength distribution curve. Furthermore, the three strength distribution curves obtained from the proof-tested population of glass slides could not be predicted from the crack growth data obtained in the present experiment.

In the course of our discussion and analysis, we concluded that the position and shape of the strength distribution curve after proof testing was highly sensitive to the exact position and shape of the crack growth data. We were able to show that slight shifts in the position, or shape of the $v\text{-}K_I$ plot resulted in substantial changes in the position and shape of the predicted strength distribution curve. As a consequence, any physical or chemical process that disturbs or changes the position of the crack growth curve, or prevents an accurate determination of the crack growth curve will cause the strength distribution curve determined from crack growth data to differ considerably from the one determined experimentally. Specific causes of the differences are (1) the experimental uncertainty inherent in obtaining $v\text{-}K_I$ data, and (2) physical and chemical effects that alter the behavior of small surface cracks so that their response to applied stress differs significantly from the response of large macroscopic cracks typical of fracture mechanics specimens.

From a practical point of view our strength data suggests that proof testing in an "inert" liquid may not be a wise procedure because only a modest degree of truncation is observed (only at high unloading rates) and because after proof-testing many specimens have strengths that lie below the proof test level. Based on these observations and results from an earlier study, which included proof test studies in dry nitrogen gas, we suggest that proof

testing be conducted in dry, gaseous environments, and that rapid rates of unloading be used to assure structural reliability. When this procedure is followed, satisfactory truncation of the strength distribution can be achieved.

Acknowledgement: This work was supported by the Office of Naval Research, Metallurgy and Ceramics Program. The technical assistance of Mark Gollup and Meers Oppenheim and the helpful technical discussions with B.R. Lawn are gratefully acknowledged.

REFERENCES

1. S.M. Wiederhorn, "Reliability, Life Prediction, and Proof Testing of Ceramics," pp. 635-55 in Ceramics for High Performance Applications, ed. by J.J. Burke, A.G. Gorum, and R.N. Katz, Brook Hill Pub. Co., Chestnut Hill, MA (1974).
2. J.E. Ritter, Jr., "Engineering Design and Fatigue Failure of Brittle Materials," pp. 667-686 in Fracture Mechanics of Ceramics, Vol. 4, ed. by R.C. Bradt, D.P.H. Hasselman and F.F. Lange, Plenum Press, N.Y. (1978).
3. J.N. Humenik and J.E. Ritter, Jr., "Susceptibility of Alumina Substrates to Stress Corrosion Cracking During Wet Processing," Bull. Am. Ceram. Soc. 59, 1205 (1981).
4. S.M. Wiederhorn, A.G. Evans, and D.E. Roberts, "A Fracture Mechanics Study of the Skylab Windows," pp. 829-41 in Fracture Mechanics of Ceramics, Vol. 2, ed. by R.C. Bradt, D.P.H. Hasselman, and F.F. Lange, Plenum Press, New York (1974).
5. S.M. Wiederhorn, A.G. Evans, E.R. Fuller, and H. Johnson, "Application of Fracture Mechanics to Space-Shuttle Windows," J. Am. Ceram. Soc. 57, 319-23 (1974).
6. J.E. Ritter, Jr., and S.A. Wulf, "Evaluation of Proof Testing to Assure Against Delayed Failure," Bull. Am. Ceram. Soc. 57, 186-190 (1978).
7. J.E. Ritter, Jr., J.M. Sullivan, Jr., and K. Jakus, Application of Fracture Mechanics Theory to Fatigue Failure of Optical Glass Fibers," J. Appl. Phys., 49, 4779-82 (1978).

8. D.G. Greene, J.E. Ritter, Jr., and F.F. Lange, "Evaluation of Proof Testing as a Means of Assuring Mission Success for the Space Shuttle Thermal Protection System," Material and Process Application-Land, Sea, Air, Space, Vol. 26, Science of Advanced Materials and Process Engineering Series, pp. 257-269 (1981).

9. D.G. Greene, J.E. Ritter, Jr. and F.F. Lange, "Fracture Behavior of Low Density Fibrous Ceramic, J. Am. Ceram. Soc. 65, 141-146 (1982).

10. J.E. Ritter, Jr., "Assessment of the Reliability of Ceramics," Fracture Mechanics of Ceramics, Vol. 5 and 6, R.C. Bradt, A.G. Evans, D.P.H. Hasselman, and F.F. Lange, eds., Plenum Press, New York, to be published.

11. J.E. Ritter, Jr., P.B. Oates, E.R. Fuller, Jr., and S.M. Wiederhorn, "Proof Testing of Ceramics: I. Experiment," J. Mat. Sci. 15, 2275-81 (1980).

12. E.R. Fuller, Jr., S.M. Wiederhorn, J.E. Ritter, Jr., and P.B. Oates, "Proof Testing of Ceramics: II. Theory," J. Mat. Sci. 15, 2282-95 (1980).

13. J.E. Ritter, Jr., K. Jakus, G.M. Young, and T.H. Service, J. Comm. Am. Ceram. Soc. 65, C134-C135 (1982).

14. S.W. Freiman, "Effects of Straight-Chain Alkanes on Crack Propagation in Glass," J. Am. Ceram. Soc. 58 339-340 (1975).

15. S.W. Freiman, D.R. Mulville and P.W. Mast, "Crack Propagation in Brittle Materials," J. Mat. Sci. 8, 1527-34 (1973).

16. H. Richter, "Experimentelle Untersuchungen zur Rissausbreitung in Spiegelglass im Geschwindigheitbereich 10^{-3} bis 5×10^{3} mm/s," Institut fur Festkorpermechanik der Fraunhofer-Gesselschaft e.V. Freiburg i. Br. Rosastrasse 9, Dezember 1974.

17. H. Richter, "Der Einfluss der Probendicke auf die Rissausbreitung in Glas," pp. 447-457, in Proceedings of the XIth International Congress on Glass, Prague 1977, Vol. II.

18. G.R. Irwin and P.C. Paris, "Fundamental Aspects of Crack Growth and Fracture," pp. 1-46 in Fracture, An Advanced Treatise, Vol. III, H. Liebowitz, ed., Academic Press, New York (1971).

19. T.A. Michalske and V.D. Frechette, "Dynamic Effects of Liquids on Crack Growth Leading to Catastrophic Failure in Glass," J. Am. Ceram. Soc. 63, 603-609 (1980).

20. S.M. Wiederhorn, S.W. Freiman, E.R. Fuller, Jr., and C.J. Simmons, "Effects of Water and Other Dielectrics on Crack Growth," J. Mat. Sci. 17, 3460-3478 (1982).

21. D.B. Marshall and B.R. Lawn, "Residual Stress Effects in Sharp Contact Cracking, I. Indentation Fracture Mechanics," J. Mat. Sci. 14, 2001-2012 (1979).

22. D.B. Marshall, B.R. Lawn and P. Chantikul, "Residual Stress Effects in Sharp Contact Cracking, II. Strength Degradation," J. Mat. Sci. 14, 2225-2235 (1979).

23. R.J. Charles and W.B. Hillig, pp. 511-27 in Symposium on Mechanical Strength of Glass and Ways of Improving It. Florence, Italy, September 25-29, 1961. Union Scientifique Continentale du Verre, Charleroi, Belgium, 1962.

24. T.A. Michalske, "The Stress Corrosion Limit: Its Measurement and Implications," Fracture Mechanics of Ceramics, Vol. 5 and 6, R.C. Bradt, A.G. Evans, D.P.H. Hasselman and F.F. Lange, eds., Plenum Press, New York, to be published.

25. T.P. Dabbs, B.R. Lawn and P.L. Kelly, "A Dynamic Fatigue Study of Soda-Lime Silicate and Borosilicate Glasses using Small Scale Indentation Flaws," Phys. Chem. Glasses, 23, 58-66 (1982).

26. S.M. Wiederhorn, "Influence of Water Vapor on Crack Propagation in Soda-Lime Glass," J. Am. Ceram. Soc. 50 407-414 (1967).

27. K. Schönert, H. Umhauer and W. Klemm, "The Influence of Temperature and Environment on the Slow Crack Propagation in Glass," pp. 474-482 in Fracture 1969. Proceedings of the Second International Conference on Fracture, Brighton, 1969.

28. C.L. Quackenbush and V.D. Frechette, "Crack-Front Curvature and Glass Slow Fracture," J. Am. Ceram. Soc. 61, 402-406 (1978).

29. H. Richter, "Rissfrontkrümmung und Bruchfläschenmarkierung im Übergangsbereich der Bruchgeschwindigkeit," Glastech. Ber. 47, 146-7 (1974).

30. J.R. Varner and V.D. Frechette, "Fracture Marks Associated with Transition Region Behavior of Slow Cracks in Glass," J. Appl. Physics, 42, 1983-1984 (1971).

31. K.C. Kapur and L.R. Lamberson, "Reliability in Engineering Design," John Wiley and Sons, New York (1977).

32. S.M. Wiederhorn, "Fracture Surface Energy of Glass," J. Am. Ceram. Soc. 52, 99-105 (1969).

TABLE 1. TEST CONDITIONS FOR SODA-LIME SILICA GLASS PROOF TESTED IN HEPTANE*

LOADING RATE (MPa/s)	UNLOADING RATE (MPa/s)	PROOF LOAD (MPa)	NUMBER TESTED	PROOF TEST SURVIVORS
33	STRENGTH TESTS	----	628	----
33	165	103	673	417
33	3.3	100.5	630	179
33	0.33	90.5	497	143

*All strength measurements were made by 4-point bending using an inner span of 19 mm and an outer span of 64 mm.

TABLE 2. TEST OF WEIBULL DISTRIBUTION

s_0 = 112 MPa, M=7

UNLOADING RATE (MPa/s)	PROOF LOAD (MPa)	FRACTION BROKEN DURING LOADING	
		MEASURED	PREDICTED
165	103.0	0.34	0.41
3.3	100.5	0.38	0.37
0.33	90.5	0.21	0.20

APPENDIX A

The Selection of K_{Ic}

In developing the computer code used in the present study, we found it necessary to establish a criterion for failure. A standard, albeit somewhat idealized, failure criterion is to assume that failure occurs when the strength, S, is equal to the applied stress, σ.[31] In fracture mechanics terms, this criterion is equivalent to assuming $K_I = K_{Ic}$ and $d K_I/da \geq 0$ for the most critical crack.

In more practical terms, however, failure by crack growth is determined by a crack velocity criterion: failure occurs when the crack is moving so rapidly that the specimen cannot be unloaded fast enough to avoid failure. The critical velocity for failure depends on the rate of unloading: as the unloading rate is increased, the critical velocity also is increased. This failure criterion is exactly applicable to proof-testing, since the number of specimens that pass the proof test is determined by the rate of unloading.

When the v-K_I curve is steep as it is for soda-lime silica glass in nitrogen gas, the two criteria are almost identical. The value of K_{Ic} is insensitive to the crack velocity, and the value selected (within region III) for K_{Ic} does not affect the truncation that results from proof testing. However, when the v-K_I curve is complicated by physical effects, such as viscous drag or cavitation, as it is for soda-lime silica glass tested in heptane, then one must be concerned with the equivalence of the two failure criteria. In particular, it must be determined whether K_{Ic} determined by "conventional" methods can be used to establish a criterion for crack stability for a proof test.

In the present study we used a value of K_{Ic} = 0.75 MPa$\sqrt{m}$ as obtained on DCB specimens that were loaded to failure in dry nitrogen gas.[32] To test the validity of this convenitonal value of K_{Ic}, the v-K_I curve for the SEN specimen, figure 1b, was used to determine a strength distribution curve for three values of "K_{Ic}": 0.75, 0.90 and 1.10 MPa-$m^{1/2}$. For each of the proof test cycles used in the present study, the strength distribution after proof testing and the number of specimens that broke during the proof test were found to be independent of the value of "K_{Ic}" used in the program. The reason for this apparent insensitivity of the strength distribution curve to K_{Ic} is the fact that the distribution curve is determined by a relatively narrow range of velocities on the v-K_I plot. As long as "K_{Ic}" lies at a value that is above this range of velocities, the strength curve will not be sensitive to its value. The main effect of changing "K_{Ic}" is to shift the position of the initial strength distribution*. Increasing the value of "K_{Ic}" increases the value of S_o and decreases the value of m for the initial distribution. Thus, "K_{Ic}" plays the role of a scaling factor in a proof test. In view of this conclusion, the fracture mechanics value of K_{Ic} (i.e. 0.75 MPa-$m^{1/2}$) was used for the present study.

---

*The initial distribution referred to here is the distribution calculated from the input data discussed in Section 2.

TABLE 1a. INPUT DATA: WEIBULL PARAMETERS

Condition	S_o	m
Experimental	112	7
Inert: calculated from v-K_I data		
SEN	123.1	6.55
DCB	130.1	6.28

TABLE 2a. CRACK GROWTH DATA

K_{Ic} = 0.75 MPa-$m^{1/2}$

K_{Iscc} = 0.2 MPa-$m^{1/2}$

Y = 1.5

Slopes and Intercepts for v-K_I curves; values based on Pa as units for stress

Condition	Region	Slope, n	ln A
SEN	1	16.59	- 233.13
	2	5.07	- 81.90
	3	245.66	-3315.52
	4	56.00	- 762.88
	5	13.02	- 180.91
	6	6.97	- 98.23
	7	382.50	-5255.06
	8	16.03	- 218.66
	9	6.60	- 88.35
DCB	1	17.10	- 237.95
	2	4.09	- 67.85
	3	125.83	-1700.19

Note: The number of significant figures given in the above parameters are included for purposes of calculation only, and do not indicate accuracy of the various parameters.

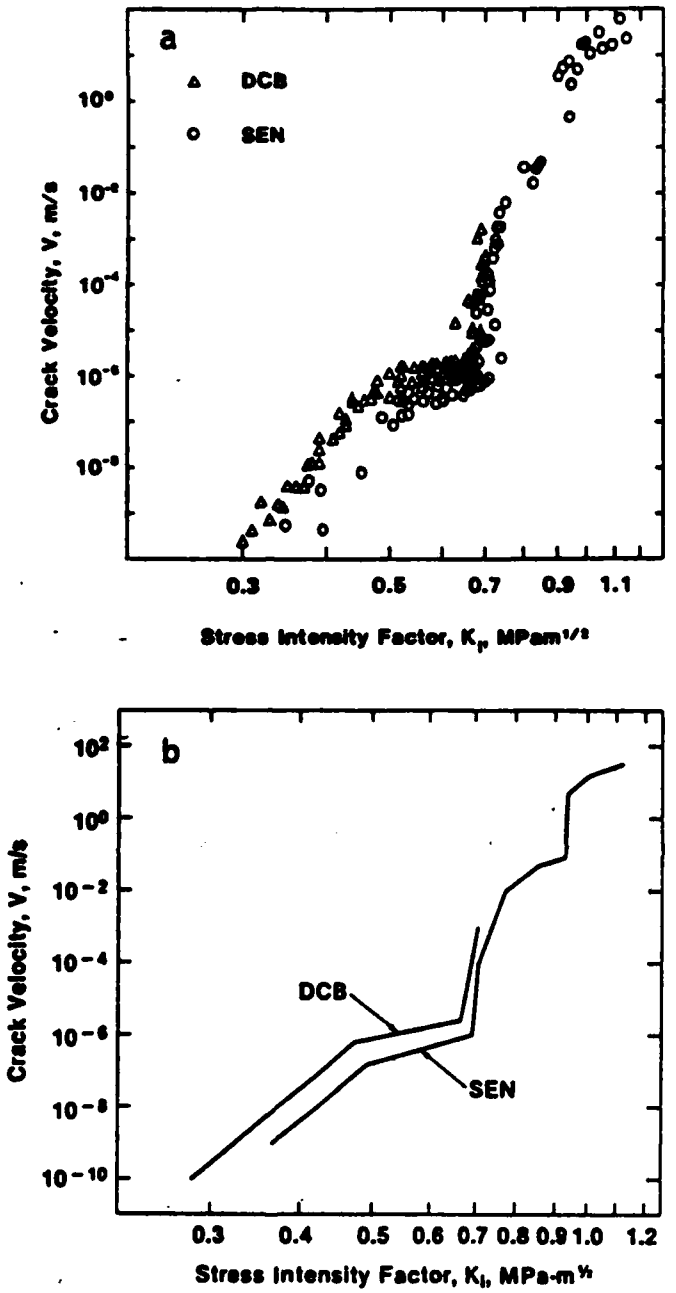

1. Crack velocity data, soda-lime silica glass in heptane. (a) Crack velocity data collected by the applied moment, double cantilever techniques and the single-edge, notch technique. (b) Piecewise, straight-line fit of the crack growth data shown in (a). Curve marked SEN represents the single edge, notch data; curved marked DCB represents the double cantilever data.

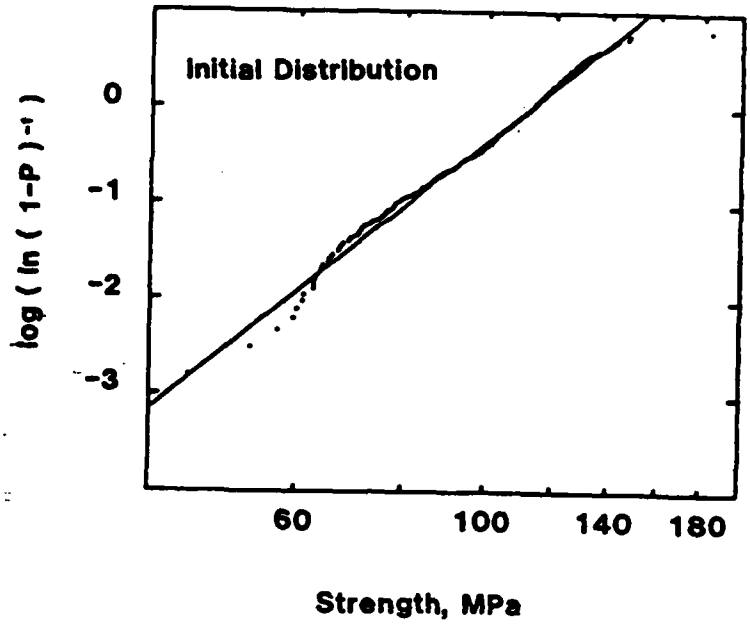

2. Initial strength distribution of 628 microscope slides broken in four-point bending, in heptane: S_0 = 112; m = 7.

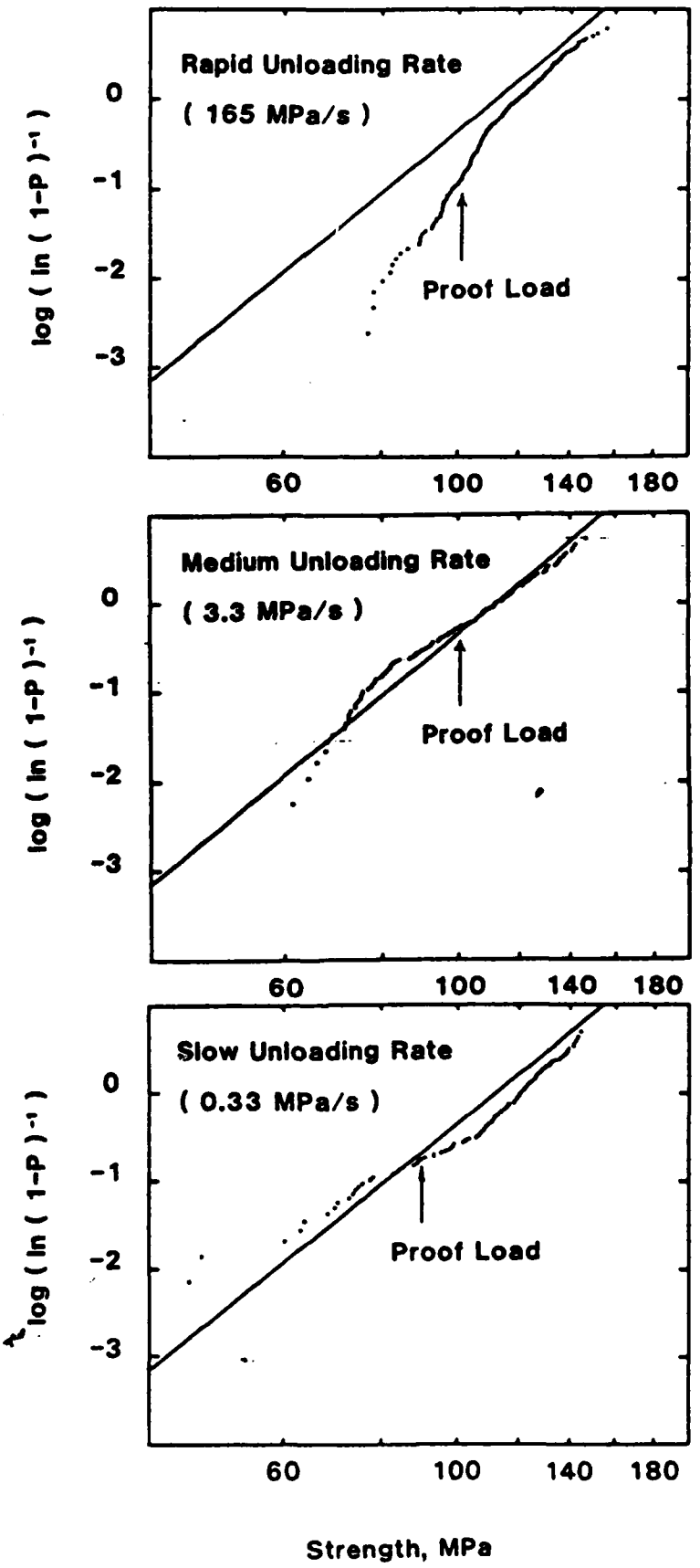

3. Strength distribution after proof testing in heptane: (a) rapid (165 MPa/s) unloading rate; (b) medium (3.3 MPa/s) unloading rate; (c) slow (0.33 MPa/s) unloading rate.

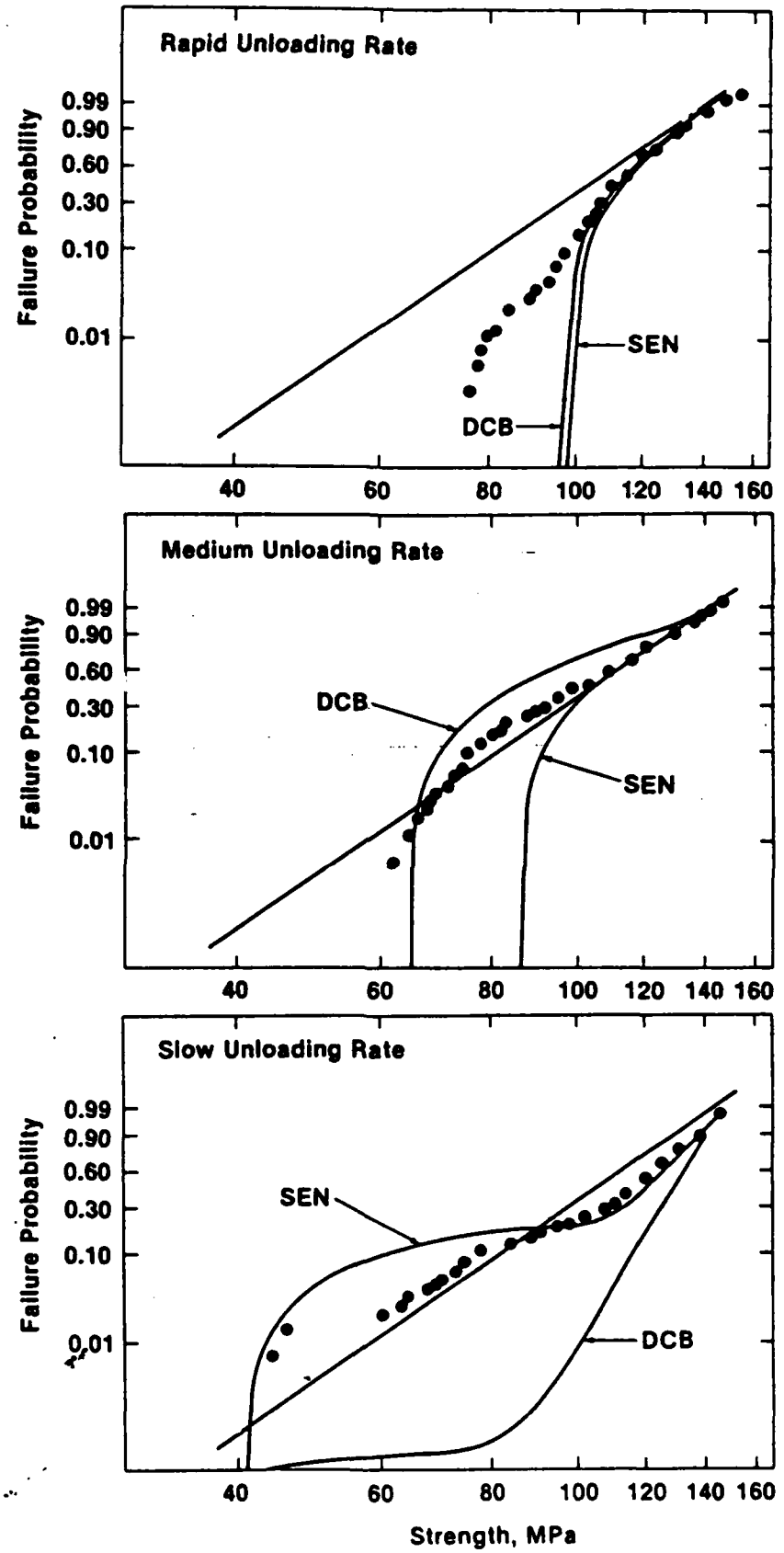

4. Strength distribution curves after proof testing in heptane, calculated from v-K, data shown in figure 1: (a) rapid (165 MPa/s) unloading rate; (b) medium (3.3 MPa/s) unloading rate; (c) slow (0.33 MPa/s) unloading rate.

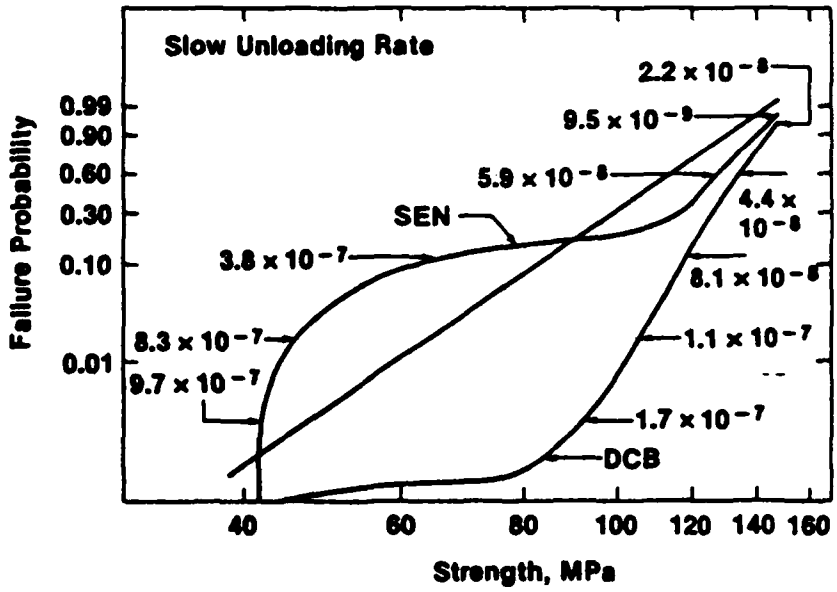

5. Maximum velocities (m/s) achieved during proof testing printed next to calculated strength distribution curves. The maximum crack velocities and the calculated strength distribution curves were obtained from the v-K_I data shown in figure 1: slow (0.33 MPa/s) unloading rate.

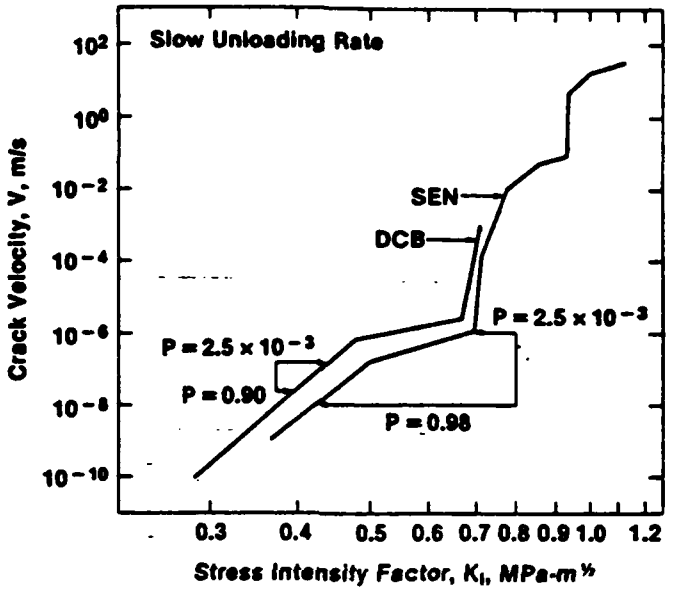

6. Range of crack velocities that determine the strength distribution curves for the slow (0.33 MPa/s) unloading rate.

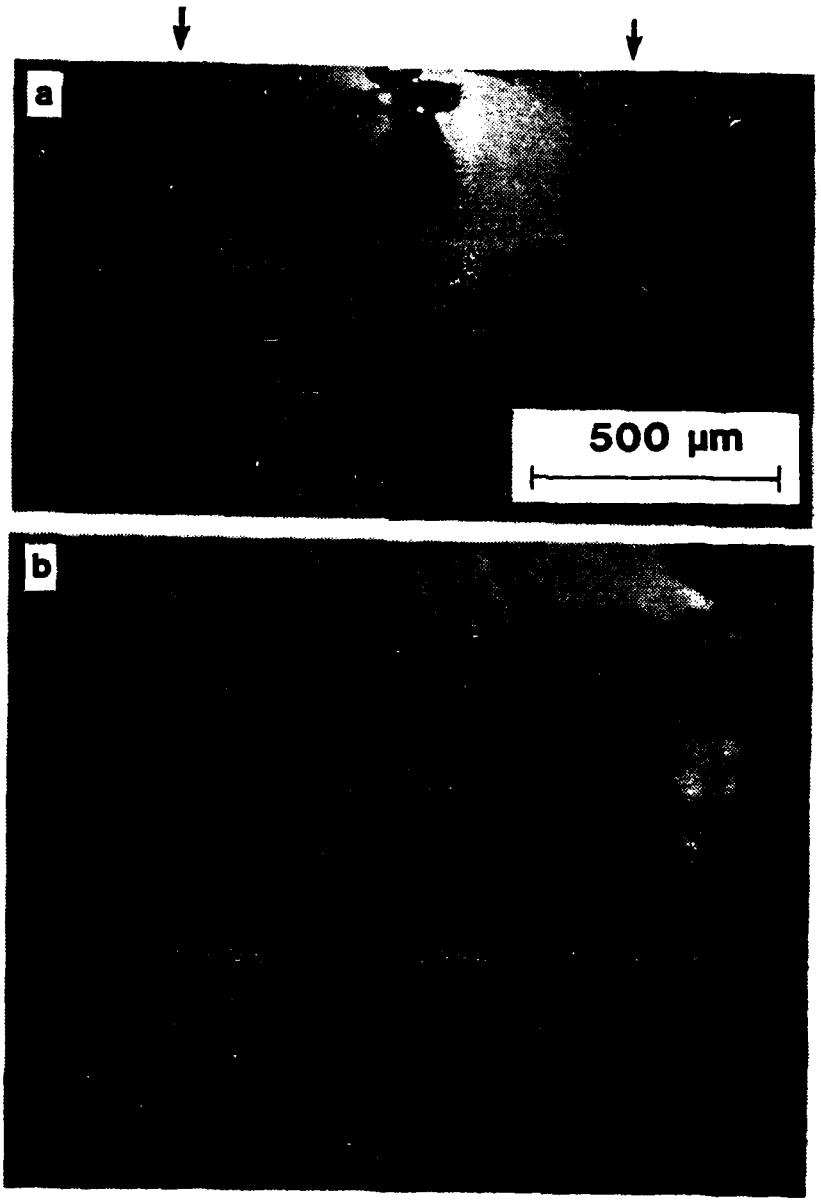

7. Successive positions of a surface crack that was propagated to failure in heptane: (a) arrows mark the transition between region II and region III crack growth; (b) higher magnification of (a) showing the shape of the crack fronts in region II.

To be published in Ferroelectrics, 1984.

FRACTURE OF FERROELECTRIC CERAMICS

R.F. COOK, S.W. FREIMAN, B.R. LAWN
Inorganic Materials Division, National Bureau of Standards, Washington. DC 20234

R.C. POHANKA
Office of Naval Research, Code 431, Arlington, Virginia

Abstract This paper surveys the temperature, microstructural and environmental variations of the fracture properties of ferroelectric ceramics. Earlier work shows that fracture toughness decreases on heating through the Curie temperature. There is also anomalous behavior in the strength at small crack sizes, indicative of a grain size effect. Further, the strength properties are known to be adversely affected by the presence of water in the atmosphere. Data from recent indentation studies on barium titanate are used to investigate these phenomena.

INTRODUCTION

Ferroelectric ceramics such as barium titanate ($BaTiO_3$) and lead zirconate titanate (PZT) are susceptible to brittle failure from small processing and handling flaws. To characterize the strength properties of brittle materials we need to understand the nature of all forces acting on the flaws. We shall address these issues in terms of data from indentation fracture studies.

INDENTATION TESTING

Reproducibility in strength data may be optimized by introducing controlled indentation flaws into prospective test specimens.[1] The driving force on such flaws comes from two main sources, the externally applied stress field and a local residual field about the elastic/plastic impression. Under equilibrium fracture conditions the strength is given by

$$\sigma = AK_c^{4/3}/P^{1/3} \quad (1)$$

where A is a dimensionless constant, K_c is the material toughness and P is the original indentation load. Departures from the predicted variation of σ on P in Eq. (1) could be effected either by a third, unaccounted driving force on the indentation flaw, or by a systematic dependence of K_c on crack size.

Accordingly, controlled flaw tests were run on $BaTiO_3$. Indentations were made on annealed bar specimens with a Vickers diamond pyramid, in air, at prescribed loads. Failure was produced in four-point flexure in a controlled environment. At low loads, failure tended to initiate from natural rather than introduced flaws, thereby imposing a lower limit on the data range.

TEMPERATURE EFFECTS

Strength variations were followed as a function of temperature for a $BaTiO_3$ material of nominal grain size 7 μm. The indentation load for these tests was fixed at 30 N, so that the cracks produced were well in excess of the grain size. The flaws were introduced at room temperature, and the strength tests were run in a heated oil bath. Figure 1 shows the results. There is a monotonic decrease in strength to the vicinity of the Curie temperature, T_c, then an apparent levelling out. The falloff between 25°C and 150°C corresponds to a reduction of $\tilde{\sim}$40% in K_c (see Eq. 1), consistent with trends noted previously in monocrystalline $BaTiO_3$.[2,3] Specimens tested after cycling through T_c showed the same strengths, within experimental scatter, as those heated directly from room temperature.

In view of this reversibility, it can be concluded that the results in Fig. 1 reflect intrinsic thermal effects in the toughness parameter. The reported appearance of domain wall

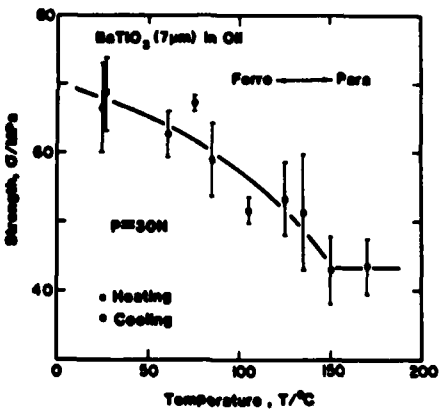

FIGURE 1 Strength as function of temperature.

markings on fracture surfaces produced below T_c suggests that crack/twin interactions could account for the trends observed here[2]; the falloff of K_c with temperature would then be attributable to the thermally activated annihilation of domain walls as the transition is approached.[4]

Analogous thermal effects have been reported for PZT.[5,6]

MICROSTRUCTURAL EFFECTS

The influence of microstructure on strength properties was investigated by systematically reducing the controlled-flaw size, via the indentation load. Data are plotted in Fig. 2 for the 7 μm (Fig. 1) and a 1 μm $BaTiO_3$. Several points may be noted:
(i) At 150°C the data fit the dependence predicted by Eq. (1) over the entire load range, for both materials. Moreover, the representative straight lines are indistinguishable, indicating that K_c is the same in both cases. This grain-size invariance of toughness above the Curie point is consistent with data on other cubic ceramics.[7]

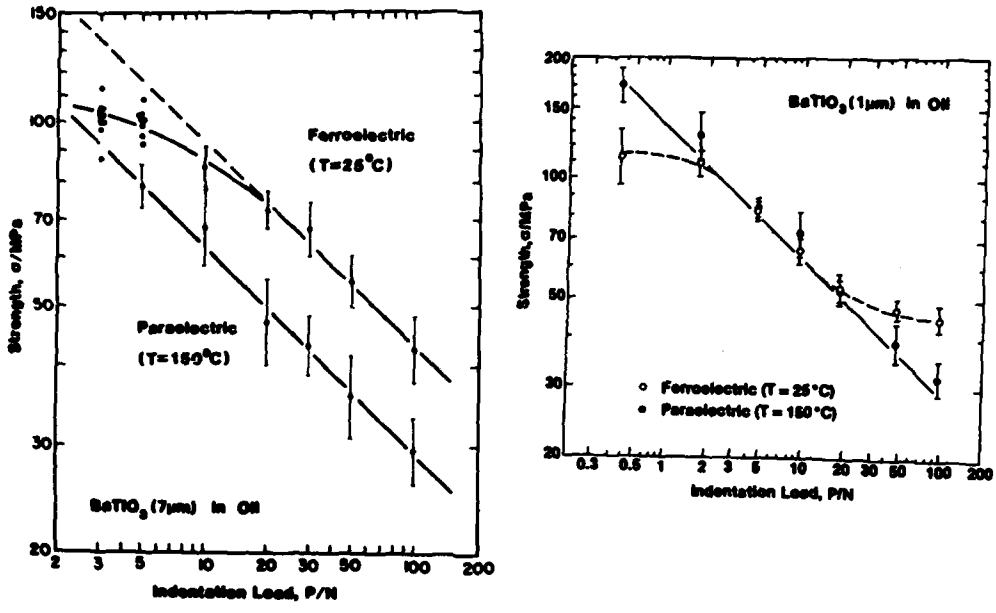

FIGURE 2 Strength as function of load.

(ii) At 25°C the data are well behaved over only part of the load range. In this well-behaved region there is overlap with the 150°C data for the 1 μm material, whereas for the 7 μm material the temperature dependence noted in the strength data of Fig. 1 is apparent. These results imply a grain-size dependence in K_c below the Curie point. A systematic study of this dependence in $BaTiO_3$ materials over a grain-size range 1-150 μm shows that K_c can vary by as much as a factor of two.[2]

(iii) At low loads the 25°C data for both materials drop off below the theoretical line. As alluded earlier, such a departure could be due either to the presence of an additional driving force on the cracks or to a tendency for K_c to increase in a systematic manner as the cracks intersect a greater number of grains. Of these two possibilities, only the first appears to be capable of accounting for the reversion to ideal behavior at the elevated temperature, since the grain geometry remains invariant on traversing the Curie point. Thus it has been suggested that the room temperature data are consistent with the existence of local

internal stresses associated with a non-cubic (tetragonal) polycrystal.[2,4] These stresses are felt more strongly as the cracks become smaller, approaching the scale of the microstructure; in this context, it is noted in Fig. 2 that the deviation occurs at a lower level of P in the 1 μm material. (iv) At high loads the 25°C data for the 1 μm material again deviates from ideal behavior. The cause of this anomaly is not understood at present, although analogous behavior has recently been reported in a La-doped lead titanate.[8]

ENVIRONMENTAL EFFECTS

The access of water to crack tips in brittle ceramics can cause subcritical growth, i.e. growth at stress levels less than that needed to maintain the equilibrium configuration implied in Eq. (1). The rate of subcritical crack growth increases dramatically with stress intensity, approximately to some power N, where N >> 1 typically. Accordingly, specimens loaded at low stressing rates are subject to more extensive subcritical growth, and hence to a greater degradation in strength. For specimens with indentation flaws, the "fatigue susceptibility" parameter N can be measured directly from the (inverse) slope of a strength vs stressing rate plot.[9]

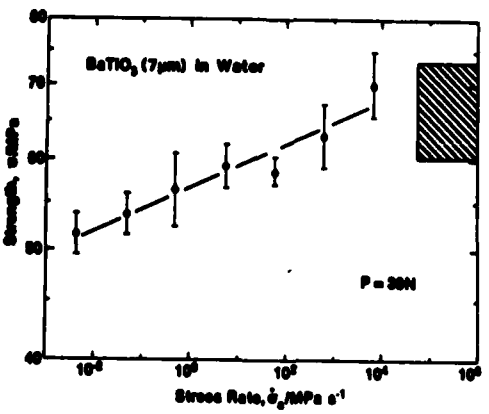

FIGURE 3 Strength as function of stressing rate.

Accordingly, such a plot is shown in Fig. 3 for the 7 μm $BaTiO_3$ tested in water at 25°C. The strength indeed falls off significantly as the stressing rate decreases (or, alternatively, as the time to failure increases). The value N = 67 obtained from these data is considerably higher than that for soda-lime glass (N = 18, representing one of the most susceptible of all brittle materials), but is within the range found for a broad spectrum of ferroelectric ceramics. Small changes in composition, particularly in the form of grain boundary impurities, could well give rise to deleterious decreases in the N parameter.

ACKNOWLEDGEMENTS

The authors thank Karl McKinney for supplying the barium titanate and Heidi Multhopp for experimental assistance. The work was funded by the U.S. Office of Naval Research.

REFERENCES

1. B.R. Lawn, in Fracture Mechanics of Ceramics, edited by R.C. Bradt, A.G. Evans, D.P.H. Hasselman and F.F. Lange (Plenum, New York, 1982), Vol. 5, p. 1.
2. R.C. Pohanka, S.W. Freiman and B.A. Bender, J. Amer. Ceram. Soc., 61, 72 (1978).
3. S.W. Freiman, K.R. McKinney and H.L. Smith, in Fracture Mechanics of Ceramics, edited by R.C. Bradt, D.P.H. Hasselman and F.F. Lange (Plenum, New York, 1974), Vol. 2, p. 659.
4. B. Jaffe, W.R. Cook and H. Jaffe, Piezoelectric Ceramics (Academic Press, London, 1971), Chap. 5.
5. R.C. Pohanka, S.W. Freiman and R.W. Rice, Ferroelectrics, 28, 337 (1980).
6. R.C. Pohanka, S.W. Freiman, K. Okasaki and S. Tashiro, in Fracture Mechanics of Ceramics, edited by R.C. Bradt, A.G. Evans, D.P.H. Hasselman and F.F. Lange (Plenum, New York, 1982), Vol. 6.
7. R.W. Rice, S.W. Freiman and P.F. Becher, J. Amer. Ceram. Soc., 64, 345 (1981).
8. T. Yamamoto, H. Igarashi and K. Okazaki, J. Amer. Ceram. Soc., 66, 363 (1983).
9. R.F. Cook, B.R. Lawn and G.R. Anstis, J. Mater. Sci., 17, 1108 (1982).

Pages 205-212 in NMAB Report
The Reliability of Multilayer Ceramic Capacitors, 1983

THE EFFECT OF CRACKS ON THE RELIABILITY OF MULTILAYER CAPACITORS

S. W. Freiman
Fracture and Deformation Division
National Bureau of Standards
Washington, DC

The purpose of this paper is twofold. First it will show to what extent the fracture of piezoelectric materials such as $BaTiO_3$ are influenced by microstructure and the phase transformation from the paraelectric to the ferroelectric state. It will be demonstrated that multiple toughening mechanisms such as twinning and microcracking account for the observed behavior and that fracture mechanics principles can be used to develop materials having an optimum resistance to cracking. Second, it will show that subcritical crack growth in capacitors will ultimately lead to failure. Again, fracture mechanics techniques will be used to make predictions as to the likely failure times for actual capacitors.

FRACTURE OF $BaTiO_3$

Pohanka and co-workers (1976) have shown that the strength of polycrystalline $BaTiO_3$ is lower in the ferroelectric state compared to that in the paraelectric state for grain sizes between 1 and 100 μm. Using a fracture mechanics approach, one obtains the following expression for the strength of the material above the Curie temperature where the material is cubic:

$$\sigma = Y \left(\frac{E\gamma_c}{a}\right)^{1/2} \qquad (1)$$

where E is Young's modulus, γ_c is the critical fracture energy of the cubic material, a is the flaw size, and Y is a measure of the flaw geometry. For the ferroelectric state, this equation must be modified to take into account both internal stresses arising due to the phase transformation and mechanisms leaching to an increase in γ:

$$\sigma + \langle\sigma_I\rangle = Y \left(\frac{E\gamma_f}{a}\right)^{1/2} \qquad (2)$$

where $\langle\sigma_I\rangle$ represents the average of the tensile and compressive stresses around the perimeter of a flaw. The flaw that propagates to failure will be the one under the largest combination of size and tensile stress. Larger flaws intersect many tensile and compressive components, leading to low values of $\langle\sigma_I\rangle$. The contribution of $\langle\sigma_I\rangle$ to failure as a function of flaw size follows the trend shown in Figure 1. In order to completely understand the fracture process, one also must know the effect of the microstructure of $BaTiO_3$ on the resistance of the material to crack growth (i.e., γ).

In $BaTiO_3$ the critical fracture energy, γ, is a function of grain size, G, in the ferroelectric state but is independent of grain size in the paraelectric state (Pohanka et al. 1982) (Figure 2). The 150°C data fit an empirical expression:

$$\gamma = - 0.02 \text{ Log } G + 3.46 \qquad (3)$$

Because the crystal structure in the paraelectric state is cubic, this type of behavior is to be expected (Rice et al. 1981). The room temperature fracture energy of $BaTiO_3$, having a tetragonal crystal structure, remains constant up to a grain size of 15 μm, increases rather sharply, and then decreases (Figure 2). This behavior can be explained on the basis of a combination of twinning and microcracking enhanced toughness over different portions of the grain size range.

1 to 5 μm

In the 1 to 5 m grain size regime, ferroelastic twinning does not occur; therefore, the fracture energy of cubic and tetragonal $BaTiO_3$ would be expected to be quite similar, as is observed. These are the lowest values of γ measured experimentally.

5 to 15 μm

Above a grain size of 5 μm, 90-degree, ferroelastic twins are produced by the cubic-to-tetragonal phase transformation (Dennis 1972). Based on the increase in the fracture energy of single-crystal $BaTiO_3$ from 0.8 to 1.4 J/m^2 due to the interaction of the crack with the twins, one would expect the γ of the polycrystalline materials to be increased proportionally. However, it is observed that fracture over this grain size range is predominantly intergranular. This means that the cracks, instead of passing through the twin structure, take the easier path around the grains. Since no crack-twin interactions take place, twinning does not influence the toughness.

Microcracking near the crack tip does affect the measrued fracture energy. That microcracking must play some role in the fracture process is shown by the spontaneous cracking of polycrystalline $BaTiO_3$ at grain sizes between 150 to 250 μm. Following Rice and Freiman (1981), one can calculate the contribution that microcracking would make to the measured fracture energy; this contribution is shown as the dashed line in Figure 2. Considering the number of assumptions and the experimental scatter in both the measured γ and the parameters needed to calculate it, the fit is quite good.

15 to 50 μm

Over this range, both microcracking and twinning contribute to the measured fracture energy. A maximum in the γ-grain size curve at $\sim$40 μm is calculated based on microcracking contributions, in good agreement with the data.

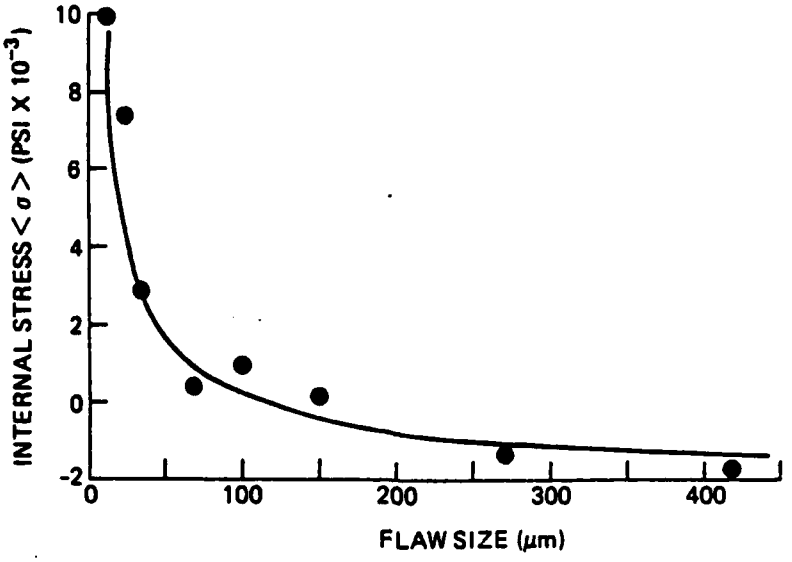

FIGURE 1 Effective internal tensile stress in fine-grained $BaTiO_3$, determined from measurements of flaw sizes, fracture stress and critical fracture energy, as a function of measured-flow size.

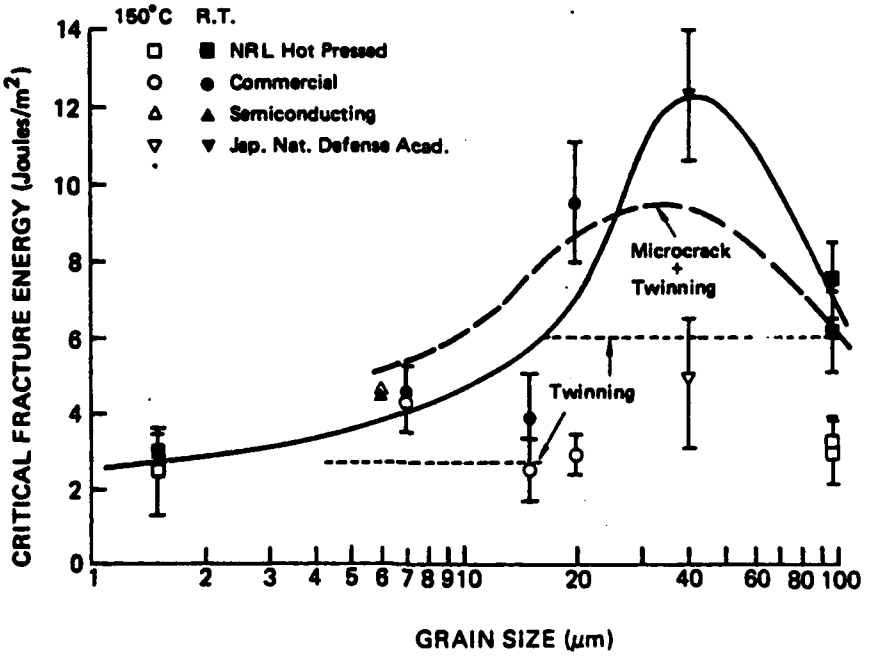

FIGURE 2 Fracture energy of $BaTiO_3$ as a function of grain size: _____ best fit to room temperature data; ----- contribution due to twinning, - - - combined effect of twinning and microcracking predicted by model of Rice and Freiman (1981).

50 to 200 μm

At grain sizes greater than about 50 μm, both twinning and microcracking still contribute to increased toughness, but linking of microcracks begins to occur, leading to decreasing fracture energy with grain size. Eventually, spontaneous failure takes place.

DESIGN DIAGRAMS FOR CAPACITORS

The above discussion relates the strength and fracture toughness of a primary capacitor material to microstructurally related processes. It also is known, however, that in the combined pressure of stress and moisture, initially small cracks will grow slowly, leading to eventual failure. In this section it will be shown how fracture mechanics techniques can be used to predict the time to failure for capacitors containing cracks under stress.

Cracks have been observed in capacitors and to some degree can be associated with premature capacitor failure. These cracks can be stressed by a variety of loading conditions. These include possible mechanical loads, stresses due to the differential thermal expansion between the capacitor and the substrate to which it is bonded, and internal stresses due to electrical field concentrations at the crack tip. Based on the two equations:

$$V = A K_I^n \tag{4}$$

and

$$\sigma = Y K_I a^{-1/2} \tag{5}$$

where V is crack velocity, K_I is the stress intensity at the crack tip, a is the crack size, and A and n are parameters that are dependent on the material and the environment. A time to failure, t, can be calculated:

$$t = B \sigma^{-n} S_i^{(n-2)} , \tag{6}$$

where B is a constant involving A and Y and S_i is the initial strength of the material (i.e., a measure of the crack size distribution before any stresses are applied). The constants n and B can be determined by measuring the strength of the capacitors as a function of stressing rate. The tests usually are performed in four-point flexure over three to four orders of magnitude in stressing rate as shown in Figure 3 for a typical capacitor composition. Approximately 100 specimens are required to obtain accurate measures of n and B.* The initial flaw size distribution is determined by

*Details of the analysis techniques for tests of this type are given by Jakus and co-workers (1978) and Ritter and co-workers (1981).

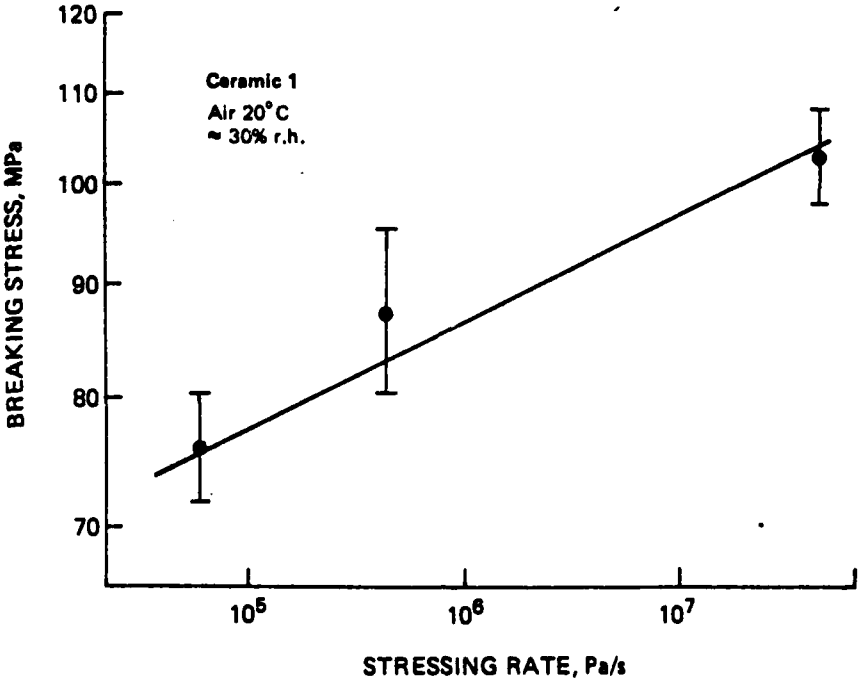

FIGURE 3 Strength-stressing rate curve for a typical capacitor material. The slope of the curve equals $(n+1)^{-1}$.

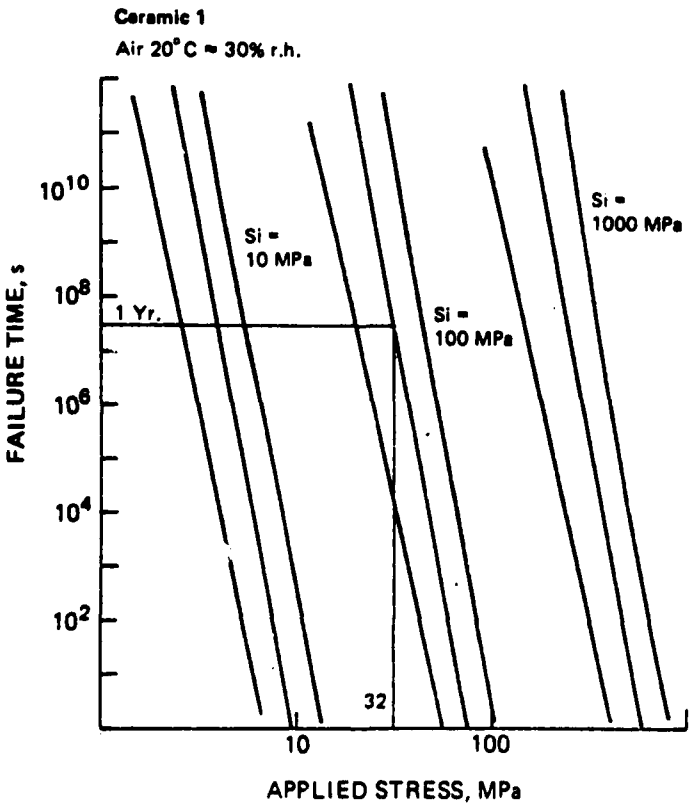

FIGURE 4 Design diagram based on the data obtained from Figure 3.

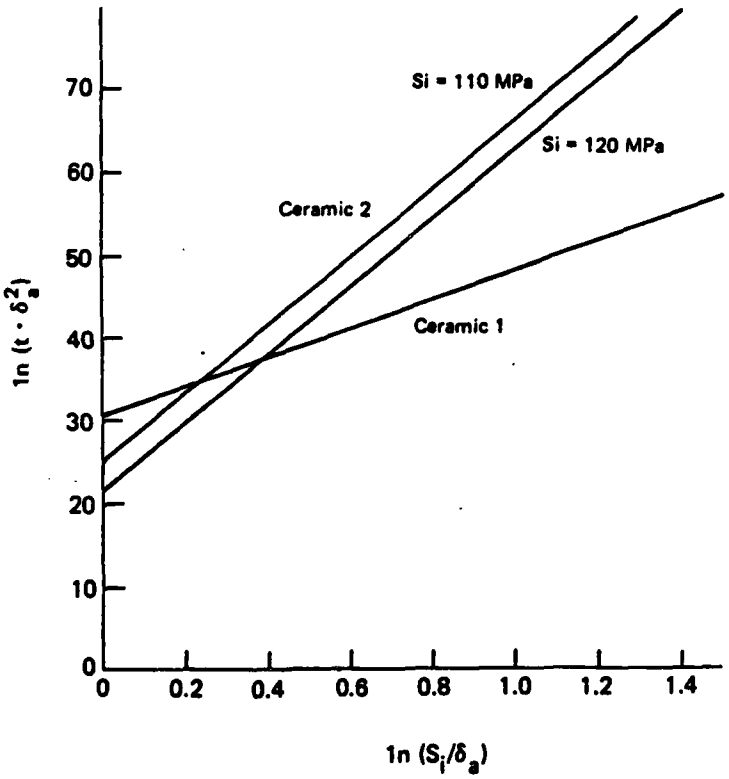

FIGURE 5 Comparison of failure time predictions for two capacitor materials. Ceramic 1: n = 19.5 and lnB = 30.95. Ceramic 2: n = 42.2 and lnB ≃ 27.0.

measuring the strength under inert conditions (e.g., dry N_2 gas) at a relatively rapid rate of loading. The distribution in inert strengths is analyzed using Weibull statistics. Weibull theory allows us to assign a probability of failure for a given level of stress. Combining these statistics for S_i with the crack growth parameters obtained from the stressing rate tests allows a design diagram such as that shown in Figure 4 to be constructed. The three sets of curves in this diagram represent the same material with three different initial flaw sizes. The central line in each set is the calculated values of failure time for a given applied stress in Equation 6. The bounding lines represent the 95 percent confidence limits on the failure times and are based on the errors in determining B and n. One can see that errors in B and n lead to large uncertainties in estimating the safe lifetime for a given applied stress. One can reduce this uncertainty, however, by reducing the applied stress to the edge of the confidence band.

Figure 5 shows the failure time data for two different capacitor compositions plotted in a way that normalizes the flaw sizes. It can be seen that the material having the larger value of n would be expected to survive for much longer times over most of the range of applied stresses.

SUMMARY AND CONCLUSIONS

Based on the above discussions, it seems clear that the application of fracture mechanics principles can contribute significantly to an understanding of the fracture processes in capacitor type materials. Both the chemical composition of the material as well as the grain size affect the material's resistance to both subcritical crack growth and catastrosphic failures. By measuring the slow crack growth parameters for a material, it is possible to predict lifetimes under stress.

There are a number of areas in need of further work however. These include:

1. The quantitative dependence of crack growth parameters on composition and microstructure,
2. The effects of internal stresses and flaw and grain sizes on crack growth,
3. Crack growth in complex stress fields, and
4. More accurate techniques for analysis of static fatigue and stressing rate data.

ACKNOWLEDGEMENTS

I would like to thank Hughes Aircraft for supplying the capacitor materials and S. M. Wiederhorn for his analysis of the stressing rate data.

REFERENCES

Dennis, M. D. 1972. Transmission electron microscopy of ferroelectric domains in barium titanate. PhD. Thesis, The Pennsylvania State University, University Park.

Jakus, K., D. C. Coyne, and J. E. Ritter, Jr., 1978. Analysis of fatigue data for lifetime predictions for ceramic materials. J. Mat. Sci. 13: 2071

Pohanka, R. C., R. W. Rice, and B. E. Walker, Jr. 1976. Effect of lateral stress on the strength of $BaTiO_3$. J. A. Ceram. Soc. 59:71.

Pohanka, R. C., S. W. Freiman, K. Okazaki, and S. Tashiro. 1982. Fracture of piezoelectric materials. 1981. Fracture Mechanics of Ceramics.

Rice, R. W., S. W. Freiman, and P. F. Becher. 1981. Grain-size dependence of fracture energy in ceramics: I experiment. J. Am. Ceram. Soc. 64:345.

Rice, R. W., S. W. Freiman. 1981. Grain-size dependence of fracture energy in ceramics: II. A model for non-cubic materials. J. Am. Ceram. Soc. 64:350.

Ritter, J. E., Jr., N. Bandyopadhyay, and K. Jakus. 1981. Statistical reproducibility of the dynamic and static fatigue experiments. Bull. Am. Ceram. Soc. 60:798.

END

FILME

2-84

DTIC